# REPORT DOCUMENTATION PAGE

AFRL-SR-BL-TR-01-

0258



sources,
t of this
lefferson

| 1. AGENCY USE ONLY *(Leave blank)* | 2. REPORT DATE | 3. RE... |
|---|---|---|
| | | Final 01 May 95 to 31 Oct 00 |

**4. TITLE AND SUBTITLE**
MURI-94 Research on Compact, High-Energy, Microwave Sources

**5. FUNDING NUMBERS**
3484/RS
61103D

**6. AUTHOR(S)**
Dr Granatstein

**7. PERFORMING ORGANIZATION NAME(S) AND ADDRESS(ES)**
University of Maryland
Energy Research Bldg, #223
Paint Branch Drive
College Park, MD 20742-3511

**8. PERFORMING ORGANIZATION REPORT NUMBER**

**9. SPONSORING/MONITORING AGENCY NAME(S) AND ADDRESS(ES)**
Air Force Office of Scientific Research
801 N. Randolph Street
Arlington, VA 22203-1977

**10. SPONSORING/MONITORING AGENCY REPORT NUMBER**
F49620-95-1-0358

**11. SUPPLEMENTARY NOTES**



**12a. DISTRIBUTION AVAILABILITY STATEMENT**
Unlimited Distribution

**12b. DISTRIBUTION CODE**

**13. ABSTRACT** *(Maximum 200 words)*

The activity at the University of Maryland was primarily devoted to research of the following four topics: 1) frequency-multiplying gyrotron amplifiers; 2) relativistic backward wave oscillators; 3) plasma-filled microwave sources; 4) synthesis of advanced ceramics for microwave tubes. The present state of art has electron beams generated in ferroelectric guns operating at 500 kV and 300 A in 250 ns pulses. Current densities are typically less than or of order 100 A/cm$^2$, although higher current densities have been recorded from localized regions.

**14. SUBJECT TERMS**

**15. NUMBER OF PAGES**

**16. PRICE CODE**

| 17. SECURITY CLASSIFICATION OF REPORT | 18. SECURITY CLASSIFICATION OF THIS PAGE | 19. SECURITY CLASSIFICATION OF ABSTRACT | 20. LIMITATION OF ABSTRACT |
|---|---|---|---|
| Unclassified | Unclassified | Unclassified | UL |

FINAL REPORT

AFOSR Grant Number F49620-95-10358

# Research on Compact, High-Energy, Microwave Sources (MURI '94)

## May 1, 1995 to October 31, 2000

Principal Investigator:
Victor L. Granatstein
Institute for Plasma Research and
Department of Electrical and Computer Engineering
University of Maryland
College Park, MD 20742-3511



December 15, 2000

# Table of Contents

## PART A: Research at the University of Maryland

# PART B: Research at Cornell University

# PART A
# Research at the University of Maryland

The work reported in this section was carried out at the University of Maryland between May 1995 and October 2000 as part of the MURI in High Energy Microwave Sources. The activity at the University of Maryland was primarily devoted to research of the following four topics:

- frequency-multiplying gyrotron amplifiers;
- relativistic backward wave oscillators;
- plasma-filled microwave sources;
- synthesis of advanced ceramics for microwave tubes.

Progress on these topics is described sections 2, 3, 4, and 5, respectively.

A detailed review of the bulk of this research was prepared during the summer of 1999 and that review forms the basis of a large portion of this report.

## 2 Frequency-Multiplying Gyro-Amplifiers

As is known, the magnetic field required for gyrotron operation increases proportionally to the operating frequency. Therefore, millimeter wave gyrotrons operating at the fundamental cyclotron resonance need superconducting magnets producing magnetic fields above 1 T. This hinders the practical mobile deployment of gyro-devices since the superconducting magnets are in general large, heavy, complicated and expensive. One obvious way to mitigate this restriction is to operate at cyclotron harmonics since the required magnetic field decreases as $s^{-1}$, where $s$ is the cyclotron harmonic number. The first theoretical studies [1, 2, 3] showed that the operation of free-running gyrotron oscillators at harmonics can be quite efficient, especially for $s = 2$. This was confirmed in the first experiments [4] in which, at a wavelength of 8.9 mm, the second-harmonic interaction led to generation of 30 kW peak power with 43% efficiency in the pulsed regime and 10 kW power with 40% efficiency in the cw regime.

For gyrotron amplifiers, it is even more attractive to consider the possibility of frequency-multiplying operation. This would combine the advantage of reducing the solenoidal magnetic field for output frequency at a harmonic of the cyclotron frequency with the possibility of using low-frequency, high-power drivers for exciting the input stage of the device at the fundamental resonance. This concept is well known in the history of microwave tube development. For instance, the theory and experiments for a traveling wave frequency multiplier are described in [5], where it is also mentioned that frequency-multiplying klystrons had been developed earlier. With respect to gyro-amplifiers, the nonlinear nature of electron bunching leading to the appearance of harmonics in the electron current density, which can be used for the excitation of successive cavities or waveguides at harmonics of the input signal frequency, is discussed in [1].

Below, we describe the development of frequency-multiplying gyro-devices driven by electron beams generated by magnetron-type injection guns. The work at UMD focuses on the study and realization of frequency-doubling and -quadrupling gyro-amplifiers driven by conventional, large-radius ($r_b \gg r_L$) gyrotron beams. In this case, a frequency-quadrupling device implies a three-stage circuit with successive frequency doubling in the second and last stages. The theoretical and experimental efforts are described in the two succeeding subsections.

## 2.1 Theory

### 2.1.1 Frequency-multiplying gyro-amplifiers

The theoretical background for this work was developed in [6, 7]. In [6], a simplified general theory of three-cavity gyroklystrons (GKLs) was formulated for the case in which the input cavity operates at the fundamental resonance, the penultimate cavity operates either at the fundamental or at the second harmonic, and the output cavity operates at one of the first four harmonics. In particular, it was shown that a so-called 1-2-4 scheme may operate with rather high efficiency. (The numbers 1, 2, and 4 here designate the resonant cyclotron harmonic number for each cavity.) In [7], the analysis took into account the restrictions important for operation of moderately relativistic (voltages below 100 kV) GKL's at high harmonics. Also, some means for mitigating these restrictions were analyzed in that paper. Specifically, it was shown that even in the presence of a realistic electron velocity spread, a 1-2-4 GKL driven by a 60 kV electron beam with a mean orbital-to-axial velocity ratio of 1.5 can operate with an efficiency greater than 30%.

### 2.1.2 The Gyro-twystron

In its simplest configuration the gyro-twystron consists of an input cavity and an output waveguide separated by a drift region. Since a waveguide is a nonresonant circuit (in the absence of reflections), the bandwidth of the gyro-twystron is restricted by the resonance properties of the input cavity, that is, by its $Q$. When a prebunching section consisting of several cavities with slightly stagger-tuned eigenfrequencies is added, the bandwidth can be significantly increased. However, the gain of the device becomes smaller in the presence of such stagger tuning.

The trade-off between the gain and bandwidth of the gyro-twystron with a multi-cavity, stagger-tuned prebunching section was analyzed using a small-signal theory in [8]. In [8], the cases of gyro-twystrons with one-, two- and three-cavity prebunching sections were studied. An assumption that the cavity lengths are much shorter than the drift sections has led to the development of a quite general formalism that allows one to analyze the most important tendencies in the bandwidth enlargement and gain degradation of such stagger-tuned devices.

This analysis was followed by the development of the nonlinear theory of such devices as described in [9]. A more or less complete study of nonlinear properties was performed for gyro-twystrons with one- and two-cavity prebunching sections. The results are illustrated in Figure 1, taken from [9]. This figure shows how in a gyro-twystron with a two-cavity prebunching section the increase in the bunching parameter, $q_0$ (responsible for the saturation

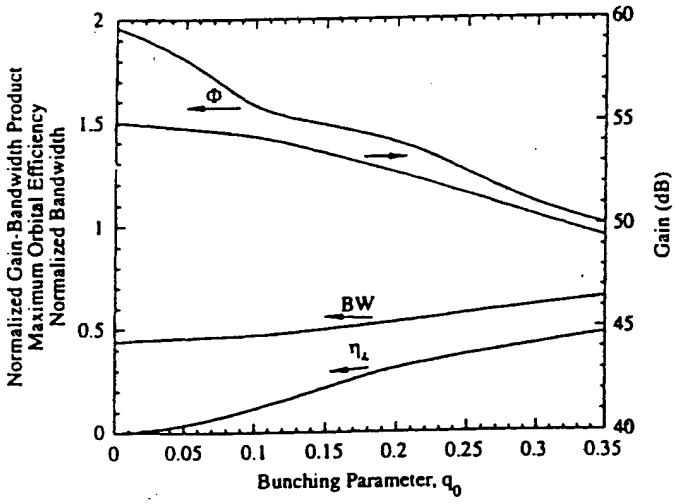


Figure 1: Large-signal gain-bandwidth and efficiency of the gyro-twystron with stagger-tuned pre-bunching cavities.

effects), changes the gain; bandwidth, BW; orbital electron efficiency, $\eta_\perp$; and normalized gain-bandwidth product, $\Phi$. The latter value is the gain-bandwidth product normalized to the value for a non-stagger-tuned device operating in a small-signal regime. This example shows that:

- in the small-signal regime, for a specified set of parameters given in [9], the stagger tuning allows one to approximately double the gain-bandwidth product;
- as the operation transitions from a small-signal regime (small $q_0$'s) to a large-signal one, this product decreases to approximately the same value as in a non-stagger-tuned gyro-twystron operating in a small-signal regime. Simultaneously, the gain drops from the 55 dB small-signal gain to the 49.5 dB large-signal gain, and the bandwidth increases by about 40% with respect to the small-signal operation.

Also, a gyro-twystron with a three-cavity prebunching section was analyzed for the set of parameters corresponding to the detailed design of the 34 GHz device reported in [10]. Our calculations based on the simplified model of the prebunching section yielded 37% maximum efficiency, 2.06% bandwidth, and 58.5 dB maximum gain, while the analysis in [10] predicted 33% efficiency, 55 dB gain, and a little more than 2% bandwidth. Thus, this comparison helps to validate the model described above.

### 2.1.3 Suppression of Backward Waves

Suppression of backward waves by forward waves in (gyro-) traveling wave amplifiers (TWA's) is a nonlinear effect. In general, the excitation of parasitic backward waves is the most serious obstacle for developing high-gain, large-bandwidth (gyro-)TWAs. To realize high gain in any TWA the interaction region should be sufficiently long. However, when its length

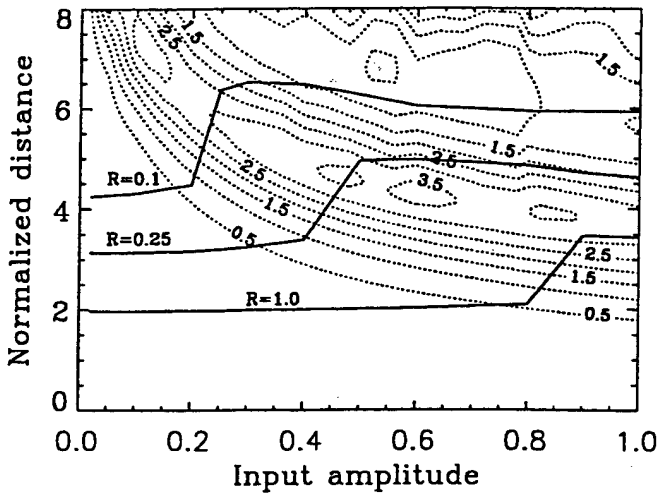


Figure 2: Contours of orbital efficiency of the forward wave operation in the gyro-TWT (dotted lines) and the start oscillation length of backward wave excitation for different values of the ratio of normalized current parameters for these waves and for the forward waves for the case when both waves interact with electrons at the fundamental cyclotron resonance $s_1 = s_2 = 1$.

exceeds a certain critical value, backward wave oscillations may appear. The problems of absolute instability suppression and reflective instabilities have been both experimentally and theoretically investigated in a series of elegant experiments by Barnett *et al.* [11] and Chu *et al.* [12]-[14], which included a detailed study of circuit losses. This led to the ultra-high gain gyro-TWT [14]-[15]. Further theoretical work has been conducted [16] that shows how a large-signal forward wave suppresses these oscillations or, in other words, increases the start oscillation length. The analysis was performed for gyro-TWT's and gyro-twystrons operating at the first two cyclotron harmonics, and for conventional (linear beam) TWT's and twystrons.

This theory allows one to analyze the problem in two steps. The first step is a standard theory describing amplification of a large-amplitude forward wave in a stationary regime. At the second step, the conditions of self-excitation of backward waves in the presence of forward waves should be analyzed. Since a small-amplitude backward wave causes only small perturbations in electron motion, corresponding equations can be linearized with respect to perturbations, which simplifies the treatment. At the same time, however, these equations contain the nonlinear terms caused by the effect of the large-signal forward wave on electrons. Certainly, in the absence of forward waves, these equations yield the standard dispersion equations known in the theory of the BWO [17] and the gyro-BWO [1].

The results of the studies of the gyro-TWT are illustrated by Figure 2. Here the dotted lines show the contours of orbital efficiency in the plane "normalized interaction length *vs.* normalized input amplitude of the forward wave," and the solid lines show the start oscillation length of the backward wave excitation for different ratios of the normalized current parameters for these waves. The increase of the start oscillation length with the

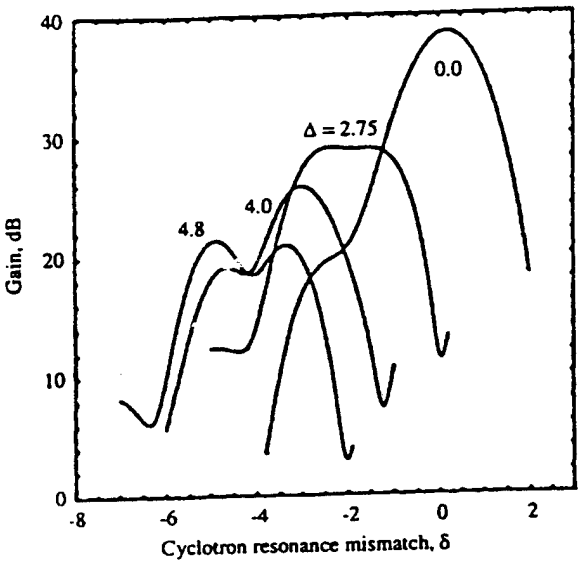


Figure 3: Gain as a function of the cyclotron resonance mismatch in the input waveguide $\delta$ for several values of the detuning parameter $\Delta$ between cutoff frequencies in the input and output waveguides.

increase in the input power, which is seen in Fig. 2, indicates the effect of suppression. Of course, as the coupling of the beam to the backward wave becomes weaker, the starting length for backward wave oscillations increases, as shown in Fig. 2. These results allow us to conclude that a device whose operation is stable to backward wave excitation in the absence of signal ("zero-drive" stability) will remain stable in the presence of the signal. Recall that, in principle, as known from the theory of mode interaction in gyrotron oscillators [18], the excitation of one mode can lead not only to the suppression of other modes, but also, under certain conditions, to their nonlinear excitation. The latter effect means that the presence of the first mode facilitates the self-excitation of the second.

### 2.1.4 Multi-stage Traveling-wave Amplifiers

Multi-stage traveling wave amplifiers allow developers to realize high gain of the total device while keeping the length of each stage shorter than the starting length of the backward wave oscillations, thus providing stable operation even in the absence of drive power (zero-drive stable regime). This motivated detailed stability studies by Chu and Lin, and their co-workers [19, 20], which led to the marginal stability design criterion for gyro-TWT's that has been validated in a number of experimental studies. In [21], a general formalism is developed that allows one to calculate the small-signal gain and bandwidth in multi-stage gyro-TWT's operating at frequencies either far from or close to cutoff. This formalism can also be applied to devices having different cutoff frequencies in different sections (a situation similar to the stagger-tuning effects discussed earlier). An example of results obtained in [21] is shown in Fig. 3. Here, the small-signal gain for a two-stage gyro-TWT operating at fundamental cyclotron resonance is shown as a function of the cyclotron resonance mismatch, $\delta$, between the Doppler shifted operating frequency and the gyrofrequency for several values

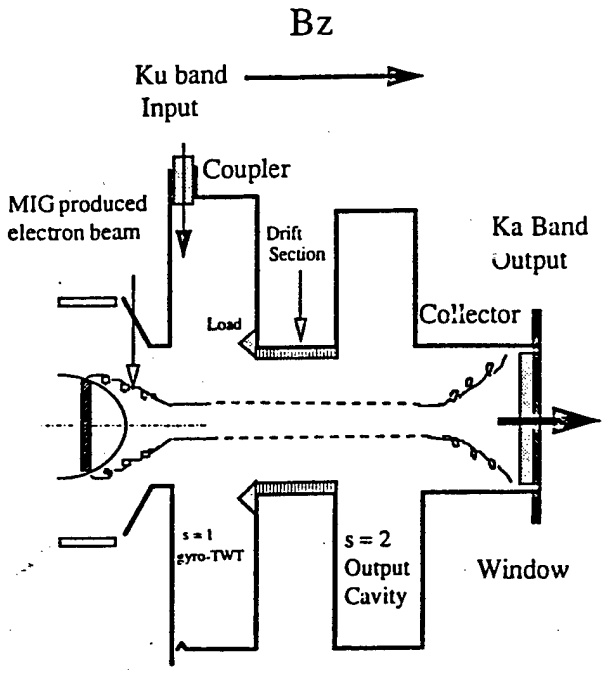


Figure 4: Schematic of a frequency-doubling inverted gyrotwystron.

of the detuning parameter, $\Delta$, characterizing the difference between cutoff frequencies of the input and output waveguides. These results illustrate the gain degradation and the bandwidth increase with the waveguides' stagger tuning.

## 2.2 Experiment

Related experimental efforts at UMD were focused on a new device called a PHIGTRON (**P**hase-coherent **H**armonic-multiplying **I**nverted **G**yrot**w**y**stron**). In contrast to the conventional gyro-twystron, which consists of an input cavity and output waveguide separated by a drift region, the input stage of the PHIGTRON is a waveguide section and the output stage is a cavity. A pictorial representation of this concept is shown in Fig. 4. The device is driven by a Ku-band, 2 kW helix TWT, and the output cavity is designed for operation at the second harmonic in Ka-band. The input waveguide and the output cavity each contains a special mode converter/filter (shown in Figs. 5 and 6), which discriminates against and spoils unwanted spurious modes. During the design phase, the simulation of mode conversion in the input gyro-TWT section was performed using the Hewlett Packard HFSS code and is reasonably consistent with the measured mode pattern that demonstrated the mode selectivity of the input coupler and the interaction circuit. This was important for stable operation of the PHIGTRON.

Depending on the preset operating parameters (in particular, the magnetic field tapering), in initial experiments at moderate power levels, the device operated either as a frequency-doubling amplifier with a $TE_{42}$ mode output (pulsed output power of 100 kW, gain of 30 dB, efficiency of 20%, and bandwidth of 1.3% around 33.7 GHz), or as a phase-locked oscillator with $TE_{03}$ mode output (pulsed output power of up to 500 kW, phase-locking gain of 35 dB,

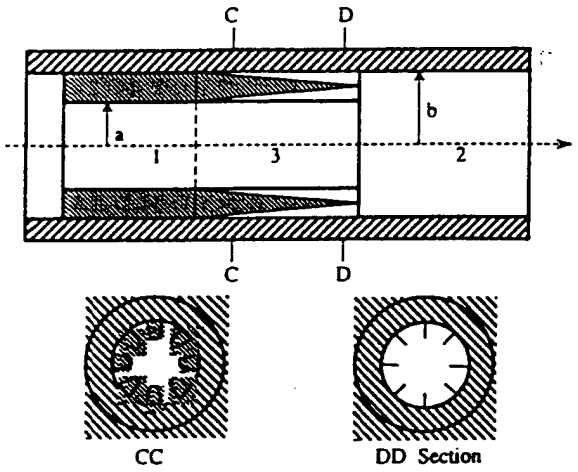


Figure 5: Mode converter for $TE_{0n}$ to $TE_{0m}$ (1. $TE_{0n}$ section, 2. $TE_{0m}$ section, and 3. Converter). $\frac{\mu_{0n}}{a} = \frac{\mu_{0m}}{b} = k_{c0}$, where $J_0'(\mu_{0n}) = J_0'(\mu_{0m}) = 0$.

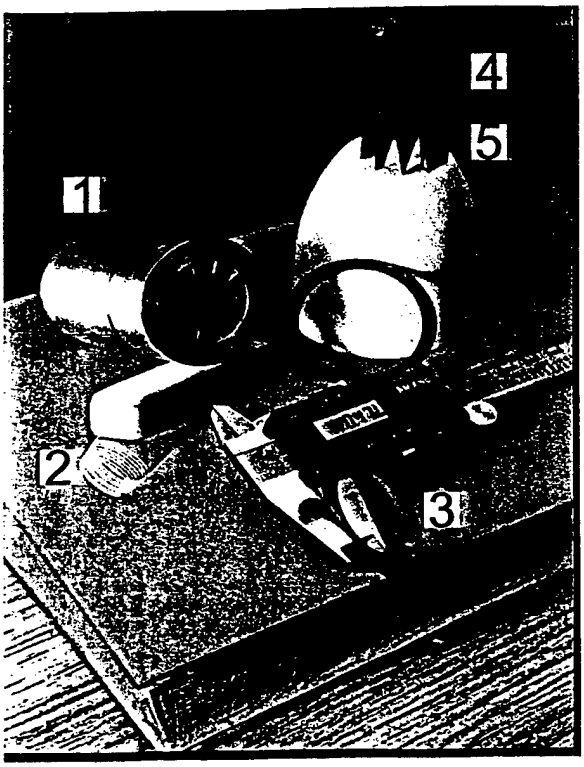


Figure 6: PHIGTRON components: 1. mode converter, 2. filament, 3. lossy ceramic spacer ring, 4. and 5. matching load (SiC-$Al_2O_3$).

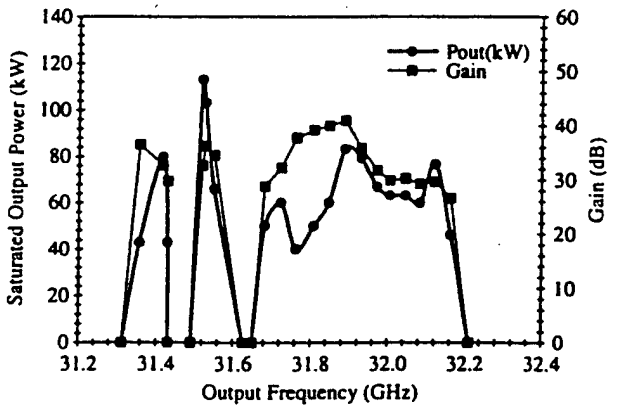


Figure 7: Results from a study of a PHIGTRON amplifier with $TE_{42}$ mode output: dependence of measured saturated power and gain on operating frequency for a fixed beam voltage of 58 kV and a current of 9.2 A.

efficiency of 32%, and locking bandwidth of $\sim$ 10 MHz around 34.46 GHz). The details of this operation are given in [22]-[24].

As with any frequency-multiplying device, the PHIGTRON is inherently a nonlinear device. As a consequence, its transfer characteristics ($P_{\text{out}}$ *vs.* $P_{\text{in}}$) are quite different from linear amplifiers. This gives rise to new physics as well as the need to give more careful consideration to determine its suitability for specific applications. An example of the physics (as well as the need for design/application trade-offs) is the fact that the PHIGTRON needs a large amplitude of the harmonic in the electron current which should excite the output stage of the device while all other harmonics (including the fundamental) should be small.

The experimental study of the PHIGTRON was accompanied by development of the theory of the inverted gyro-twystron [25]. In particular, in [25] it was shown that the electron prebunching in the input waveguide provides a better harmonic content in the electron current density than the standard ballistic bunching occurring in GKL's that have a short input cavity followed by a long drift region. This fact is important for the efficient operation of a frequency-doubling PHIGTRON.

The aforementioned 1.3% bandwidth observed in the experiments is much wider than the width of a resonance curve for the output cavity mode with one axial variation ($TE_{4,2,1}$ mode). To explain this, it is convenient to start with Fig. 7, reproduced from [22]. This figure shows that as the frequency increases, the output power first exhibits two narrow isolated peaks that are followed by a large (1.3%) continuous bandwidth. Here it should be noted that gyrotron cavities are usually formed by slightly irregular open waveguides excited at frequencies close to cutoff. In such cavities, as the number of axial variations, $l$, increases, the diffraction quality factor, $Q_D$, decreases as $1/l^2$ [26, 27]. Correspondingly, the width of the resonance curves becomes wider. Therefore, it can be assumed that in the case shown in Fig. 7, first, two modes with $l = 1$ and $l = 2$ were excited, which have a relatively

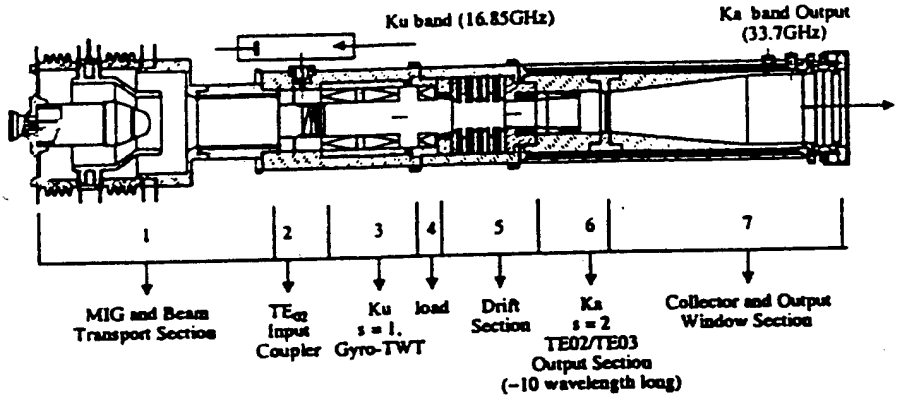


Figure 8: Schematic of the PHIGTRON experiment with harmonic multiplying scheme 1-2.

narrow resonance width, $\omega/Q$. Then, a set of low-$Q$ modes with $l \geq 3$ and overlapping resonance curves was excited in a continuous fashion. The theory describing a simultaneous excitation of modes with $l = 3$, 4, and 5 was developed [28] and its results were found to be in reasonable agreement with the experiment [22](see also [29]).

The next step in the experiments was the study of the Ka-band PHIGTRON at much higher power levels. The experiment is shown schematically in Fig. 8. The $TE_{02}$ input gyro-TWT section operates at the fundamental cyclotron frequency, while the second harmonic output cavity is complex, providing for a $TE_{02}$ to $TE_{03}$ transition. For this device, beam voltage was 50 $kV_{\perp}$ beam current was 42 A, beam velocity ratio ($\alpha$) was 1.5, the axial magnetic field was tapered from 5.7 to 6.8 kG, input frequency was 16.85 GHz, and output frequency was 33.7 GHz. The Ka-band PHIGTRON was tested in both a "high-power" mode and a distinct (beam current of only 25 A) "wideband" mode. The output parameters of each of these modes are compared with those of state-of-the-art Ka-band GKL's in Table 1. It is clear that, compared with the second-harmonic GKL described in [30], significant improvement in all the important performance parameters (power, efficiency, gain, bandwidth) has been achieved in the PHIGTRON. As may be seen from this table, the performance achieved in the frequency-doubling PHIGTRON even compares favorably with the results of leading GKL experiments operating at the fundamental cyclotron resonance [31, 32].

Plans for future experiments include the development of a three-stage, frequency-quadrupling PHIGTRON with a novel extended-interaction output cavity. Experiments will also begin with a two-stage, frequency-doubling gyro-TWT as guided by the theory developed in [33].

# 3 Relativistic Overmoded Backward-Wave Oscillators

Operation of backward wave oscillators (BWOs) is based on the coherent Cherenkov radiation of electromagnetic (EM) waves by electron beams. As is known, Cherenkov radiation occurs

Table 1: PHIGTRON performance parameters compared with Ka-band GKL's.

| Device | $P_{out}$ | Efficiency | Gain | Bandwidth | Output mode |
|---|---|---|---|---|---|
| PHIGTRON (high power) | 720 kW | 34% | 33 dB | 0.3% | $TE_{03}$ |
| PHIGTRON (wide band) | 400 kW | 35% | 30 dB | 0.7% | $TE_{03}$ |
| IAP $2^{nd}$ harmonic GKL [30] | 260 kW | 18% | 17 dB | 0.1% | $TE_{02}$ |
| IAP fundamental GKL [31] | 750 kW | 24% | 20 dB | 0.6% | $TE_{02}$ |
| NRL fundamental GKL [32] | 225 kW | 32% | 30.3 dB | 0.82% | $TE_{01}$ |

when electrons move a little faster than an EM wave. To slow down the wave, various slow-wave (quasi-) periodic structures are used whose fields contain space harmonics with phase velocities smaller than the speed of light. The generation of high-power microwaves in such structures is mostly restricted by the microwave breakdown.

An obvious way to mitigate this restrictions, and thus increase the power-handling capabilities of HPM devices, is to increase the cross section of the interaction region. This implies operation in one of the high-order modes of a slow-wave structure. The spectrum of such modes gets denser as the SWS diameter increases. Therefore, the issue of an accurate design and characterization of overmoded SWSs becomes very important.

Below, we describe the results of the studies of HPM sources with overmoded slow-wave structures. We then present the theoretical results of the analysis of the effect of the zeroeth spatial harmonic of the EM wave on BWO operation, the role of cyclotron resonance effects and the correct description of space charge forces.

## 3.1 Experimental Studies

We discuss here two aspects of our experimental studies: the characterization of slow wave structures (SWSs), and overmoded oscillators.

### 3.1.1 Characterization of Overmoded Slow Wave Structures

In practically all experiments with relativistic BWOs generating high-power microwaves the rippled wall SWSs are used. One of the new numerical tools which can be used for analyzing the fields in a rippled wall SWS is the code MAGY [34]. Although this code, in general, is developed for a self-consistent description of the interaction between electrons and slow/fast electromagnetic waves, it allows one, in particular, to study the fields of any SWS since it is based on the use of generalized telegrapher's equations which account for coupling between the waves caused by an arbitrary profiling of the SWS' wall. Figure 9, taken from Ref. [34],

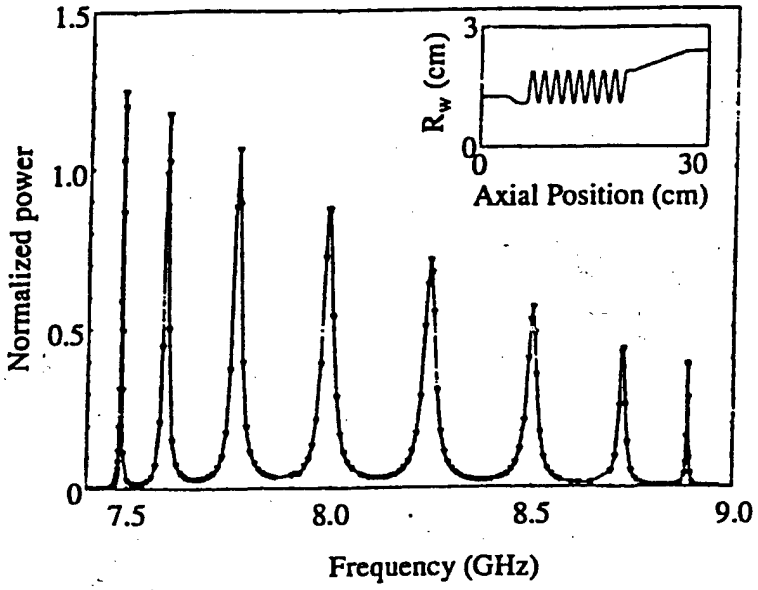


Figure 9: The resonance curve of the cold cavity. The geometry is shown in the inset.

shows, as an example, the resonance curve of an eight-period long SWS which was calculated by using the MAGY. (For details, see Ref. [34].) The first steps in characterizing open and closed SWSs are described in a paper by W. Main et al. [35]. In this work the dispersion diagram of an X-band SWS was calculated numerically by using the 2-D code Superfish and measured experimentally by using a network analyzer. As shown in Fig. 10a, taken from Ref. [35], the results are in excellent agreement. Figure 10b shows the electric field patterns for two modes with different axial structures. These field distributions were also measured experimentally by using a small movable aluminum bead and experimental data agreed very well with numerical results obtained by using the Superfish. The Q-factors of both the closed and open cavities were measured by using an HP8510C vector network analyzer. These measurements allow us to determine not only the Q-factors of various axial modes of an open slow-wave cavity but also the reflection coefficients of these modes from the open end.

The continuation of the studies of open slow-wave cavities coupled to a radiating antenna was described in paper by S. Kobayshi et al [36]. In the process of this work the frequencies, field patterns, and Q-factors of symmetric TM modes with different axial indices were calculated by using two codes, MAGIC and MAGY, and measured experimentally. Also important was the study of the matching section between the open slow-wave cavity and an output waveguide on the reflection coefficient and Q-factors of open cavity modes. The matching section studied was a three-period long corrugated waveguide, shown in Fig. 11, in which the large radius was kept constant and equal to the large radius of the cavity while the depth of corrugations was varied in three different ways. Without going into details described in Ref. [36], let us mention only that it was shown that such an interface section can significantly reduce Q-factors of all modes except for the modes close to the ends of the passband. Such a reduction may lead to a substantial increase in the starting and optimal currents of relativistic BWOs, thus allowing for high-efficiency, high-power generation. Recently, the analysis of overmoded SWSs with various wall radius profiles was also carried

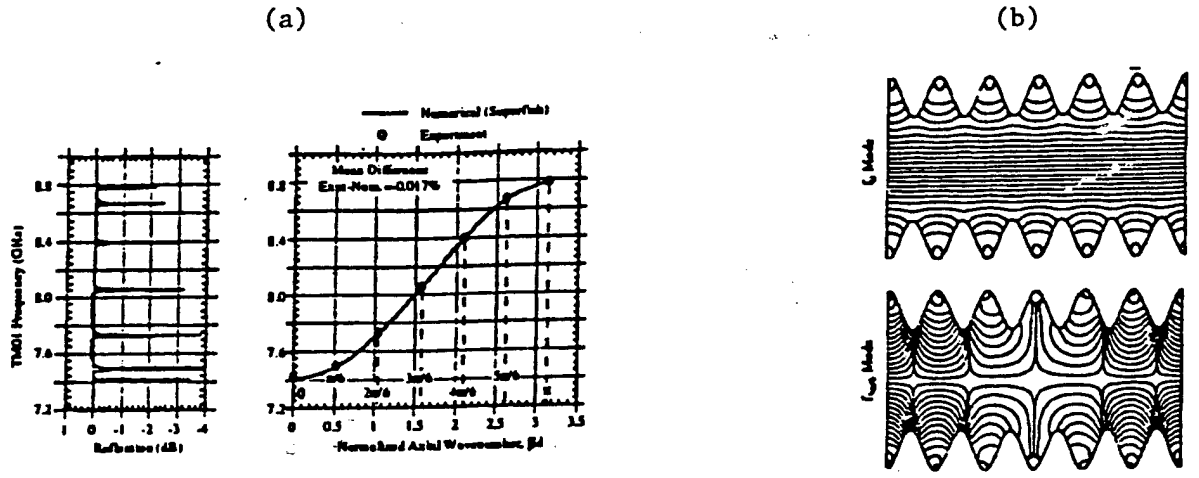


Figure 10: (a) The dispersion diagram of an X-band slow wave structure having a passband of 7.4 to 8.7 GHz for the $TM_{01}$ mode as calculated by Superfish, presented as a smooth line. Only half of the first Brillouin zone is shown. Also shown is the measured reflection data and all seven $TM_{01}$ resonance peak of the closed six period slow wave cavity (open circles). (b) The electric field line pattern associated with two of the seven axial modes ($0.5\pi/6$).

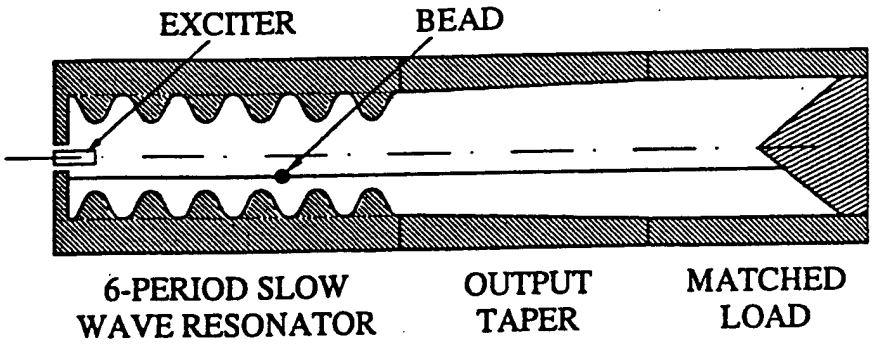


Figure 11: A schematic diagram of the open periodic cavity with a tapered matching section and the experimental setup used for the frequency and field profile measurements (see text for details).

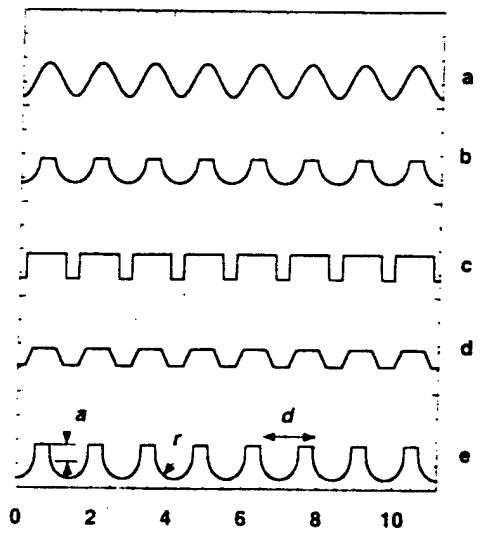


Figure 12: Examples of wall radius profiles as functions of the axial coordinate.

out [37]. The examples of profiles studied are shown in Fig. 12. Figure 13 shows calculated dispersion diagrams for the six lowest modes of an oversized SWS, which illustrates the spectrum density in such a system.

### 3.1.2 Overmoded Oscillators

There were two sets of experiments carried out at UMD. In the first [38], an oversized SWS with a mean diameter to wavelength ratio on the order of 3 was designed for operation in the frequency range of 5-6 GHz at the surface waves. (Recall that surface waves are the waves in which all space harmonics are slow; i.e. the fields of all harmonics are localized near the SWS walls.) For these experiments a novel carbon-epoxy cathode coating technology was developed which provided an azimuthally uniform electron emission over a wide range of electric fields at the cathode (from 60 kV/cm to 600 kV/cm). Corresponding densities of the cathode current were in the range of 350-1600 A/cm$^2$. As a result, a thin (thickness of about 2 mm), large diameter (up to 95% of the SWS diameter), non-rotating electron beam with good symmetry and azimuthal uniformity, which was guided by a strong (up to 14 kG) magnetic field, successfully propagated over distances up to 1 m.

The microwave generation experiments were mostly carried out at about 10 kG guiding magnetic field. The length of the SWS was varied from 10 to 35 periods. (From the 8-period SWS no radiation was observed.) A maximum power of about 320 MW was generated in a 10-period SWS driven by an 827 kV, 9.0 kA electron beam with a corresponding efficiency of about 4%. Pulse shortening was not observed in any of the shots.

These experiments clearly demonstrated the possibility of producing a highly coherent ($\Delta f/f < 0.5\%$) single-mode radiation in oversized BWOs. At frequencies above those corresponding to fundamental $TM_{01}$ mode interaction no significant power was observed.

In the second set of experiments [37], some improvements in the microwave structure were made which allowed operation at 8.3 GHz frequency, 0.5 GW power with 15% efficiency. This

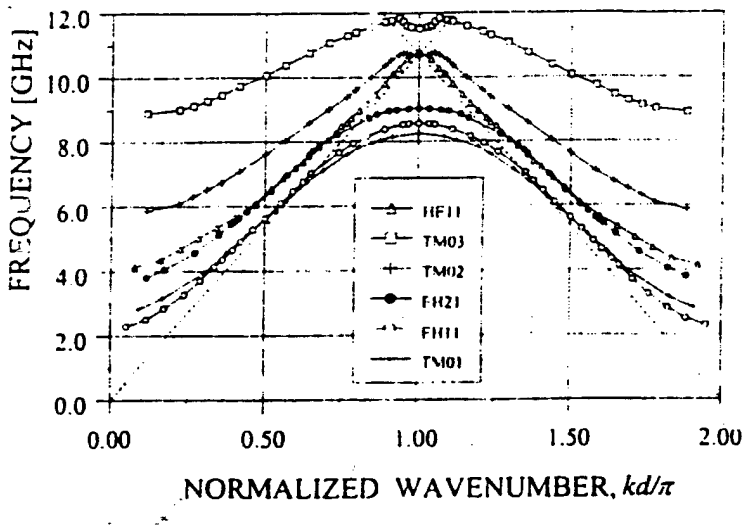


Figure 13: Calculated dispersion diagrams for the six lowest modes of a periodic oversized structure with optimal profile (maximual radius 4.9 cm; period 1.4 cm; height of rectangles 0.2 cm; radius of semicircle 0.5 cm). 511-kV beam line - dotted; light line - dashed.

power was measured calorimetrically. The total radiated microwave energy per pulse was 10.2 J. However, the increment in the radiated power from about 150 MW to 0.5 GW was accompanied by a pulse shortening effect.

## 3.2 Theoretical studies

Here we discuss two aspects of our theoretical studies: zeroeth spatial harmonics and cyclotron resonance effects.

### 3.2.1 Zeroeth space harmonics

As is known. in BWOs the condition for Cherenkov synchronism relates the motion of beam electrons to the phase velocity of the first negative ($k_{z1} = k_{z0} - 2\pi/d$, where $d$ is the SWS period) spatial harmonic of the wave. However, in analyzing the interaction between relativistic electrons and the EM wave in a BWO, there are at least two reasons for taking the zeroeth spatial harmonic into account. The first reason is the decrease of the ratio of harmonic amplitudes, $A_{-1}/A_0$, with the voltage increase, and the second is the parametric coupling between these harmonics in the case of propagation of an intense electron beam near a rippled wall of an SWS.

To explain the decrease in the ratio of harmonic amplitudes, recall that in general when the voltage, $V_b$, increases, the electron velocity approaches the speed of light and therefore it is not necessary to significantly slow down the synchronous wave. This leads to the use of shallow SWSs in which the amplitude of the minus first harmonic becomes smaller as the voltage increases. At the same time, if we assume that the BWO efficiency does not depend drastically on the voltage (which was confirmed by numerous calculations), then

the radiated power increases proportionally to the beam power. For shallow SWSs with the dominant zeroeth spatial harmonic, $A_0$ grows with increasing $V_b$. So, as the voltage increases, the ratio $A_{-1}/A_0$ becomes smaller because $A_{-1}$ decreases simultaneously as $A_0$ increases. It seems intuitively clear that when electrons pass through a finite length SWS the interaction with not only the synchronous, small-amplitude space harmonic but also with the non-synchronous, large-amplitude harmonic can be important. This was confirmed by several studies [39, 40, 41, 42] in which it was shown, in particular, that not only the amplitude's ratio $A_{-1}/A_0$, but also the phase relation between harmonics are important for interaction processes. The latter effect was analyzed in Refs. [41] and [42].

The role of the zeroeth spatial harmonic can be even more important in a relativistic BWO driven by a high-current, thin annular electron beam propagating near the SWS walls. In such a system the voltage depression which depends on the clearance between the beam and the wall is periodically modulated with the period equal to the period of the SWS. This leads to the parametric coupling between the zero and minus first space harmonics which, as shown in Ref. [43], modifies the starting conditions, changes the efficiency and leads to quasi-periodic modulation in electron axial velocities.

Another case when the interaction with the forward wave should be undoubtedly taken into account is the operation near $\pi$-point. This is the case when the beam line $\omega = k_z v_z$ intersects the dispersion curve of an SWS near its maximum at $k_z = \pi/d$. Therefore, the axial wavenumber of the minus first space harmonic of the backward wave, $k_{-1}^{(b)} = -k_0 + 2\pi/d$, and that of the zeroeth spatial harmonic of the forward wave, $k_0^{(f)} = k_0$, are close since $k_0 \approx \pi/d$, so both of these harmonics interact with electrons synchronously. An interesting feature of this operation is the fact at $\pi$-point the group velocity determined as $v_{gr} = d\omega/dk_z$ is equal to zero. Therefore, the process of the microwave energy transfer through an SWS is determined by the second derivative since the dispersion characteristic of the SWS near the $\pi$-point can be expanded in a Taylor series as

$$\omega \simeq \omega_0(\pi/d) + \frac{1}{2}\frac{d^2\omega}{dk_z^2}|_{k_z=\pi/d}(k_z - \pi/d)^2.$$

Correspondingly, the wave envelope equation has the form of a non-stationary Schrödingren equation in which the role of the term describing the effect of the potential well on the motion of a charged particle is played now by the source term proportional to the power of interaction between electrons and the SWS field.

More than a decade ago this kind of operation was analyzed in Refs. [44, 45, 46] (see also references therein) mostly in application to the TWT operating near the borders of the passband where an amplifier is especially prone to parasitic self-excitation. Later, a similar theory was developed in Ref. [47] with an emphasis on the operation of relativistic BWOs. This theory was used for calculating the starting currents, operating frequencies and efficiencies for two BWOs. In some cases a reasonable agreement between theoretical and experimental results was demonstrated, although in several cases there was a certain discrepancy which can be attributed to the effects ignored in calculations (high-order modes, electron velocity spread, etc.).

### 3.2.2 Cyclotron resonance effects

At certain magnetic fields we can simultaneously satisfy the Cherenkov synchronism condition for the first negative spatial harmonic, $\omega \approx k_{-1}^{(b)} v_z$, and fulfill the cyclotron synchronism condition for the zeroeth spatial harmonic, $\omega - k_0 v_z \simeq s\Omega$. Here $s$ is the cyclotron harmonic number and $k_0$ is positive for the forward wave and negative for the backward one. When the cyclotron harmonic number is positive ($s > 0$) the normal Doppler effect takes place, and therefore, the cyclotron resonance can lead only to absorption of electromagnetic waves by a beam of electrons moving initially along linear trajectories. On the contrary, in the case of the anomalous Doppler effect which corresponds to negative cyclotron harmonics an initially linear electron beam can coherently radiate waves; see Ref. [48] and references therein. The cyclotron absorption causing a dip in the dependence of the radiated power on the magnetic field was observed in many experiments with relativistic BWOs (see e.g. Refs. [49] and [50]). Later, a semi-analytical theory [51] was developed for describing this effect and the method of cyclotron selection based on the cyclotron absorption of unwanted modes was successfully used in a very impressive experiment [52].

A more detailed theoretical study of relativistic BWOs operating near the cyclotron resonance was recently presented in Ref. [53]. In this paper a self-consistent, non-stationary theory was developed which allows one to describe the increase in starting currents due to cyclotron interaction, the appearance of automodulation and stochastic oscillations and the suppression of oscillations. It was also shown that at magnetic fields equal to or larger than that corresponding to the exact resonance the cyclotron effects may enhance the efficiency. This effect occurs in a relatively narrow (less than 5%) region of magnetic field values. The existence of similar effects in relativistic BWOs operating near cutoff was shown later in Ref. [54]. In Fig. 14, taken from Ref. [53], the cyclotron dip calculated numerically and measured experimentally is shown. References [53] and [54] considered the cyclotron resonance with the zeroeth spatial harmonic of the backward wave. As was mentioned in the beginning of this subsection, the cyclotron resonance with the zeroeth harmonic of the forward wave is also possible, as shown in Fig. 15. In the case of operation near the $\pi$-point such a resonance occurs at low magnetic fields. Such low magnetic fields imply lower magnet weights, which is attractive for the development of lightweight HPM sources. The linear theory of describing the cyclotron effects in relativistic BWOs operating at low magnetic fields was presented in Ref. [55] where the effect of magnetic fields on the starting current was analyzed.

### 3.2.3 Space Charge Effects

Correct description of space charge effects is a very important issue for designing relativistic BWOs driven by intense electron beams. This issue was addressed in Ref. [56]. By varying the number of space charge harmonics taken into account and comparing the results, the authors concluded that the ac space-charge effects can be adequately described if the first five harmonics are accounted for [56]. As they pointed out, the field of these harmonics may have a significant effect on the Poynting flux; it was shown that the Poynting flux at the end of the SWS differs significantly from that calculated at the output after dumping the electron beam. Correspondingly, the efficiency of the BWO with a two-period SWS can be about 58% at the end of the SWS and only 35% at the device output. The optimization

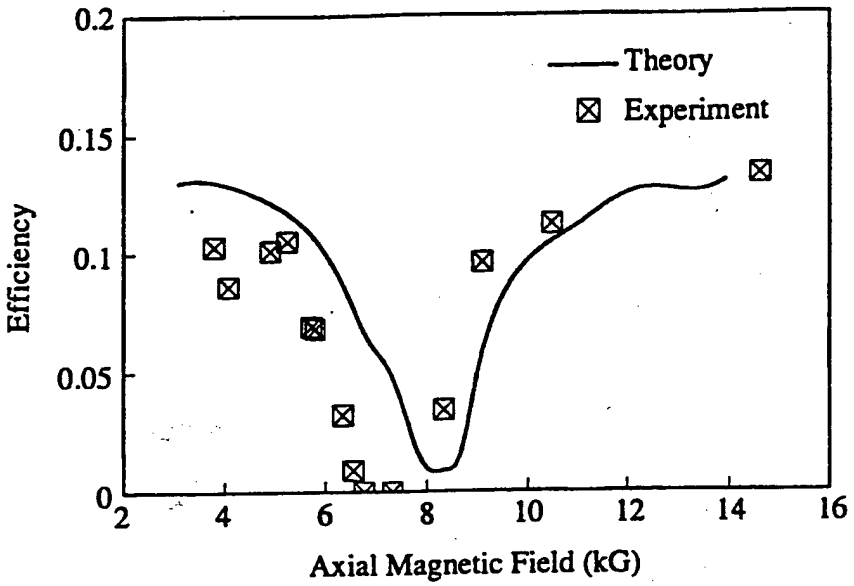


Figure 14: Cyclotron resonance.

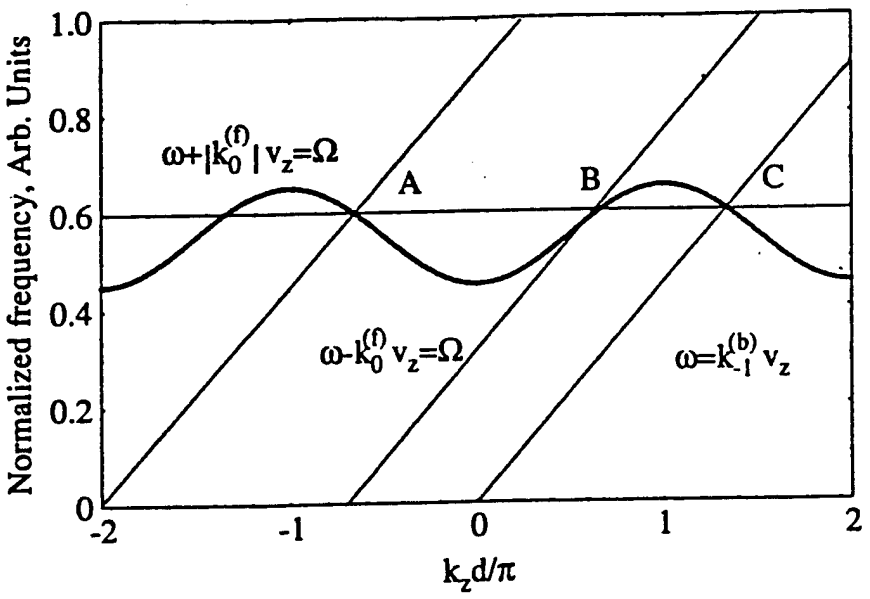


Figure 15: Dispersion diagram showing possible cyclotron resonances with the zero spatial harmonic of the backward (A) and forward (B) wave. The Cherenkov synchronism (C) occurs at $k_{-1}^{(b)} = -|k_0^{(f)}| + 2\pi/d$.

Table 2: High-efficiency BWO parameters.

| | | |
|---|---|---|
| $R_{\max}$ | 5.380 | cm |
| $R_{\min}$ | 4.500 | cm |
| $D_1$ | 4.500 | cm |
| $D_2$ | 5.175 | cm |
| Periods | 3.5 | with period $D_1$ |
| | 9.5 | with period $D_2$ |
| $B_z$ | 10.0 | kG |
| $R_{\text{beam}}$ | 4.200 | cm |

of the design of an S-band BWO driven by a 500 kV, 5 kA beam has led to the choice of parameters of the interaction region summarized in Table 2, taken from Ref. [56].

# 4 Plasma-Filled HPM Sources

The efforts to generate high-power microwave radiation by using intense relativistic electrons beams (REBs) renewed interest in plasma-filled microwave sources [57]-[59]. There were several reasons for this renewed interest:

1. **Facilitating extraction of microwave power from plasmas using REB's**: Indeed, since relativistic electrons move with velocities close to the speed of light, the plasma waves that should be in Čerenkov synchronism with electrons should also have such phase velocities. Therefore, these waves can easily be coupled to free space where the waves propagate with the speed of light.

2. **Compensation of space charge**: Pressed for even more power, HPM sources are usually driven by high voltage, high current electron beams. When an electron beam propagates in a metallic tube, however, it is subject to a limiting current determined by space charge effects. When the charge of the beam electrons is neutralized by plasma ions, therefore, this limiting current increases. In the case of relativistic electrons the electric self-field is partially compensated by the magnetic self-field, and this compensation increases with the voltage. Therefore, as the beam voltage increases, the plasma neutralization factor, and correspondingly the plasma density required for beam transport decreases.

3. **Reduction or elimination of the required guiding magnetic field**: The magnetic field required for guiding the electron beam can also be reduced or completely eliminated as follows from the arguments above. Correspondingly, the size, weight, complexity, and reliability of HPM sources can be greatly improved.

4. **Higher output microwave power**: Since the current handling capability of plasma-filled devices is higher than that of their evacuated counterparts under the same conditions, the output microwave power is expected to increase as well.

5. **Electronic frequency tunability**: It was expected that electronic frequency tunability could be achieved through exersizing control over the plasma density.

The progress in the development of plasma-filled HPM sources prior to the beginning of the MURI94 program was reviewed in a number of papers [57, 58].

## 4.1 Theoretical Studies

In the framework of MURI94, active theoretical and experimental studies of plasma-filled HPM sources were carried out at the Unviersity of Maryland. Theoretical efforts were focused on such fundamental issues as

- the gain and bandwidth enhancement in plasma-filled TWTs
- space charge effects
- ponderomotive effects and nonstationary phenomena in plasma-filled mcirowave sources
- modeling of plasma-loaded BWOs in the overdense regime ($\omega_{\text{plasma}} > \omega_{\text{radiation}}$).

It should be emphasized that the studies of these fundamental issues were always related to experiments with plasma-filled microwave oscillators and amplifiers.

### 4.1.1 Beneficial effects of space charge

Pressed for more power, HPM sources are often driven by beam currents so large that space charge effects are a major limiting factor. In order to better understand the detailed physics, the University of Maryland studied space charge effects in plasma-filled TWT's [60]. In this work a simple, one-dimensional model of a TWT was considered and the plasma was characterized by a simple dielectric permittivity tensor which had only two non-zero components (one axial and one transverse). As a result, it became possible to account for plasma effects in the same manner as theoreticians account for space charge effects in vacuum TWT's by introducing modified "depression coefficients." In plasma-filled TWTs, these coefficients describe dielectric responses of plasma-filled waveguides at the wave frequency and its harmonics. It was shown that in the presence of plasma these depression coefficients can be either positive or negative (in contrast to the vacuum case when they are always positive). Therefore, these effects can lead to the improvement of electron bunching and efficiency enhancement in plasma-filled TWT's, while in vacuum TWT's space charge effects always deteriorate the bunching.

The presence of plasma also modifies the radial structure of the synchronous wave when parameters of an SWS and plasma are chosen so that the hybrid modes can be formed [61]). As a result, for a solid pencil-like electron beam propagating near the axis, the coupling impedance to the hybrid mode can be increased. This is illustrated by Fig. 16, which shows the results of the study of a plasma-filled, coupled-cavity TWT. Figure 16 shows that the efficiency can be increased from less than 45% to more than 60% due to plasma filling. Also, the optimal interaction length shortens due to the increase in the coupling impedance, thus making the TWT more compact.

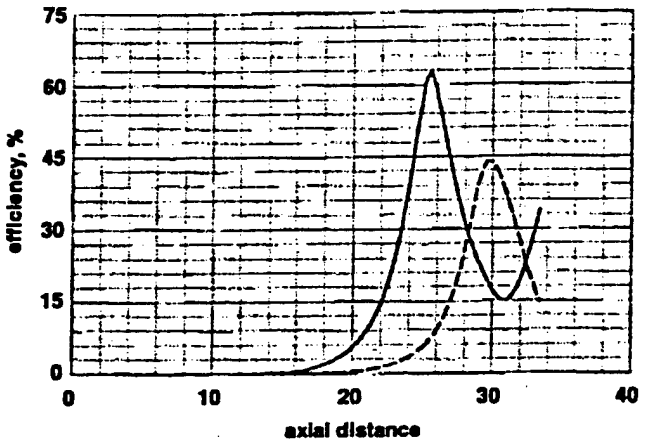


Figure 16: The efficiency of a coupled-cavity TWT with (solid) and without (dashed) accounting for the ac space charge force of electrons in the presence of plasma [60].

### 4.1.2 Modification of the radial structure

Modification of the radial structure of the wave and the small-signal gain increase were described in more detail in [62], devoted to the analysis of a plasma-loaded, helix TWT. As shown in Fig. 17, in the presence of a dense plasma (when the plasma frequency is larger than the operating frequency, and an SWS wave and a plasma electrostatic wave, *i.e.*, Trivelpiece-Gould wave, form a hybrid mode) the linear gain (growth rate) can be substantially increased compared to a vacuum helix TWT. Note that in the case of $n_p = 1 \times 10^{12}$ cm$^{-3}$ shown in Fig. 17, the ratio of the Poynting flux in the plasma region to the total Poynting flux does not exceed 0.2. Thus, the electromagnetic energy can easily be extracted from the interaction region. In general, as shown in [62], this takes place only in the case of the excitation of the hybrid mode. Needless to say, such a dramatic increase in the wave growth rate as that shown in Fig. 17 may lead to significant shortening of the interaction region, thus making a tube much more compact.

### 4.1.3 Ponderomotive effects

Ponderomotive effects in plasma-filled microwave tubes were analyzed in [63, 64], where it was shown that these effects may lead to various nonstationary phenomena. Recall that the ponderomotive force $f_p$ is the force that acts on electrons moving in a slightly inhomogeneous electromagnetic field. In [63], the axial dependence of the intensity of the axial component of the electric field $|E_z|^2$ acting on electrons was taken into account, *i.e.*, it considered the case when the additional force, $f_p \sim d|E_z|^2/dz$, acts on electrons. The relativistic, plasma-filled BWO operating near cutoff was studied using both the fluid model of plasmas and particle-in-cell (PIC) simulations. (Note that a PIC representation of plasma is necessary, particularly in the case of very large density perturbations where the fluid approximation is not valid.)

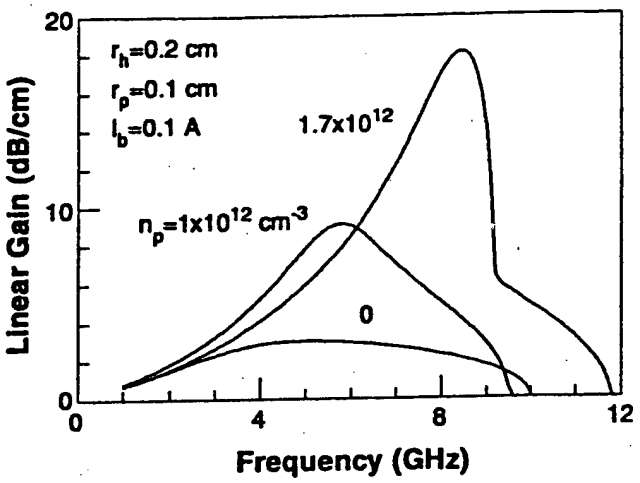


Figure 17: Calculated growth rate in a TWT with and without plasma loading. Note the greatly enhanced gain due to the plasma [62].

The analysis performed in [63] showed that, at low plasma densities, the ponderomotive effects may cause cavitation of plasma electrons in regions of low amplitudes of the wave electric field. This happens when the ponderomotive force of the radiation dominates the space charge force of plasma electrons. Time evolution of the outgoing radiation in such a case exhibits, first, the onset of constant amplitude radiation, and then the beating effect associated with the excitation of a plasma wave. In the presence of plasma waves the system may exhibit some mode hopping effects, *e.g.*, from a mode with two axial variations to a mode with three variations.

In [64], a plasma-filled TWT was studied. It considered the case of a plasma column of small radius at finite magnetic fields when the ponderomotive force caused by the radial inhomogeneity of $|E_z|^2$, *i.e.*, $f_p \sim d|E_z|^2/dr$, can be important and may lead to excitation of transverse magnetosonic oscillations in plasma. The formalism developed in [64] allows one to describe the effect of magnetosonic oscillations by one additional term in the first-order wave equation for the traveling wave. This equation can be written as

$$\frac{da}{d\tau} + \frac{da}{d\xi} - i\gamma|a|^2 a = -\frac{1}{2\pi}\int_0^{2\pi} e^{i\varphi} d\varphi_0. \qquad (1)$$

Here $a$ is the complex amplitude of the wave envelope, $\tau$ and $\xi$ are the normalized time and axial coordinates, respectively, the term in the right-hand side is a source term that is proportional to the high frequency component of the electron current density in a beam of electrons homogeneously distributed over the phases $\varphi_0$ at the entrance. The last term on the left-hand side is just a new term which appears due to magnetosonic oscillations. The coefficient $\gamma$ in it is proportional to $(n_0/v_{ph})(dv_{\rm ph}/dn_0)$, *i.e.*, it characterizes the sensitivity of the wave phase velocity to perturbations in the plasma density. This term corresponds to a reactive cubic nonlinearity that changes the phase of the wave.

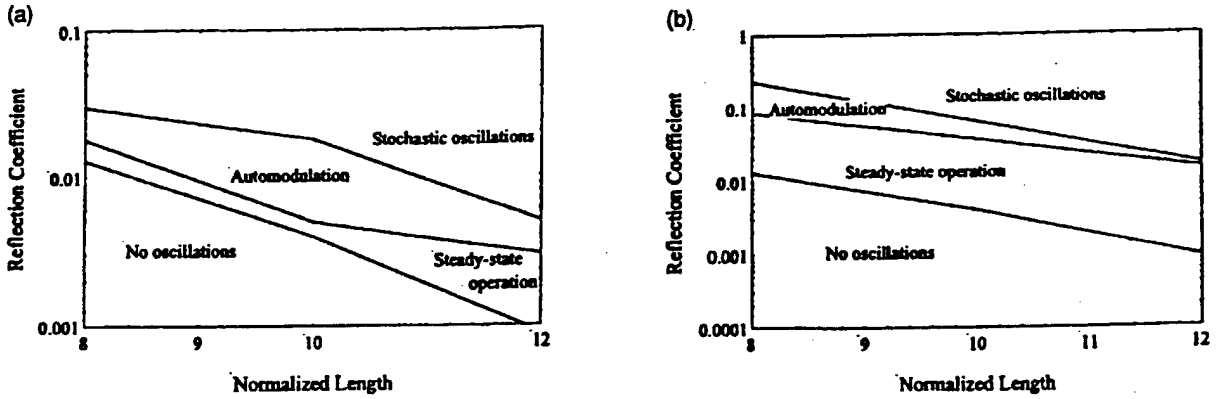


Figure 18: Regions of steady state operation, automodulation, and stochastic oscillations in a TWT with feedback (a) in the absence of plasma, and (b) in the presence of magnetosonic oscillations.

When in such a TWT a certain feedback exists (which, for instance, can be caused by some wave reflections from the output), the tube may exhibit not only steady state operation, but also automodulation and stochastic oscillations. The presence of magnetosonic waves reduces the threshold values of the reflection coefficient for the appearance of automodulation and stochasticity, as illustrated by Fig. 18. This study shows that, to provide stable operation of plasma-filled TWT's, the issue of the sensitivity of the wave phase velocity to perturbations in the plasma density caused by magnetosonic oscillations should be taken into account. Since the phase velocity is unavoidably sensitive to the plasma density perturbations, the output should be well matched for minimizing wave reflections.

### 4.1.4 Modeling of plasma-loaded BWO's in the overdense regime ($\omega_{\text{plasma}} > \omega_{\text{radiation}}$) and the "Dense Spectrum"

The spectrum of the low frequency modes ($\omega_{\text{radiation}} < \omega_{\text{plasma}}$) in a plasma-filled, spatially periodic structure is drastically modified by the periodic boundaries of the SWS in a way that produces a fundamentally different kind of spectral behavior, a "dense-spectrum." The interaction of ballistic electron beam modes with the dense spectrum of plasma modes was shown to be unstable [65], and this is important for plasma microwave electronics, especially for operation in the overdense regime ($\omega_{\text{plasma}} > \omega_{\text{radiation}}$) where hybrid modes may play an important role. The issue is whether an electron beam can selectively excite only few modes out of the entire dense spectrum.

Recent results [66] indicate that some of these modes interact with an electron beam more strongly than others. Figure 19 shows the mode chart of a corrugated wall SWS filled with a high density ($5 \times 10^{12}$ cm$^{-3}$), radially inhomogeneous plasma column driven by a relativistic electron beam. The figure shows the frequency-wavenumber plane for various

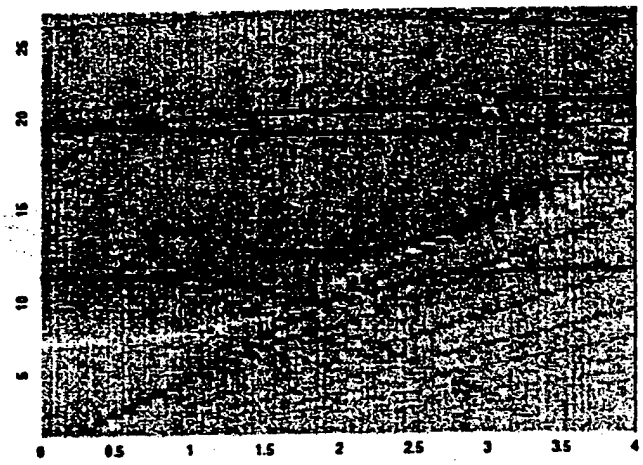


Figure 19: The frequency-wavenumber mode chart for a corrugated wall SWS filled with a high density ($5 \times 10^{12}$ cm$^{-3}$), radially inhomogeneous plasma column driven by a REB. The "interaction strength" for various modes is shown in gray scale. The darker the line, the stronger is the interaction. By properly choosing the beam parameters, a few of these modes can be selectively excited.

modes, and the "interaction strength" is indicated in gray scale. By properly choosing the beam parameters, a few of these modes can be selectively excited.

This issue is further demonstrated in Fig. 20(a,b). There, the frequencies of all 8 axial modes associated with both the $TM_{01}$ and hybrid modes in a finite length, 8-period, plasma-loaded, corrugated cavity are calculated as a function of the backgroung plasma density in the overdense regime. The plasma had a radially inhomogeneous profile plasma channel (overdense regime). The measured spectrum (Fig. 20(a)) compares favorably with the calculated one (Fig. 20(b)), and also with the hot tests [66].

## 4.2 Experimental Studies

Experimental activities were mostly focused on characterization of plasma-filled slow-wave structures (SWSs) and on 'hot' experiments with plasma-loaded relativisitc backward wave oscillators (BWOs).

### 4.2.1 Electromagnetic Properties of SWS's Loaded with Radially Inhomogeneous Plasma

Spatially periodic electrodynamic structures are an essential part of HPM sources of coherent Čerenkov radiation. The presence of plasma changes the dispersion characteristics of SWS's and also leads to the appearance of plasma modes. Plasma influence on the electromagnetic dispersion properties of waveguides can be described by the parameter $\omega_p/\omega$, where $\omega_p$ and $\omega$ are the electron plasma frequency and the frequency of the vacuum waveguide mode.

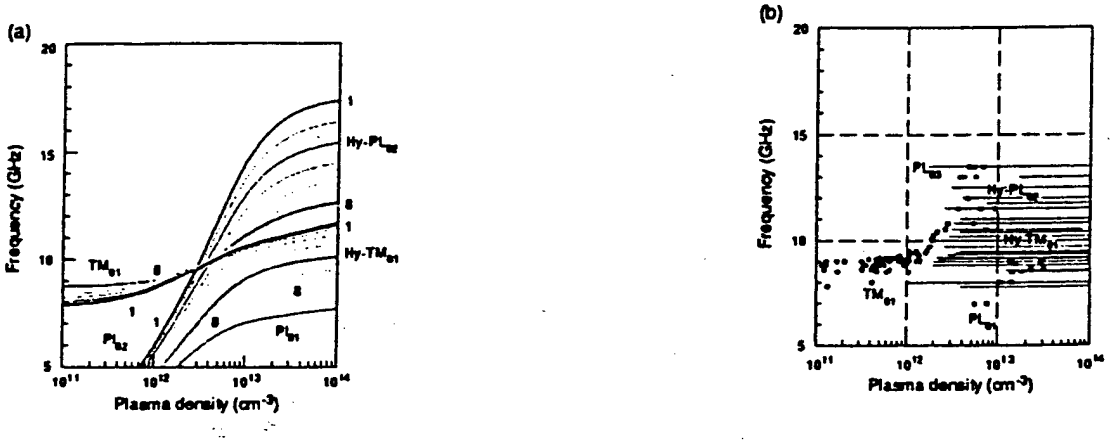


Figure 20: Frequency as a function of peak plasma density for a finite length, slow wave, corrugated-wall structure loaded with a high density, radially inhomogeneous plasma column: (a) the calculated axial modes (labeled 1 through 8) of both the plasma branches and the electromagnetic branches overlap in frequency, and (b) the measured curve, using the techniques described earlier. Note that the tunability range can be 8-17GHz.

respectively. The plasma upshifts the electromagnetic branches of vacuum TM modes in waveguides, as approximately given by $\omega_0^2 = \omega_p^2 + \omega^2$, where $\omega_0$ is the upshifted frequency of the plasma-filled resonator. If a strong guiding magnetic field ($B_z$) is applied ($\Omega = eB_z/\gamma m > \omega_0,\ \omega_p$), only TM modes will be upshifted. TE modes will remain unaffected because these modes have a zero longitudinal component of electric field ($E_z$), while in plasma oscillations the axial component of electric field is the most important. These frequency upshifts in plasma-loaded structures have been observed in experiments where microwave generators were driven by REB's. This property of plasma-loaded microwave sources is of importance since it allows one to realize an electronic frequency tunability by exercising control over the plasma density. It is therefore important to characterize the electromagnetic properties (dispersion curves) of plasma-loaded SWS's, first, without beams ("cold"). This information can then be used to develop predictive capabilities and as an input for some of the codes used to simulate plasma-loaded HPM devices.

### 4.2.2 Corrugated X-band SWS's Loaded with Low Density Plasma ($< 10^{12}$ cm$^{-3}$)

In this Section the measurement of the complete dispersion curve of three plasma-loaded, spatially periodic structures performed at UMD will be described. First, a description of the approach will be given, using the specific example of the sinusoidally corrugated cavity loaded with plasma whose density varies up to $2 \times 10^{12}$ [36, 67, 68].

From the reflected power oscillogram shown in Fig. 21 (the excitation frequency is 8.95 GHz) one can see that resonant conditions for $TM_{01n}$ modes are satisfied for $n = 8$ at $t = 736\ \mu sec, n = 7$ at $t = 573\ \mu sec$, and so on up to $n = 1$ at $t = 323\ \mu sec$. A series of

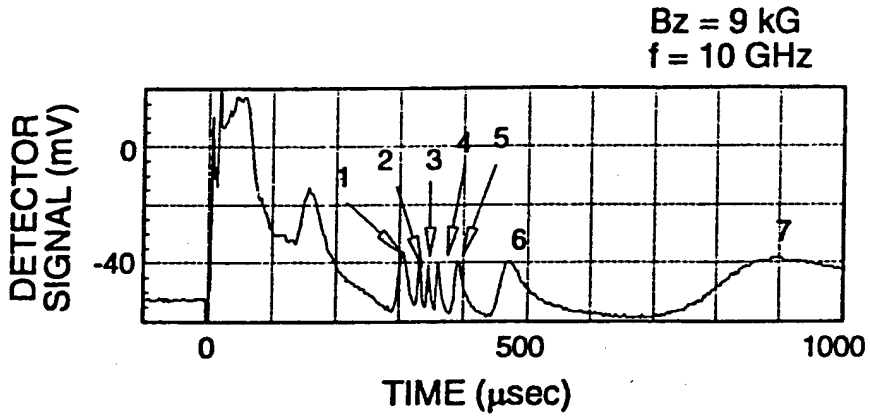


Figure 21: A reflected power oscillogram as a function of time used to measure the dispersion characteristics of a finite length, plasma-loaded SWS. The resonant conditions for $TM_{01n}$ axial modes are satisfied for $n = 8$ at $t = 736$ $\mu$s, $n = 7$ at $t = 573$ $\mu$s, and so on up to $n = 1$ at $t = 323$ $\mu$s. A series of pulsed measurements performed with different excitation frequencies were used to construct the dispersion curve.

pulsed measurements performed with different excitation frequencies was used to plot the plasma density as a function of the applied frequency for the discrete $TM_{01n}$ resonance of the corrugated cavity. The final step is to assign wave numbers to the modes in order to finish constructing the dispersion diagram. The order in which the individual modes appear in the oscillogram as the applied frequency is changed clearly indicates the appropriate mode number $n = 1$ to 8. The problem of assigning resonant wave numbers $k_z$ to this index was solved by using the same approach (and experimental data) presented earlier for empty cavities [69], where the resonances of evacuated closed and open (*i.e.*, coupled to a radiating antenna) corrugated cavities were measured. Very good agreement between measurements and calculated resonant frequencies implies that for an open corrugated cavity, the wave number $k_{zn}$ is given by $k_{zn} = n\pi/L_0$ as in a smooth, close cavity case ($L_0$ is the total cavity length).

The final result of this procedure, shown in Fig. 22(a,b) is the dispersion diagram of the plasma-filled corrugated cavity, for two values of guiding magnetic field. The points connected with the solid line are experimental. The lowest curve is for $n_p = 0$, the next one up is for $n_p = 10^{11}$ cm$^{-3}$, and so on for 2, 5, and $8 \times 10^{11}$ cm$^{-3}$. The independently calculated [68] dispersion curves for an infinitely long, corrugated waveguide loaded with the same plasma densities are superimposed in the figure. The geometry used for these calculations was close to the experimental parameters ($R_p = 0.75$ cm, $R_0 = 1.499$ cm, $h = 0.406$ cm, $d = 1.67$ cm). One can see that the calculated frequency upshift of the dispersion curve of the $TM_{01}$ mode due to the presence of the plasma is very close to the measured data ($\Delta\omega/\omega < 2\%$), as long as the plasma density is below $5 \times 10^{11}$ cm$^{-3}$. Above this value, the measured upshift is somewhat less than anticipated by theory. Also, the

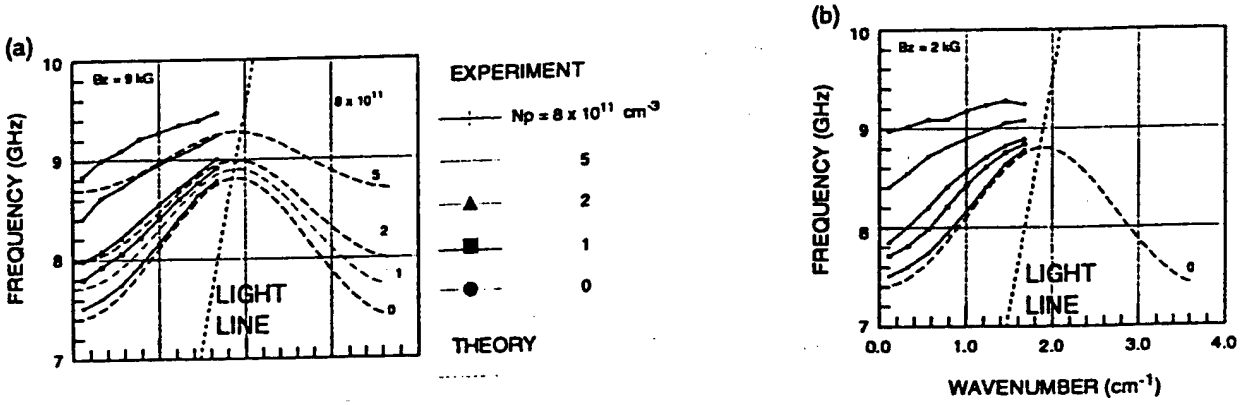


Figure 22: Reconstructed dispersion diagrams of a plasma-filled corrugated cavity. Solid lines represent experimental data, and the dashed line represents theory [35, 68, 69].

plasma causes flattening of the dispersion diagram, especially above a plasma density of $5 \times 10^{11}$ cm$^{-3}$, although the measured flattening is less than predicted by the calculation. The allowed passband (the difference between the upper cutoff and the lower cutoff) for the $TM_{01}$ mode in vacuum is about 1.25 GHz. When the plasma density is $8 \times 10^{11}$ cm$^{-3}$ this difference is reduced to less than 0.6 GHz.

In conclusion, the resonant cavity approach, in combination with multiprobe diagnosis, allows for the characterization of the electromagnetic properties of SWS's loaded with inhomogeneous plasma.

### 4.2.3 Electromagnetic Properties of Realistic Coupled Cavity TWT Structures Loaded with Plasma

Plasma-based microwave devices have the potential to advance the technological and scientific base of microwave tubes for DoD applications [70], and also to have a large impact on commercial and industrial applications through the development of transferable, commercially available technologies.

For that reason, two realistic coupled cavity TWT (CCTWT) structures were loaded with plasma and the dispersion characteristics were measured. Both structures possessed no azimuthal symmetry, as is usually the case, due to "banana shaped" coupling slots between adjacent cavities. The first structure was made by Communications and Power Industries (CPI, formerly Varian [71]) and the second one was made in Russia (VEI, Moscow [72]). Both are SWS's, with azimuthally asymmetric coupling slots between adjacent cavities. The results of the measurements performed at the UMD are shown in Figs. 23 and 24, respectively.

The Russian CCTWT is less sensitive to the plasma density. Both are operating in the overdense regime $\omega_{\text{radiation}} \leq \omega_{\text{plasma}}$, as indicated in the figures. Notice that both structures

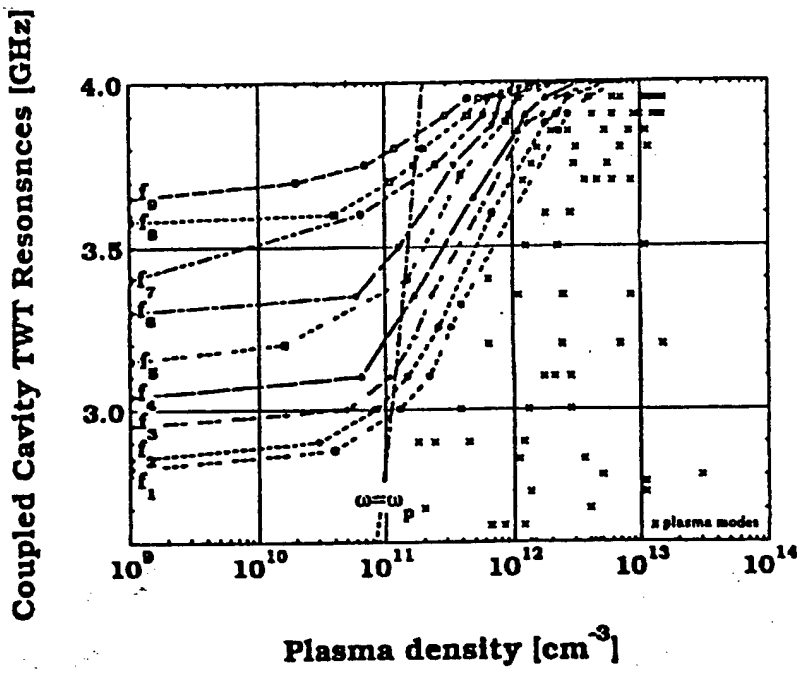


Figure 23: Effects of plasma on the eigenfrequencies of axial modes in a CPI coupled-cavity, ten-period-long SWS [71]. The symbols connected by lines represent the axial modes of the SWS as modified by the plasma; the x's represent additional plasma modes [65].

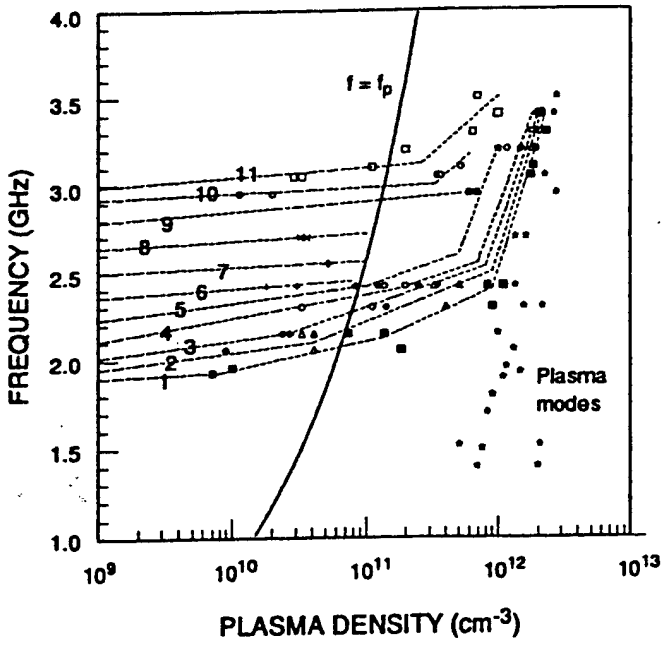


Figure 24: Same as Figure 23, except for a VEI coupled-cavity SWS [72].

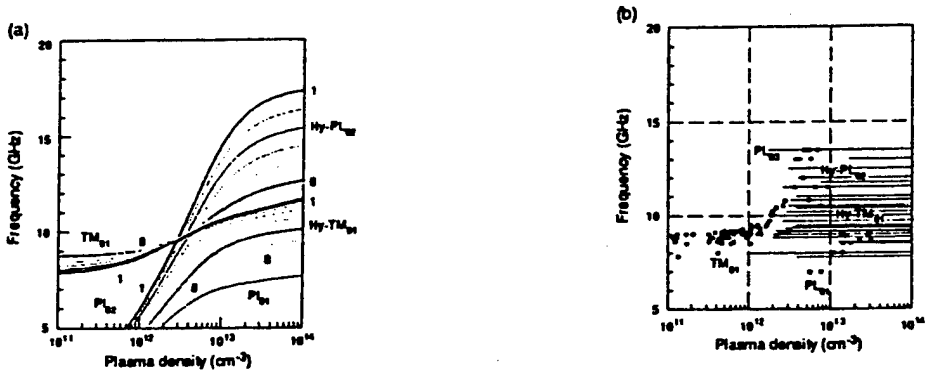


Figure 25: Frequency as a function of peak plasma density for a finite length, slow wave, corrugated-wall structure loaded with a high density, radially inhomogeneous plasma column: (a) the calculated axial modes (labeled 1 through 8) of both the plasma branches and the electromagnetic branches overlap in frequency, and (b) the measured curve, using the techniques described earlier. Note that the tunability range can be 8-17 GHz.

are characterized by a transition in the slope of the dispersion curves around the point where $\omega_{\text{plasma}} \cong \omega_{\text{radiation}}$. Periodic plasma modes are dominant above this critical point.

### 4.2.4 Electromagnetic Properties of Corrugated SWS Loaded with High Density Plasma ($> 10^{12}$ cm$^{-3}$)

In contrast to cavities loaded with low density plasma, when the plasma density is high ($\omega_{\text{radiation}} \leq \omega_{\text{plasma}}$), the dispersion curves of the plasma modes and those of the vacuum SWS electromagnetic modes overlap in frequency. This case can lead to the formation of hybrid modes [61] and to electronic frequency tunability over a wide frequency range [67].

A finite length slow wave corrugated-wall structure loaded with a high density, radially inhomogeneous plasma column was used as an example. The calculated axial modes (labeled 1 through 8) of both the plasma branches and the electromagnetic branches overlap in frequency, as shown in Fig. 25(a).

The tunability range in this case can possibly be from 8-17 GHz. The dispersion curves were also measured using the techniques described earlier, and are shown in Fig. 25(b). Note the agreement between the calculation and the measurement [68]. Moreover, the hot test results reported below confirm both the calculation and cold test results.

### 4.2.5 Operation of Plasma-loaded Relativistic BWO

A relativistic (500 kV) BWO filled a radially nonuniform, preionized plasma of high peak density ($n_p \leq 10^{14}$ cm$^{-3}$) was studied experimentally, and some of the most interesting

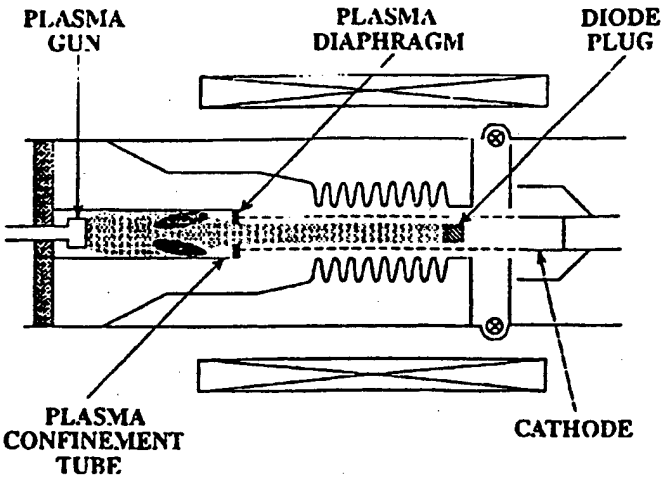


Figure 26: A schematic diagram of a modified plasma-loaded BWO with steps taken to protect both the output and the electron gun region from plasma penetration.

results will be described below. It should be emphasized that in this high density regime, the peak plasma frequency is higher that the operating frequency, and is therefore labeled "overdense." It is in this overdense regime that the most beneficial effects of the plasma, such as wideband electronic tunability, substantial space charge neutralization, and power enhancement, are pronounced.

The presence of high density plasma in the rf interaction region may create difficulties in *both* the diode and output regions. In the output region the guiding magnetic field decreases along the axis of the system away from the solenoid. A resonant microwave absorbing layer (upper hybrid frequency absorption) will be created somewhere in the output region, where the microwave frequency equals the upper hybrid frequency, *i.e.*, $\omega^2 = \omega_p^2 + \Omega_c^2$ ($\Omega_c$ is the electron cyclotron frequency). This layer is capable of absorbing a considerable fraction of the output microwave energy and may also contribute to "microwave pulse shortening." On the opposite end of the system, plasma in the resonator may also stream into the electron gun (diode) region, where it can significantly reduce its impedance and cause deterioration of the electron beam quality. This influence may be substantial for $\omega_p R_b/c > 1$.

In order to overcome those difficulties in the electron gun and in the output region and still allow high density operation in the corrugated rf interaction region, a greatly improved experimental geometry was successfully adopted as shown in Fig. 26 [66]. The plasma gun was mounted inside a long stainless steel tube extending into the uniform magnetic field region. This tube shields the output region from the magnetically active plasma and prevents absorption of microwave energy in this region, and also acts as part of a coaxial output coupler. The plasma diaphragm also serves as a beam collector. The relativistic electron gun was protected from plasma penetration by placing a cylindrical "plug" (1.4 cm in diameter) close to the anode plane. This geometry allowed hollow beam propagation into the interaction region, but prevented plasma penetration into the gun region. As a result, the modified experimental apparatus allowed us to investigate the influence of plasma density on BWO

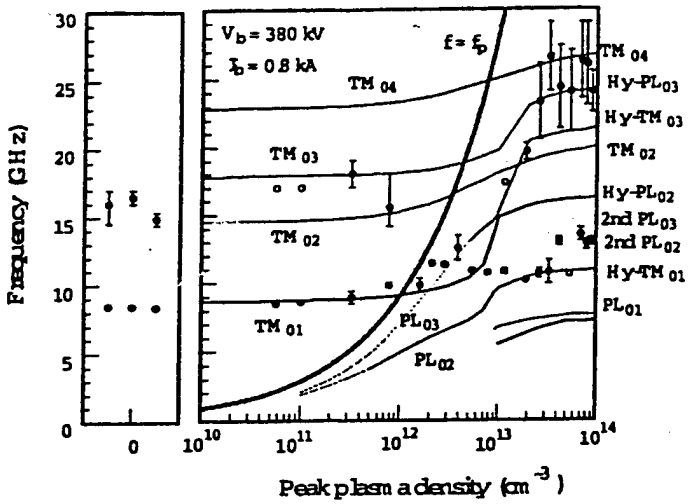


Figure 27: Electronic tunability, as a function of peak plasma density for modified plasma-loaded BWO [67] (380 kV, 0.8 kA). The measured hot test results are shown as open and closed circles, while the solid lines are the calculated modes (labeled as TM, PL for plasma, and Hy for hybrids). A tunability range of over 300% was demonstrated (from 8-26 GHz). The thick solid line represents the condition $\omega = \omega_p$, and all the "territory" to the right of this line is the "overdense regime."

operation over a very wide density range (up to $5 \times 10^{13}$ cm$^{-3}$) without adversely affecting the gun and output regions.

Three of the most interesting quantitative results, namely i) electronic tunability by exercising control over the plasma density, ii) plasma influence on microwave pulse duration, and iii) plasma influence on microwave power, will be presented here.

Electronic tunability, as function of peak plasma density, is demonstrated in Fig. 27 for a 380 kV, 0.8 kA relativistic BWO. This important figure allows us to "close the circle" in terms of understanding the wideband frequency tunability capabilities of a plasma-loaded BWO, by combining the results of hot tests (Fig. 27) with those of cold test (Fig. 25(b)) and the calculation (Fig. 25(a)) of the same plasma-loaded corrugated SWS discussed earlier. As can be seen, the results compare favorably with both the cold test and modeling. It should be emphasized that the calculation (solid lines in Fig. 27) are derived from the calculation presented earlier (Fig. 25(a)) by choosing a specific beam voltage of 380 kV.

Most interesting is the plasma influence on microwave pulse duration, shown in Fig. 28, where the pulse duration as a function of peak plasma density is plotted. Not only is the plasma not contributing to microwave pulse shortening, it actually leads to a substantial pulse lengthening, by a factor of three, over the vacuum value (left frame). (For more details see [67].)

The plasma influence on peak microwave power is shown in Fig. 29, again for a 380 kV, 0.8 kA beam. For the case of $n_p \approx 3 \times 10^{12}$ cm$^{-3}$, the peak microwave power is enhanced by a factor of about four compared with the vacuum value under the same conditions.

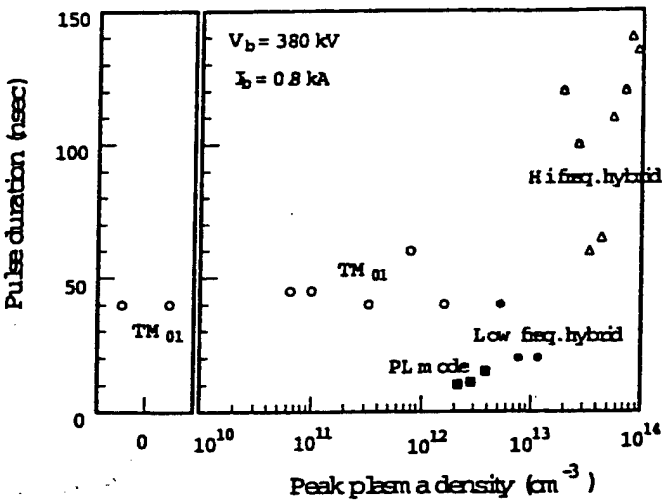


Figure 28: Microwave pulse duration as a function of peak plasma density for a corrugated-wall BWO (external plasma gun). Notice that the pulse duration at plasma densities $> 2 \times 10^{13}$ cm$^{-3}$ is three times longer than the vacuum values (380 kV, 0.8 kA).

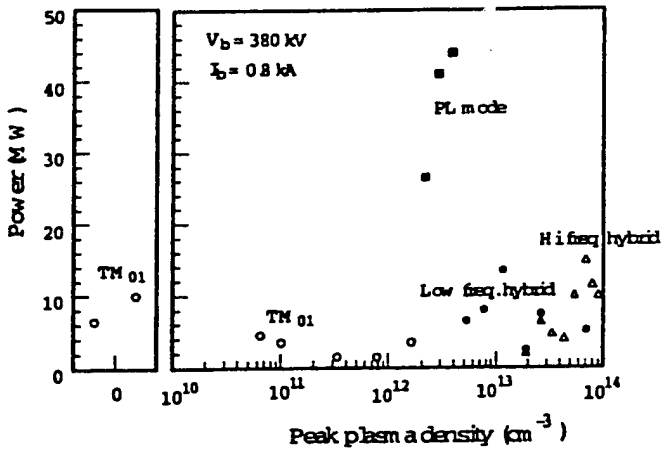


Figure 29: The plasma's influence on peak microwave power (380 kV, 0.8 kA). For the case of $n_p \approx 3 \times 10^{12}$ cm$^{-3}$, the peak microwave power is enhanced by a factor of about four compared with the vacuum value under the same conditions.

## 4.3 Summary of achievements

- Wideband electronic frequency tunability of 300% (8 GHz to 24 GHz) was demonstrated by excersizing control over the background plasma density.
- Plasma-loaded microwave devices have the potential to advance the technological and scientific base of microwave tubes, and also to impact commercial and industrial applications through the development of commercially viable technologies (examples include high current density plasma cathodes, new beam transport techniques, and high efficiency, tunable microwave sources for plasma, semiconductor and materials processing).
- The presence of plasma does not contribute to pulse shortening. On the contrary, it was found that the presence of plasma in relativistic backward wave oscillators leads to both increase in microwave pulse duration and peak output power.
- Demonstrated ability to generate, control, and diagnose plasmas over a wide density range, from $10^9$ to $10^{14}$ $cm^{-3}$.
- Impact of research in relativistic plasma microwave electronics. Activity in this field was found to be scientifically challenging and rewarding, as evident from the extensive list of publications. Furthermore, students educated in this research moved to play important roles in DoD laboratories after graduation.
- Development of novel diagnostics.

# 5 Summary of Synthesis of Advanced Ceramics for Microwave Tubes

## 5.1 Scope of Research Performed

As part of MURI 1994, the Univ. of Maryland chose CPI (Communication Power Industries, formerly Varian) as an industrial partner in order to jointly develop, test and operate an advanced, gyrotron based microwave processing facility. CPI, based on specification developed by the University of Maryland designed the system. The key component in the system was a 28 GHz, 15 kW CW gyrotron. The design specifications were very challenging. A fast response computer control of the gyrotron output power over an extremely wide range (10 W to 10,000 W). The gyrotron and its associated components were designed for integration with an existing microwave furnace at the Univ. of Maryland. As a first step, the gyrotron tube was designed, built and tested. Next, the gyrotron tube was integrated in a cabinet with its own power supplies, cooling and a computerized control system. The system was delivered to the University of Maryland in June 1998, and integrated with an existing, highly overmoded applicator (furnace). In order to integrate the gyrotron with the applicator, special components like high power cooled windows; low loss circular transmission lines with $90^0$ bends; and arc detectors were developed and tested.

## 5.2 Motivation for the Research

The availability of the 28 GHz microwave processing system was expected to open new possibilities for synthesis of advanced ceramics for microwave tubes for Air Force and DOD applications. This promising line of research can lead to breakthroughs in the synthesis of new class of structural and functional materials with superior properties. The new materials can have beneficial impact on microwave windows and radomes, substrates for high-speed semiconductors, as well as UV transparent materials. A short description of these new possibilities, to be investigated under the sponsorship of other programs, is given below.

The mechanical, thermal, optical and dielectric properties of materials depend to a large extent on their method of fabrication. Research in processing of materials with microwave energy demonstrated the potential for synthesis of advanced materials with superior properties, not attainable by any other means. Pressureless, near net shape microwave processing is also expected to substantially reduce the cost of those advanced materials, due to the elimination of the need for machining (this step is very expensive-often accounting for 90% of total cost).

A specific example of great importance to thermal management in microwave sources is the need replace beryllium oxide (BeO) and beryllium oxide/silicone carbide (BeO/SiC) composites commonly used in medium and high power microwave tubes. This is a critically important issue for the Air Force and DOD since BeO is not acceptable from environmental point of view- it is both toxic and long term carcinogenic. Microwave processing can lead to advanced ceramics with improved thermal conductivity, to replace beryllium oxide (BeO) and beryllium oxide/silicone carbide (BeO/SiC) composites.

Currently available alternatives are characterized by too low thermal conductivity. If those alternative materials are incorporated into existing microwave sources, a prohibitively expensive redesign will be required. Aluminum nitride (AlN) is a candidate to replace BeO in these demanding applications. Unfortunately, the thermal conductivity of the commercially available material (50 W/mK) is well below the theoretical value (200 W/mK). Microwave processing at the University of Maryland convincingly demonstrated that it is possible to synthesize high quality, high thermal conductivity AlN with thermal conductivity exceeding 205 W/mK, as well as high quality AlN/SiC composites.

# References


[1] A. V. Gaponov, M. I. Petelin, and V. K. Yulpatov, "The Induced Radiation of Excited Classical Oscillators and its Use in High Frequency Electronics," *Izv. VUZov. Radiofiz.*, vol. 10, p. 1414, 1967 [*Radiophys. Quantum Electron.*, vol. 10, p. 794, 1967].

[2] G. S. Nusinovich and R. E. Erm, "Efficiency of a CRM-monotron with a Gaussian Axial Structure of the High Frequency Field," *Elektron. Tekhn.*, Ser. 1, *Elektron. SVCh.*, No. 8, p. 55, 1972.

[3] B. G. Danly and R. J. Temkin, "Generalized Nonlinear Harmonic Gyrotron Theory," *Phys. Fluids*, vol. 29, p. 561, 1986.

[4] D. V. Kisel, G. S. Korablev, V. G. Pavelyev, M. I. Petelin, and Sh. E. Tsimring, "An Experimental Study of a Gyrotron, Operating at the Second Harmonic of the Cyclotron Frequency, with Optimized Distribution of the High Frequency Field," *Radiotekhn. i. Elektron.*, vol. 19, p. 782, 1974 [*Radio Eng. Electron. Phys.*, vol. 19, p. 95, 1974].

[5] D. J. Bates and E. L. Ginzton, "A Traveling Wave Frequency Multiplier," *Proc. IRE*, vol. 45, p. 938, 1957.

[6] G. S. Nusinovich and O. Dumbrajs, "Two-harmonic Prebunching of Electrons in Multicavity Gyro-devices," *Phys. Plasmas*, vol. 2, p. 568, 1995.

[7] G. S. Nusinovich, B. Levush, and O. Dumbrajs, "Optimization of Multistage Harmonic Gyro-devices," *Phys. Plasmas*, vol. 3, p. 3133, 1996.

[8] G. S. Nusinovich, W. Chen, and V. K. Tripathi, "Linear Theory of a Gyro-twystron with Stagger-tuned Cavities," *IEEE Trans. Plasma Sci.*, vol. 26, p. 468, 1998.

[9] W. Chen, G. S. Nusinovich, and V. L. Granatstein, "Nonlinear Theory of Gyro-twystrons with Stagger-tuned Cavities," *IEEE Trans. Plasma Sci.*, vol. 27, p. 429, 1999.

[10] C. S. Kou, M. H. Wu, and F. Tseng, "Nonlinear Analysis of Multi-cavity Gyro-twystron," *Int. J. Infrared and Millimeter Waves*, vol. 18, p. 1857, 1997.

[11] L. R. Barnett, L. H. Chang, H. Y. Chen, K. R. Chu, W. K. Lau, and C. C. Tau, "Absolute Instability Competition and Suppression in a Millimeter Wave Gyrotron Traveling-wave Tube," *Phys. Rev. Lett.*, vol. 63, p. 1062, 1989.

[12] K. R. Chu, L. R. Barnett, W. K. Lau, L. H. Chang, A. T. Lin, and C. C. Lin, "Nonlinear Dynamics of the Gyrotron Traveling-wave Amplifier," *Phys. Fluids. B*, vol. 3, p. 2403, 1991.

[13] K. R. Chu, L. R. Barnett, H. Y. Chen, S. H. Chen, C. Wang, Y. S. Yeh, Y. C. Tsai, T. T. Yang, and T. Y. Dawn, "Stabilization of Absolute Instabilities in the Gyrotron Traveling-wave Amplifier," *Phys. Rev. Lett.*, vol. 74, p. 1103, 1995.

[14] K. R. Chu, H. Y. Chen, C. L. Hung, T. H. Chang, L. R. Barnett, S. H. Chen, and T. T, Yang, "Ultrahigh Gain Gyrotron Traveling-wave Amplifier," *Phys. Rev. Lett.*, vol. 81, p. 4760, 1998.

[15] K.R. Chu, H.Y. Chen, C.L. Hung, T.H. Chang, L.R. Barnett, S.H. Chen, T.T. Yang, and D. Dialetis, "Theory and Experiment of Ultra-high Gain Gyrotron Traveling Wave Amplifier," *IEEE Trans. Plasma Sci.*, vol. 27, p. 391, 1999.

[16] G. S. Nusinovich, M. Walter, and J. Zhao, "Excitation of Backward Waves in Forward Wave Amplifiers," *Phys. Rev. E*, vol. 58, p. 6594, 1998.

[17] H. R. Johnson, "Backward Wave Oscillators," *Proc. IRE*, vol. 43, p. 684, 1955.

[18] G. S. Nusinovich, "Mode Interaction in Gyrotrons," *Int. J. Electron.*, vol. 51, p. 457, 1981.

[19] A. T. Lin, K. R. Chu, C. C. Lin, C. S. Kou, D. B. McDermott, and N. C. Luhmann, Jr., "Marginal Stability Design Criterion for Gyro-TWT's and Comparison of Fundamental with Second Harmonic Operation," *Int. J. Electron.*, vol. 72, p. 873, 1992.

[20] K. R. Chu and A. T. Lin, "Gain and Bandwidth of the Gyro-TWT and CARM Amplifiers," *IEEE Trans. Plasma Sci.*, vol. 16, p. 90, 1988.

[21] G. S. Nusinovich and M. Walter, "Linear Theory of Multi-stage Forward Wave Amplifiers," *Phys. Rev. E.*, vol. 60, p. 4811, 1999.

[22] H. Guo, S. H. Chen, V. L. Granatstein, J. Rodgers, G. Nusinovich, M. Walter, B. Levush, and W. J. Chen, "Operation of a Highly Overmoded, Harmonic-multiplying, Wideband Gyrotron Amplifier," *Phys. Rev. Lett.*, vol. 79, p. 515, 1997.

[23] H. Guo, S. H. Chen, V. L. Granatstein, J. Rodgers, G. S. Nusinovich, M. Walter, J. Zhao, and W. J. Chen, "Operation of a High Performance, Harmonic-multiplying. Wideband Inverted Gyro-twystron," *IEEE Trans. Plasma Sci.*, vol. 26, p. 451, 1998.

[24] J. Rodgers, H. Guo, V. L. Granatstein, S. H. Chen, G. S. Nusinovich, M. Walter, B. Levush, and W. J. Chen, "Highly Efficient, Phase-locked Oscillator Operation of the Harmonic-multiplying Inverted Gyro-twystron," *IEEE Trans. Plasma Sci.*, vol. 27, p. 412, 1999.

[25] G. S. Nusinovich and M. Walter, "Theory of the Inverted Gyro-twystron," *Phys. Plasmas*, vol. 4, p. 3394, 1997.

[26] L. A. Weinstein, *Open Resonators and Waveguides*. Boulder, CO: Golem Press, 1969.

[27] S. N. Vlasov, G. M. Zhislin, I. M. Orlova, M. I. Petelin, and G. G. Rogacheva, "Irregular Waveguides as Open Resonators," *Izv. VUZov. Radiofiz.*, vol. 12, p. 1236, 1969. [*Radiophys. Quantum Electron.*, vol. 12, p. 972, 1969].

[28] G. S. Nusinovich and J. Zhao, "Axial Mode Locking in Gyro-devices," *Digest 23rd International Conference on Infrared and Millimeter Waves*, Colchester, U.K., p. 76. 1998.

[29] J. Zhao, G. S. Nusinovich, H. Guo, J. C. Rodgers, and V. L. Granatstein, *IEEE Trans. Plasma Sci.*, vol. 28, p. 597, 2000.

[30] E. V. Zasypkin, M. A. Moiseev, I. G. Gachev, and I. I. Antakov, "Study of High Power Ka-band Second-harmonic Gyroklystron Amplifier," *IEEE Trans. Plasma Sci.*, vol. 24, p. 666, 1996.

[31] I. I. Antakov, A. V. Gaponov, E. V. Zasypkin, E. V. Sokolov, V. K. Yulpatov, L. A. Aksenova, A. P. Keyer, V. S. Musatov, V. E. Myasnikov, L. G. Popov, B. A. Levitan, and A. A. Tolkachev, "Gyroklystrons-Millimeter Wave Amplifiers of the Highest Power," in *Proceedings 1993 International Symposium on Strong Microwaves in Plasmas*, Moscow-N. Novgorod-Moscow, p. 587, 1994.

[32] J. P. Calame, M. Garven, J. J. Choi, K. Nguyen, F. Wood, M. Blank, B. G. Danly, and B. Levush, "Experimental Studies of Bandwidth and Power Production in a Three-cavity, 35 GHz Gyroklystron Amplifier," *Phys. Plasmas*, vol. 6, p. 285, 1999.

[33] K. R. Chu, H. Guo, and V. L. Granatstein, "Theory of the Harmonic Multiplying Gyrotron Traveling Wave Amplifier," *Phys. Rev. Lett.*, vol. 78, p. 4661, 1997.

[34] M. Botton, T. M. Antonsen, Jr., B. Levush, K. T. Nguen, and A. N. Vlasov, "MAGY: A time-dependent code for simulation of slow and fast microwave sources," IEEE Trans. Plasma Sci., v. 26, pp. 882-892 (1998).

[35] W. Main, Y. Carmel, K. Ogura, J. Weaver, G. S. Nusinovich, S. Kobayashi, J. P. Tate, J. Rodgers, A. Bromborsky, S. Watanabe, M. R. Amin, K. Minami, W. W. Destler, and V. L. Granatstein, "Electromagnetic properties of open and closed overmoded slow-wave resonators for interaction with relativistic electron beams," IEEE Trans. Plasma Sci., v. 22, pp. 566-577 (1994).

[36] S. Kobayashi, M. Botton, Y. Carmel, T. M. Antonsen, Jr., J. Rodgers, A. G. Shkvarunets, A. N. Vlasov, L. Duan, and V. L. Granatstein, "Electromagnetic properties of periodic cavities coupled to a radiating antenna," IEEE Trans. Plasma Sci., v. 26, pp. 947-954 (1998).

[37] A.N. Vlasov, A.G. Shkvarunets, J.C. Rodgers, Y. Carmel, T.M. Antonsen, Jr., T.M. Abuelfadl, D. Lingze, V.A. Cherepenin, G.S. Nusinovich, M. Botton, and V.L. Granatstein, "Overmoded GW-class surface-wave microwave oscillator," IEEE Trans. Plasma Sci., v. 28, p. 550 (2000).

[38] D. K. Abe, Y. Carmel, S. M. Miller, A. Bromborsky, B. Levush, T. M. Antonsen, Jr., and W. W. Destler, "Experimental studies of overmoded relativistic backward wave oscillators," IEEE Trans. Plasma Sci., v. 26, pp. 591-604 (1998).

[39] S. D. Korovin, S. D. Polevin, A. M. Roitman, and V. V. Rostov, "The effect of forward waves in the operation of a uniform relativistic backward wave tube," Pis'ma Zh. Tekh. Fiz., v. 20, p. 12-16 (1994) [Tech. Phys. Lett., v. 20, pp. 5-7 (1994)].

[40] L. D. Moreland, E. Schamiloglu, R. W. Lemke, S. D. Korovin, V. V. Rostov, A. M. Roitman, K. J. Hendricks, and T. A. Spencer, "Efficiency enhancement of high power vacuum BWOs using nonuniform slow wave structures," IEEE Trans. Plasma Sci., v. 22, pp. 554-565 (1994).

[41] L. D. Moreland, E. Schamiloglu, R. W. Lemke, A. M. Roitman, S. D. Korovin, and V. V. Rostov, "Enhanced frequency agility of high-power relativistic backward wave oscillators," IEEE Trans. Plasma Sci., v. 24, pp. 554-565 (1996).

[42] A. N. Vlasov, G. S. Nusinovich, and B. Levush, "Effect of the zero spatial harmonic in a slow electromagnetic wave on operation of relativistic backward-wave oscillators," Phys. Plasmas, v. 5, pp. 1402-1412 (1997).

[43] G. S. Nusinovich and A. N. Vlasov, "Parametric effect of a spatially periodic voltage depression on operation of Cerenkov sources of electromagnetic radiation," Phys. Plasmas, v. 1, pp. 774-779 (1994).

[44] A. P. Kuznetsov and S. P. Kuznetsov, "Nature of the instability in a TWT in the region of the limit of the passband," Izv. VUZov, Radiofiz., v. 23, pp. 1104-1112 (1980) [Radiophys. and Quant. Electron., v. 23, pp. 736-743 (1980)].

[45] L. V. Bulgakova and S. P. Kuznetsov, "Unsteady-state nonlinear processes accompanying the interaction of an electron beam with an electromagnetic field near the boundary of transmission band: I. The high-frequency boundary," Izv. VUZov, Radiofiz., v. 31, pp. 207-221 (1988) [Radiophys. and Quant. Electron., v. 31, pp. 155-166 (1988)].

[46] L. V. Bulgakova and S. P. Kuznetsov, "Nonstationary nonlinear processes in the interaction of a an electron beam with an electromagnetic field near the limit of the transmission band of an electrodynamic system: II. Low-frequency limit," Izv. VUZov, Radiofiz., v. 31, pp. 612-621 (1988) [Radiophys. and Quant. Electron., v. 31, pp. 452-460 (1988)].

[47] S. M. Miller, T. M. Antonsen, Jr., B. Levush, A. Bromborsky, D. K. Abe, and Y. Carmel, "Theory of relativistic backward wave oscillators operating near cutoff," Phys. Plasmas, v. 1, pp. 730-740 (1994).

[48] G. S. Nusinovich, M. Korol, and E. Jerby, "Theory of the anomalous Doppler cyclotron-resonance-maser amplifier with tapered parameters," Phys. Rev. E., v. 59, pp. 2311-2321 (1999).

[49] V. S. Ivanov, S. I. Krementsov, V. A. Kutsenko, M. D. Raizer, A. A. Rukhadze, and A. V. Fedotov, "Investigation of a relativistic Cherenkov self-generator," Zh. Tekh. Fiz., v. 51, pp. 970-975 (1981) [Sov. Phys. Tech. Phys., v. 26, pp. 580-583 (1981)].

[50] R. A. Kehs, A. Bromborsky, B. G. Ruth, S. E. Graybill, W. W. Destler, Y. C. Carmel, and M. C. Wang, "A high-power backward-wave oscillator driven by a relativistic electron beam," IEEE Trans. Plasma Sci., v. 13, pp. 559-562 (1985).

[51] E. B. Abubakirov, N. S. Ginzburg, N. F. Kovalev, and M. I. Fuks, "Effect of fast cyclotron wave on the operation of Cherenkov microwave devices with relativistic electron beams," Radiotekh. i Elektron., v. 34, pp. 1058-1066 (1989) [Sov. J. Commun. Technol. Electr., v. 34, pp. 129-136 (1989)].

[52] E. B. Abubakirov, V. I. Belousov, V. N. Varganov, V. A. Gintzburg, N. F. Kovalev, N. G. Kolganov, M. I. Petelin, and E. I. Soluyanov, "Cyclotron-resonance mode selection in Cherenkov relativistic-electron RF sources," Pis'ma Zh. Tekh. Fiz., v. 9, p. 533-536 (1983) [Sov. Tech. Phys. Lett., v. 9, pp. 230-231 (1983)].

[53] A. Vlasov, G. Nusinovich, B. Levush, A. Bromborsky, W. Lou, and Y. Carmel, "Relativistic backward-wave oscillators operating near cyclotron resonance," Phys. Fluids B, v. 5, pp. 1625-1638 (1993).

[54] S. M. Miller, T. M. Antonsen, Jr., B. Levush, and A. N. Vlasov, "Cyclotron resonances in relativistic BWOs operating near cutoff," IEEE Trans. Plasma Sci., v. 24, pp. 859-869 (1996).

[55] A. N. Vlasov, A. S. Ilyin, and Y. Carmel, "Cyclotron effects in relativistic backward-wave oscillators operating at low magnetic fields," IEEE Trans. Plasma Sci., v. 26, pp. 605-614 (1998).

[56] B. Levush, T. M. Antonsen, Jr., A. N. Vlasov, G. S. Nusinovich, S. M. Miller, Y. Carmel, V. L. Granatstein, W. W. Destler, A. Bromborsky, C. Schlesiger, D. K. Abe, and L. Ludeking, "High-efficiency relativistic backward wave oscillator: theory and design," IEEE Trans. Plasma Sci., v. 24, pp. 843-851 (1996).

[57] Y. Carmel, W. R. Lou, T. M. Antonsen, Jr., J. Rodgers, B. Levush, W. W. Destler, and V. L. Granatstein, "Relativistic Plasma Microwave Electronics: Studies of High Power Plasma-filled Backward Wave Oscillators," *Phys. Fluids B*, vol. 4, p. 2286, 1992.

[58] M. V. Kuzelev, A. A. Rukhadze, P. S. Strelkov, and A. G. Shkvarunets, "Relativistic High Current Plasma Microwave Electronics: Advantages, Progress, and Outlook," *Fiz. Plazmy*, vol. 13, p. 1370, 1987 [*Sov. J. Plasma Phys.*, vol. 13, p. 793, 1987].

[59] G. Nusinovich, Y. Carmel, T. Antonsen, D. Goebel, J. Santoru, "Recent Progress in the Development of Plasma-filled Traveling Wave Tubes and Backward Wave Oscillators," *IEEE Trans. Plasma Sci.*, vol . 26, p. 628, 1998.

[60] G. S. Nusinovich, L. A. Mitin, and A. N. Vlasov, "Space Charge Effects in Plasma-filled Traveling Wave Tubes," *Phys. Plasmas*, vol. 4, p. 4394, 1997.

[61] N. I. Karbushev, Y. A. Kolosov, E. I. Ostrensky, and A. I. Polovkov, "Hybrid Plasma Slow Wave Structures for Linacs and Microwave Power Sources," in *Pulsed RF Sources*

*for Linear Colliders*, R. C. Fernow, Ed. *AIP Conference Proceedings 337*. Woodbury, NY: 1995.

[62] S. Kobayashi, T. M. Antonsen, Jr., and G. S. Nusinovich, "Linear Theory of a Plasma-loaded, Helix Type, Slow Wave Amplifier," *IEEE Trans. Plasma Sci.*, vol. 26, p. 669, 1998.

[63] S. M. Miller, T. M. Antonsen, Jr., and B. Levush, "Ponderomotive Effects in Plasma-filled Backward Wave Oscillators," *IEEE Trans. Plasma Sci.*, vol. 26, p. 680, 1998.

[64] Yu. P. Bliokh, M. G. Liubarskii, V. O. Podobinskii, Ya. B. Fainberg, G. S. Nusinovich, S. Kobayashi, Y. Carmel, and V. L. Granatstein, "Chaotic Oscillations Enhanced by Magnetosonic waves in Plasma-filled Traveling Wave Tubes," *Phys. Plasmas*, vol. 5, p. 4061, 1998.

[65] W. R. Lou, Y. Carmel, T. M. Antonsen, Jr., W. W. Destler and V. L. Granatstein, "New Modes in a Plasma with Periodic Boundaries: the Origin of the Dense Spectrum," *Phy. Rev. Lett.*, vol. 67, p. 2481, 1991.

[66] A. Shkvarunets, S. Kobayashi, J. Rodgers, Y. Carmel, T. Antonsen, L. Duan, and V. L. Granatstein, "Operation of a Relativistic Backward Wave Oscillator Filled with a Preionized, High Density, Radially Inhomogeneous Plasma," *IEEE Trans. Plasma Sci.*, vol. 3, p. 646, 1998.

[67] S. Kobayashi, *Studies of a Relativistic Backward Wave Oscillator Loaded with Radially Inhomogeneous Plasma Column*, Ph.D. Dissertation, University of Maryland, College Park, MD, 1999.

[68] A. Shkvarunets, S. Kobayashi, J. Weaver, Y. Carmel, J. Rodgers, V. L. Granatstein, and W. W. Destler, "Plasma Influence on the Dispersion Properties of Finite Length, Corrugated Waveguide," *Phys. Rev. E*, vol. 53, p. 2045, 1996.

[69] A. Shkvarunets, S. Kobayashi, J. Weaver, Y. Carmel, J. Rodgers, T. Antonsen, V. L. Granatstein, and W. W. Destler, "Electromagnetic Properties of Corrugated and Smooth Waveguides Filled with Radially Inhomogeneous Plasma," *IEEE Trans. Plasma Sci.*, vol. 24, p. 905, 1996.

[70] D. Goebel, Y. Carmel and G. Nusinovich, "Advances in Plasma-filled Microwave Sources," *Phys. Plasmas*, vol. 6, p. 2225, 1999.

[71] TWT structure, courtesy of W. James, Communications and Power Industries (CPI).

[72] TWT structure, courtesy of V. I. Perevodchikov, M. A. Zavjalov, and A. L. Shapiro, VEI, Moscow, Russia. Work performed as collaborative efforts of the University of Maryland and VEI, sponsored in part by a NATO Collaborative Linkage Grant.

# Refereed Journal Publications Arising from MURI 94 at the University of Maryland


1. G. S. Nusinovich, B. Levush, and O. Dumbrajs, "Optimization of multistage harmonic gyro-devices," *Phys. Plasmas*, vol. 3, pp. 3133-3144, 1996.

2. B. Levush, T. M. Antonsen, Jr., A. N. Vlasov, G. S. Nusinovich, S. M. Miller, Y. Carmel, V. L. Granatstein, W. W. Destler, A. Bromborsky, C. Schlesiger, D. K. Abe, and L. Ludeking, "High-efficiency relativistic backward wave oscillator: theory and design," *IEEE Trans. Plasma Sci.*, vol. 24, pp. 843-851, 1996.

3. J.P. Calame, A. Birman, Y. Carmel, D. Gershon, B. Levush, A.A. Sorokin, V.E. Semenov, D. Dadon, L.P. Martin, and M. Rosen, "A dielectric mixing law for porous ceramics based on fractal boundaries," J. Appl. Phys., vol. 80, pp. 3992-4000, 1996.

4. A. Shkvarunets, S. Kobayashi, J. Weaver, Y. Carmel, J. Rodgers, T. Antonsen, V. L. Granatstein, and W. W. Destler, "Electromagnetic properties of corrugated and smooth waveguides filled with radially inhomogeneous plasma," *IEEE Trans. Plasma Sci.*, vol. 24, pp. 905-918, 1996.

5. A. Shkvarunets, S. Kobayashi, J. Weaver, Y. Carmel, J. Rodgers, V. L. Granatstein, and W. W. Destler, "Plasma influence on the dispersion properties of finite length, corrugated waveguide," *Phys. Rev. E*, vol. 53, p. 2045, 1996.

6. S. M. Miller, T. M. Antonsen, Jr., B. Levush, and A. N. Vlasov, "Cyclotron resonances in relativistic BWOs operating near cutoff," *IEEE Trans. Plasma Sci.*, vol. 24, pp. 859-869, 1996.

7. H. Guo, S. H. Chen, V. L. Granatstein, J. Rodgers, G. Nusinovich, M. Walter, B. Levush, and W. J. Chen, "Operation of a highly overmoded, harmonic-multiplying, wideband gyrotron amplifier," *Phys. Rev. Lett.*, vol. 79, p. 515, 1997.

8. K. R. Chu, H. Guo, and V. L. Granatstein, "Theory of the harmonic multiplying gyrotron traveling wave amplifier," *Phys. Rev. Lett.*, vol. 78, p. 4661, 1997.

9. G. S. Nusinovich and M. Walter, "Theory of the inverted gyro-twystron," *Phys. Plasmas*, vol. 4, p. 3394, 1997.

10. G. S. Nusinovich, L. A. Mitin, and A. N. Vlasov, "Space charge effects in plasma-filled traveling wave tubes," *ibid.*, p. 4394, 1997.

11. A. N. Vlasov, G. S. Nusinovich, and B. Levush, "Effect of the zero spatial harmonic in a slow electromagnetic wave on operation of relativistic backward-wave oscillators," *Phys. Plasmas*, vol. 5, pp. 1402-1412, 1997.

12. S.H. Gold and G.S. Nusinovich, "Review of high-power microwave source research," *Rev. Sci. Instru.*, vol. 68, pp. 3945-3974, 1997.

13. V.L. Granatstein, B. Levush, B.G. Danly, and R.K. Parker, "A quarter century of gyrotron research and development," *IEEE Trans. Plasma Sci.* (25th Anniversary Special Issue), vol. 25, pp. 1322-1335, 1997. INVITED PAPER.

14. H. Guo, S. H. Chen, V. L. Granatstein, J. Rodgers, G. S. Nusinovich, M. Walter, J. Zhao, and W. J. Chen, "Operation of a high performance, harmonic-multiplying, wideband inverted gyro-twystron," *IEEE Trans. Plasma Sci.*, vol. 26, p. 451, 1998.

15. G. S. Nusinovich, W. Chen, and V. K. Tripathi, "Linear theory of a gyro-twystron with stagger-tuned cavities," *ibid.*, pp. 468-474, 1998.

16. D. K. Abe, Y. Carmel, S. M. Miller, A. Bromborsky, B. Levush, T. M. Antonsen, Jr., and W. W. Destler, "Experimental studies of overmoded relativistic backward wave oscillators," *ibid.*, pp. 591-604, 1998.

17. A. N. Vlasov, A. S. Ilyin, and Y. Carmel, "Cyclotron effects in relativistic backward-wave oscillators operating at low magnetic fields," *ibid.*, pp. 605-614, 1998.

18. G. Nusinovich, Y. Carmel, T. Antonsen, D. Goebel, J. Santoru, "Recent progress in the development of plasma-filled traveling wave tubes and backward wave oscillators," *ibid.*, pp. 628-645, 1998.

19. A. Shkvarunets, S. Kobayashi, J. Rodgers, Y. Carmel, T. Antonsen, L. Duan, and V. L. Granatstein, "Operation of a relativistic backward wave oscillator filled with a preionized, high density, radially inhomogeneous plasma," *ibid.*, pp. 646-652, 1998.

20. S. Kobayashi, T. M. Antonsen, Jr., and G. S. Nusinovich, "Linear theory of a plasma-loaded, helix type, slow wave amplifier," *ibid.*, pp. 669-679, 1998.

21. S. M. Miller, T. M. Antonsen, Jr., and B. Levush, "Ponderomotive effects in plasma-filled backward wave oscillators," *ibid.*, pp. 680-692, 1998.

22. M. Botton, T. M. Antonsen, Jr., B. Levush, K. T. Nguyen, and A. N. Vlasov, "MAGY: A time-dependent code for simulation of slow and fast microwave sources," *ibid.*, pp. 882-892, 1998.

23. K. Tanaka, K. Minami, X. Zheng, Y. Carmel, A. Vlasov, and V. Granatstein, "Propagating quasi-TE modes in a vacuum axisymmetric corrugated wall waveguide," *ibid.* pp. 940-946, 1998.

24. S. Kobayashi, M. Botton, Y. Carmel, T. M. Antonsen, Jr., J. Rodgers, A. G. Shkvarunets, A. N. Vlasov, L. Duan, and V. L. Granatstein, "Electromagnetic properties of periodic cavities coupled to a radiating antenna," *ibid.*, pp. 947-954, 1998.

25. A. Birnboim, D. Gershon, J. Calame, A. Birman, Y. Carmle, Y. Bykov, A. Eremeev, V. Holoptsev, V. Semenov, D. Dadon, L.P. Martin, M. Rosen, and R. Hutcheon, "Comparative study of microwave sintering of zinc oxide at 2.45, 30 and 83 GHz," *J. Am. Ceram. Soc.*, vol. 81, pp. 493-501, 1998.

26. L.P. Martin, D. Dadon, M. Rosen, D. Gershon, K.I. Rybokov, A. Birman, J. Calame, B. Levush, Y. Carmel, R. Hutcheon, "Effects of anomalous permittivity on microwave heating of zinc oxide," *J. Appl. Phys.*, vol. 83, pp. 432-437, 1998.

27. Yu. P. Bliokh, M. G. Liubarskii, V. O. Podobinskii, Ya. B. Fainberg, G. S. Nusinovich, S. Kobayashi, Y. Carmel, and V. L. Granatstein, "Chaotic oscillations enhanced by magnetosonic waves in plasma-filled traveling wave tubes," *Phys. Plasmas*, vol. 5, pp. 4061-4069, 1998.

28. G. S. Nusinovich, M. Walter, and J. Zhao, "Excitation of backward waves in forward wave amplifiers," *Phys. Rev. E*, vol. 58, p. 6594-6605, 1998.

29. G.S. Nusinovich, "Review of the theory of mode interaction in gyrodevices," *IEEE Trans. Plasma Sci.*, vol. 27, pp. 313-326, 1999.

30. J. Rodgers, H. Guo, V. L. Granatstein, S. H. Chen, G. S. Nusinovich, M. Walter, B. Levush, and W. J. Chen, "Highly efficient, phase-locked oscillator operation of the harmonic-multiplying inverted gyro-twystron," *ibid.*, pp. 412-421, 1999.

31. G.S. Nusinovich, B. Levush and B.G. Danly, "Gain and bandwidth in stagger-tuned gyroklystrons and gyrotwystrons," *ibid.*, pp.422-428, 1999.

32. W. Chen, G. S. Nusinovich, and V. L. Granatstein, "Nonlinear theory of gyro-twystrons with stagger-tuned cavities," *ibid.*, pp. 429-437, 1999.

33. T.M. Antonsen, Jr., A.A. Mondelli, B. Levush, J.P. Verboncoeur, and C.K. Birdsall, "Advances in modeling and simulation of vacuum electronic devices," *Proc. IEEE*, vol. 87, "Special Issue on New Vistas for Vacuum Electronics," eds. V.L. Granatstein and C.M. Armstrong, pp. 804-839, 1999.

34. A.N. Vlasov, A.G. Shkvarunets, J.C. Rodgers, Y. Carmel, T.M. Antonsen, Jr., T.M. Abuelfadl, D. Lingze, V.A. Cherepenin, G.S. Nusinovich, M. Botton, and V.L. Granatstein, "Overmoded GW-class surface-wave microwave oscillator," *IEEE Trans. Plasma Sci.*, vol. 28, pp. 550-560 (2000).

35. J. Zhao, G. S. Nusinovich, H. Guo, J. C. Rodgers, and V. L. Granatstein, *ibid.*, pp. 597-605, 2000.

36. J. Zhao, H. Guo, G.S. Nusinovich, J.C. Rodgers and V.L. Granatstein, "Studies of a three-stage inverted gyrotwystron," *ibid.*, pp. 657-664, 2000.

37. A.T. Lin, H. Guo, and V.L. Granatstein, "Dynamic simulation of mode-selective interaction cavity for wide-band high-power gyrotron applications," *ibid.*, pp. 782-789, 2000.

# Part B: Research at Cornell University

## 1 Introduction

The work reported in this section was carried out at Cornell University between May 1995 and April 2000 as a subcontract from the University of Maryland funded under the Muri HPM program. A detailed review of the work was prepared during the summer of 1999 and this review comprises the bulk of the report. We conclude the report with an additional section which summarizes the more recent results obtained in the program.

## 2 Traveling Wave Tube Amplifiers

### 2.1 Introduction

The distributed interaction in a slow wave structure arises because both the electrons and the wave propagate with similar velocities. As a result, the average field experienced by the particles along the interaction is nonzero. Pierce [12] was the first to develop the linear nonrelativistic theory of the interaction in a traveling wave structure and during the fifties and sixties substantial efforts were directed to improving the performance of TWT's. This work, which was mainly aimed at low power amplifiers and oscillators, is summarized, for example in the book by Gilmour [4]. Typical devices use helix slow wave structures. One dimensional codes were initially developed by Nordsiek [5] and others to model the non linear processes in the microwave interaction. In parallel with this the construction of high energy electron accelerators lead to the development of high power klystrons in L and S bands. More recent work (see, for example, Caryotakis [6]) has resulted in the production of 70 MW X-Band klystrons. These tubes, which operate with a repetition rate of $\sim$ 60 Hz., and have a pulse duration of $\sim$ 1.5$\mu$s, use a short nonuniform traveling wave tube output. They differ from the amplifiers described here in that the bunching is produced by a series of decoupled $TM_{010}$ mode cavities spaced to optimize the beam modulation. The TWT amplifier employs a traveling wave section to bunch the beam as well as to extract the microwave energy. The klystron is inherently a narrow band device whereas the TWT allows the possibility of tuning the amplifier over at least a few percent of the center frequency. In addition the conventional tube uses a thermionic cathode and operates in ultra high vacuum. The HPM devices described in this chapter employ field emission diodes and relatively poor vacuum. The applications envisioned require ultra high powers $\sim$ GW powers with $\sim kJ$ pulses and tube conditioning is typically not available. The first application of pulse power technology to HPM was reported in 1970 by Nation [1] who demonstrated BWO operation using a relativistic electron beam propagating through a corrugated waveguide. Traveling wave interactions using these technologies are the subject of the remainder of this chapter.

A typical amplifier configuration is illustrated in Figure 1. It consists of two disk loaded waveguides (coupled cavities) separated by a sever. Both structures are tapered in order minimize reflections and to control the phase velocity of the wave to optimize the power

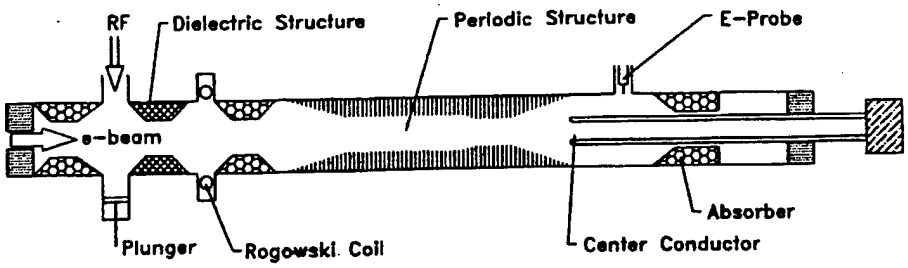


Figure 1: Typical TWT experimental arrangement showing amplifier stages separated by a sever

extraction. Before we proceed it is instructive to have some typical values of the system parameters. The beam energy typically is in the range 0.5-0.9 MeV, the current is between 0.2 and 1.5 kA, and the beam radius ($R_b$) 2.5-3.0 mm for X band operation. The period ($L$) of the metallic structure is in the range $6 - 12$mm according to the phase advance per cell chosen. The internal radius of the disks ($R_{int}$) varies between 6 and 12mm according to the design efficiency and structure length.

It consists of two disk loaded waveguides (coupled cavities) separated by a sever. Both structures are tapered in order minimize reflections and to control the phase velocity of the wave to optimize the power extraction. Before we proceed it is instructive to have some typical values of the system parameters. The beam energy typically is in the range 0.5-0.9 MeV, the current is between 0.2 and 1.5 kA, and the beam radius ($R_b$) 2.5-3.0 mm for X band operation. The period ($L$) of the metallic structure is in the range $6 - 12$mm according to the phase advance per cell chosen. The internal radius of the disks ($R_{int}$) varies between 6 and 12mm according to the design efficiency and structure length.

In a uniform and semi-infinite structure, neglecting reflections from the amplifier output, and in the framework of a linear relativistic theory, the spatial growth is determined by the imaginary part of the wavenumber $k$ which for a synchronous electron beam, is given by [13],

$$\mathrm{Im}(k) = \frac{\sqrt{3}}{2}\left[\frac{1}{2S_w}\frac{\omega}{c}\frac{eIZ_{int}}{mc^2}\frac{1}{(\gamma\beta)^3}\right]^{1/3} ; \qquad (1)$$

where $S_w$ is the cross-sectional area for wave propagation ($S_w = \pi R_{int}^2$) and $R_{int}$ is the internal radius of the disks). The coupling between the beam and the wave is represented by the product of the current ($I$) and the interaction impedance ($Z_{int}$). It is proportional to the square of electric field experienced by the electrons and is inversely proportional to the total power ($P$) associated with the specific mode i.e.,

$$Z_{int} \equiv \frac{S_w}{2P}\frac{2}{R_b^2}\int_0^{R_b} \mathrm{d}r r E_z^2(r) . \qquad (2)$$

All of the quantities are evaluated in the absence of the beam.

The result quoted in Eq.(1) is similar to that given by Pierce except that the definition of the interaction impedance uses $(R_{\rm int})^{-1}$ rather than the wavenumber $(k)$. This is convenient in a disk loaded waveguide because $R_{\rm int}$ may be kept constant while tapering the phase velocity. In addition, the formulation in [13] accounts for relativistic effects that shift the location of maximum spatial growth rate from the synchronous flow condition.

## 2.2 Single-Stage TWT

The first experiments [9, 10, 14, 15, 16, 17] on high-power disk loaded traveling wave amplifiers were carried out during the late eighties. They indicated that 100 MW at 8.76 GHz could be achieved before the system oscillated. The fact that the input is not isolated from the output, allows waves to be reflected backwards and the feedback can cause the system to oscillate. The effect of reflections was revealed as a narrowing of the amplifier bandwidth, due to the interference associated with the waves bouncing between both ends of the system. For a system of length $d$ the interference is characterized by the passive bandwidth $\Delta \mathrm{f}_{\rm pass} \simeq v_{\rm gr}/2d$ where $v_{\rm gr}$ is the group velocity in the vicinity of the frequency of interest. If the ratio of amplitudes (output/input) of the interference peak is $G(f_0)$, then the relation between the active bandwidth $\Delta \mathrm{f}_{\rm act}$ and its passive counterpart is,

$$\Delta \mathrm{f}_{\rm pass} \cdot 1 = \Delta \mathrm{f}_{\rm act} \cdot G(f_0) = \text{const.}, \tag{3}$$

In other words, the product of the gain and the bandwidth is constant and is equal the bandwidth of the structure without the beam [14].

## 2.3 Two-Stage TWT

In order to isolate the input of the amplifier from the output, the TWT driven was split into two sections [10, 16] separated by a sever, a section of waveguide made of lossy material whose radius is often below cut-off. The experiments on the two-stage TWT indicated that power levels in excess of 400 MW (corresponding to an rf conversion efficiency of more than 45% ) are achievable with no indication of rf breakdown. In this case, however, the output spectrum was 300 MHz wide and up to 50% of the power was measured in asymmetric sidebands. This was shown to be due to amplified noise at frequencies selected by the interference of the two waves bouncing between the ends of the last stage. An amplifier or an oscillator are the two extremes of possible regimes of operation and any practical device operates somewhere in between [17].

## 2.4 Particle Code Work

For an adequate simulation of a system that includes tapers and severs, a macro-particle approach was developed. A macro-particle in this context is a cluster of electrons "glued" together that all have the same velocity, and a ratio of charge to mass $(e/m)$ that is the same as that of an electron. It is further assumed that: *(a)* a strong guiding magnetic field confines the motion of the electrons to the longitudinal direction, *(b)* the basic form of the interacting field, $E_z(r,z,t) = E_0 \mathrm{I}_0[r\sqrt{k^2-(\omega/c)^2}]\cos[\omega t - \int_0^z \mathrm{d}z' k(z') + \psi]$, is preserved

and the interaction affects the amplitude $E_0$ and the phase $\psi$ but does not affect the radial behavior. *(c)* The time variations ($e^{j\omega t}$) are determined by either the input field or the modulation of the beam. *(d)* No electrons are reflected and *(e)* there is no correlation between the transverse location of the electrons (macro-particles) and their longitudinal dynamics. Based on these assumptions the dynamics of the interaction in traveling wave amplifier is determined by three equations:

$$\begin{aligned} \frac{\mathrm{d}}{\mathrm{d}\zeta}\frac{a}{\sqrt{\alpha}} &= \sqrt{\alpha}\left\langle e^{-j\chi_i}\right\rangle , \\ \frac{\mathrm{d}}{\mathrm{d}\zeta}\chi_i &= \frac{\Omega}{\beta_i} - K , \\ \frac{\mathrm{d}}{\mathrm{d}\zeta}\gamma_i &= -\frac{1}{2}\left[ae^{j\chi_i} + \mathrm{c.c.}\right]; \end{aligned} \tag{4}$$

These equations describe the amplitude dynamics, the phase dynamics and the single particle energy conservation respectively. The other definitions used here are: $\zeta = z/d$, $d$ is the total interaction length, $\Omega = \omega d/c$, $K = kd$, $a = eE_0 d/mc^2$, $\gamma_i = [1-\beta_i^2]^{-1/2}$; $\chi_i$ is the phase of the $i$'th particle relative to the $\mathrm{TM}_{01}$ mode and the coupling coefficient is denoted by $\alpha(\equiv eIZ_{\mathrm{int}}d^2/mc^2S_{\mathrm{w}})$. Figure 2 illustrates the behavior of a bunched beam in a uniform structure. The first five frames illustrate the phase-space of a partially bunched beam. After one quarter of the interaction length, the particles in phase with the wave lose momentum whereas those in anti-phase gain momentum. After propagation through three quarters of the interaction region the process is more pronounced and in addition, the phase shift associated with the cumulative effect of the particles on the wave, becomes evident. When the shift of the bottom approaches $\pi$, saturation is reached since particles that were originally decelerated are now re-accelerated by the field. The phase-space saturation is revealed in the fifth frame ($\zeta = 1$). The last frame illustrates the efficiency, $\eta(\zeta) \equiv [\langle\gamma(0)\rangle - \langle\gamma(\zeta)\rangle]/[\langle\gamma(0)-1\rangle]$, and the relative energy spread along the interaction region; clearly the two are correlated both reaching a maximum at saturation. Beyond saturation both are reduced. The braces<> indicates an average of the quantity enclosed.

## 2.5 Structure Tapering

Whenever high efficiency is required the structure has to be tapered i.e. one adapts the phase velocity of the wave to that of the electrons. When the wave phase velocity varies, the interaction impedance also changes. Figure 3 shows the typical dependence of $Z_{\mathrm{int}}$ and $R_{\mathrm{ext}}$ on the phase velocity for constant $R_{\mathrm{int}}$, frequency $f = 9GHz$, disk thickness of 1mm and phase advance per cell of $\pi/2$. This last choice is different to that used in acceleration structures ($2\pi/3$) and is dictated by the need to impose rapid flow of the power that develops namely, maximum group velocity. As for possible tapering, there are at least three conceptual schemes: *(a)* impose synchronous condition i.e. the phase velocity of the wave equals the average velocity of the particles [ $\beta_{\mathrm{ph}} = \langle\beta_i\rangle$]. *(b)* Preserve the average phase stationary i.e. $\mathrm{d}\langle\chi_i\rangle/\mathrm{d}\zeta = 0 \rightarrow \beta_{\mathrm{ph}} = 1/\left\langle\beta_i^{-1}\right\rangle$. The third *(c)* is to make the phase stationary relative to

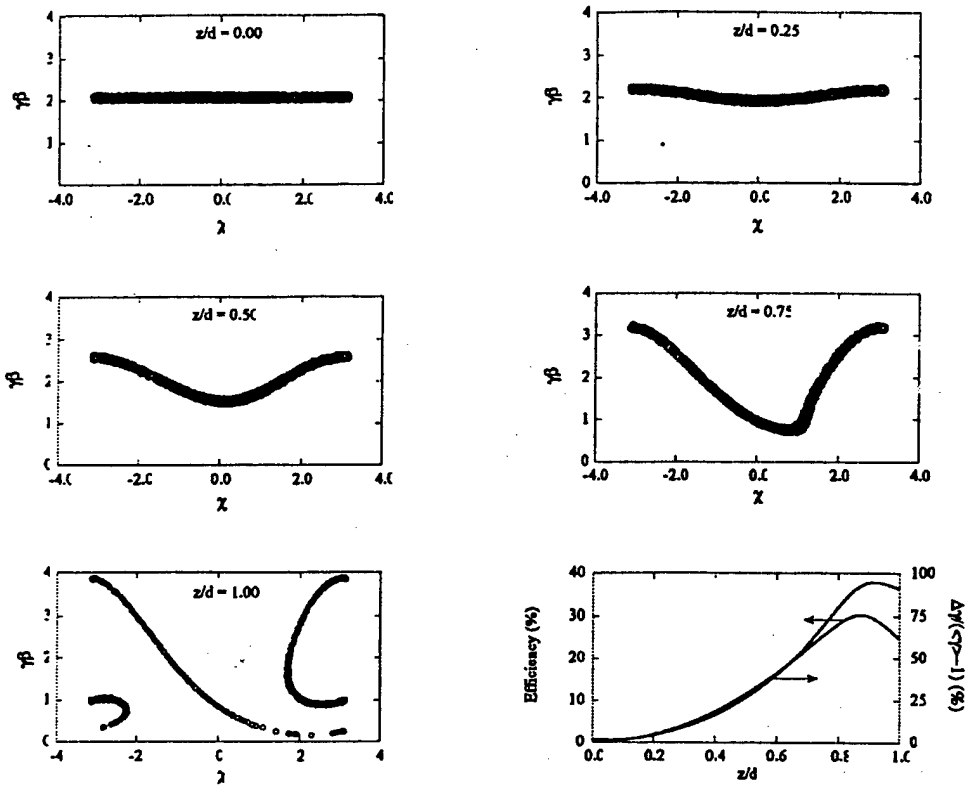


Figure 2: Simulated behavior of a bunched beam in a uniform slow wave amplifier structure. The first five frames illustrate the phase-space of a partially bunched beam. The last frame shows the rf conversion efficiency and the relative energy spread along the interaction region

the local interacting wave $\mathrm{d}[\langle\chi_i\rangle + \psi]/\mathrm{d}\zeta = 0$ where $\psi$ is the phase of $a$. Figure 4 illustrates the efficiency for the three cases.

## 2.6 Transit Time Isolation

One of the basic assumptions of the macro-particle approach is the absence of reflections. In practice, the approach may be used even when reflections are present, since during one rf round trip in the structure, the input is constant. Based on this the problem of reflections could be eliminated by designing a structure in which the time it takes the first reflection to return to the input end of the amplifier is equal to or greater than the electron pulse duration [18]. The transit time isolation principle was successfully demonstrated experimentally [19, 20] and power levels of 160 MW were achieved at 9 GHz. On the time scale of the pulse duration the use of the macro-particle approach is valid and experiments support its predictions.

# 3 Recent High Power TWT Amplifier Research

Studies of relativistic TWT's in the framework of the MURI Program on HPM generation were carried out at Cornell University. Most of this activity was focused on the development of a coherent, phase stable, X band TWT amplifier and on maximizing its rf power and

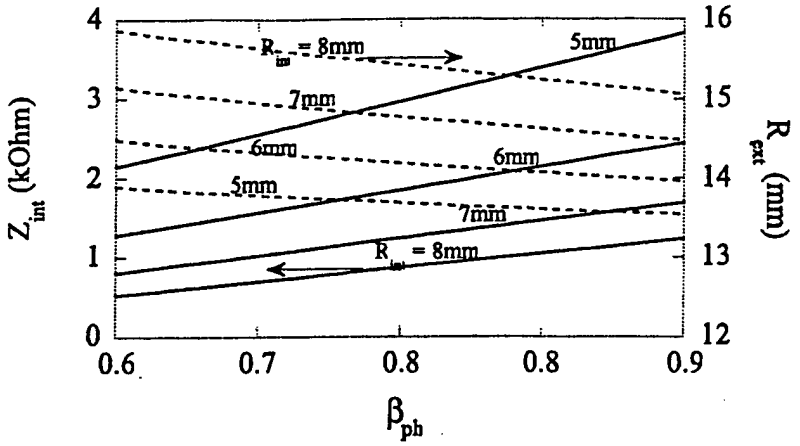


Figure 3: The dependence of $Z_{\text{int}}$ and $R_{\text{ext}}$ on the phase velocity for a structure having a constant $R_{\text{int}}$. The frequency is $f = 9GHz$, disk thickness 1mm, and the phase advance per cell $\pi/2$.

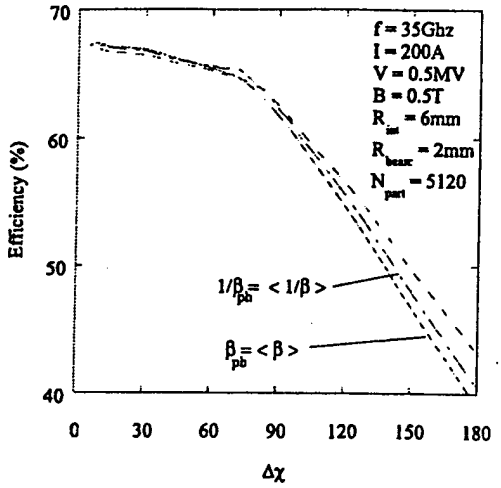


Figure 4: Efficiency as a function of tapering. a) Local synchronism, b) Average phase stationary and c) Phase stationary relative to local wave

energy conversion efficiencies. Some new work has recently started on a Ka band amplifier system.

## 3.1 Quasi-Periodic Structures

The 160 MW power levels described above, which were generated using the time isolation method, resulted in electric field gradients larger than 200 MV/m. Although no rf breakdown was experienced, any further increase in the power levels require an increase the volume of the last two or three cells in order to minimize the electric field on the metallic surfaces - in other words, the system becomes quasi-periodic. The main problems of an extraction section based on a quasi-periodic disk loaded structure are: a) to minimize the reflections at both ends of the structure in order to avoid oscillation and, b) to taper the output section in order to avoid breakdown and compensate for the velocity decrease of the electrons.

To optimize these conflicting requirements an analytical technique has been developed

[21, 22, 23] which permits the analysis and design of a quasi-periodic structure consisting of one or more symmetric arms and a set of coupled cavities.

## 3.2 High Efficiency Output Structures

The method developed relies on a model which consists of a cylindrical waveguide to which a number of pill-box cavities and radial arms, are attached. In principle the number of cavities and arms is arbitrary. The boundary condition problem is formulated in terms of the amplitudes of the electromagnetic field in the cavities and arms. The matrix elements that relate these amplitudes with the source term are analytic functions and no a-priori knowledge of the functional behavior of the electromagnetic field is necessary. In the framework of this analysis it was shown that the interaction is controlled by a *matrix interaction impedance* ($Z_{n,m}$), that is a generalization [24] of the scalar interaction impedance [Eq.(2)].

In order to illustrate the potential of the macro-particle approach applied in the framework of quasi-periodic structures, consider a system with uniform $R_{\text{int}}$ and $R_{\text{ext}}$. These values are determined by maximizing the largest eigen-value of the interaction impedance matrix at 9 GHz – as illustrated in the left frame of Figure 5. Overlaid is also the efficiency assuming a single macro-particle injected into the system in one period of the wave. Note that the two are virtually identical. The middle frame in Figure 5 illustrates the variation in space of the efficiency for an initial phase distribution of $-9° < \chi(0) < 9°$ and the right frame shows the phase-space at the input and the output. They clearly reveal the impact of each cavity and the arm on the total efficiency. Moreover, the right frame reveals the momentum reduction of all particles and the phase spread accompanying this process.

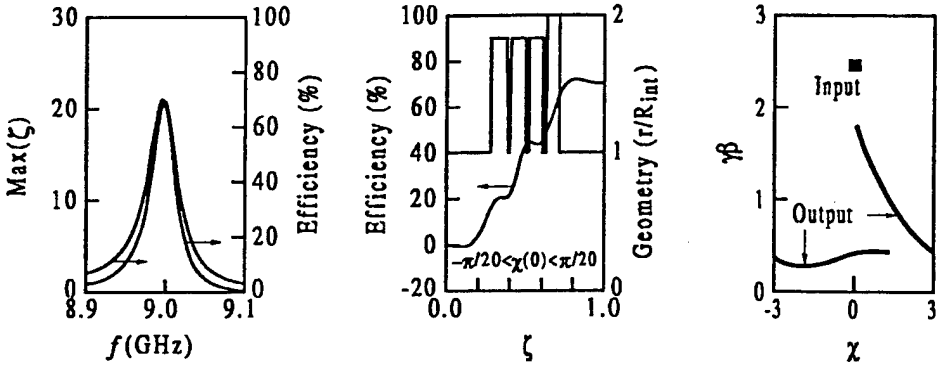


Figure 5: *left:* Largest eigen-value of the interaction impedance matrix as a function of the frequency, *Center:* efficiency development in space and *Right:* the phase space of the particles at the input and output of the structure.

## 3.3 Axial Extraction

The quasi-periodic approach discussed previously enables one to examine the electromagnetic characteristics of a structure with a tilted output [24] arm, rather than radial arm usually used.

Motivated by the desire to minimize reflections and broaden the bandwidth we take advantage of the fact that the interacting mode is a surface wave therefore it may be gradually decoupled from the beam by adiabatically increasing the radius of the structure. The concept was proven experimentally [25]. We found, in fact, that the system is substantially less sensitive to beam and wave conditions than originally anticipated. The lack of sensitivity is in part associated with the fact that in relativistic traveling wave structure, the bandwidth of the interaction [26] is larger than in a corresponding nonrelativistic device - see Figure 6.

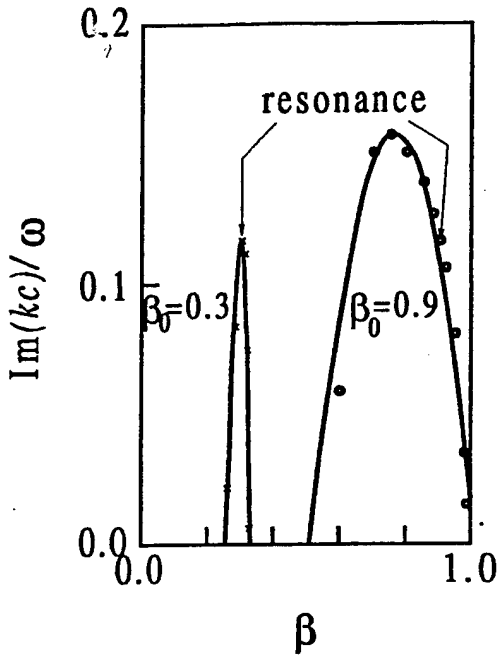


Figure 6: Comparison of spatial wave growth of nonrelativistic and relativistic TWT's. For the nonrelativistic case the maximum spatial growth occurs at resonance, whereas in a relativistic device, the peak occurs at a lower velocity. Gain is also observed for a wide range of relativistic electron velocities

## 3.4 High Efficiency Amplifier Operation

In recent experiments [27] several configurations (See Figure 1) of a two stage traveling wave amplifier were investigated. In the device illustrated we use a Teflon dielectric buffer amplifier immediately following the rf input port. This absorbs the rf power, but does not produce amplification. The absorbed power modulates the beam so that a weakly modulated beam enters the second stage which is located immediately after a silicon carbide sever. The first stage of the amplifier has a phase velocity approximately equal to the speed of light at the center of the amplifier passband. It serves to efficiently bunch the 700 kV beam. A short, 4 cell, transition section leads to a 7 cell output section where the cold wave phase velocity is about 0.78 c.

Tight bunching is critical to efficient operation, since decreasing the local wave phase velocity to match the decreasing electron velocity cannot increase the efficiency once the

bunch has expanded to have a length comparable to a half wavelength. The output has a tapered section expanding to the radius of the cylindrical guide. Re-acceleration of the electrons is prevented by decoupling the wave from the beam in this region by use of a hollow central beam dump. The slow wave structure supports a $TM_{01}$ mode which is efficiently mode converted to a TEM coaxial wave at the beam dump. The amplified wave is detected, but not extracted from the system in this region. There are two additional silicon carbide absorbers located in the amplifier, one at the entrance and the second in the coaxial section. It is essential to minimize reflections from the ends of the amplifier to prevent oscillation. It was shown experimentally that in the case of an cathode immersed in a uniform axial magnetic field that up 60 MW of microwave power, at 9 GHz, for $\sim$ 80nsec before significant pulse shortening developed. Beyond this value both the rf and beam pulse durations became shorter until at 150 MW the pulse duration had dropped to 10nsec. In these experiments the current was about 500A and the guiding field 10kG. For a beam generated in a converging axial guiding magnetic field of 5kG and a structure with $R_{\text{int}} = 11.75$mm up to 77 MW were measured without indications of pulse shortening, corresponding to a 55% conversion efficiency.

We show in Fig. 7 typical rf output pulses shown as a function of time on the same figure as the bean current and voltage traces. In Fig. 8 we show the signal obtained from mixing the output signal with that from a local oscillator, and the FFT (Fig. 9) of the mixed signal. Finally, in Fig 10 we demonstrate that the output signal varies linearly with the input signal for outputs up to about 60 MW and that the small signal gain was 32.5 dB at 9.21 GHz and 35.7 dB (not shown) at 9.48 GHz. Similar results were obtained with an $R_{\text{int}} = 8.0$mm structure, except that in this case the gain was greater than 45 dB. The smaller diameter structure has a $TM_{01}$ mode passband of 2.0 GHz compared with the 4.0 GHz for the 11.75 mm diameter structure. In both cases the measured 3 dB bandwidth of the amplifier was greater than 500 MHz.

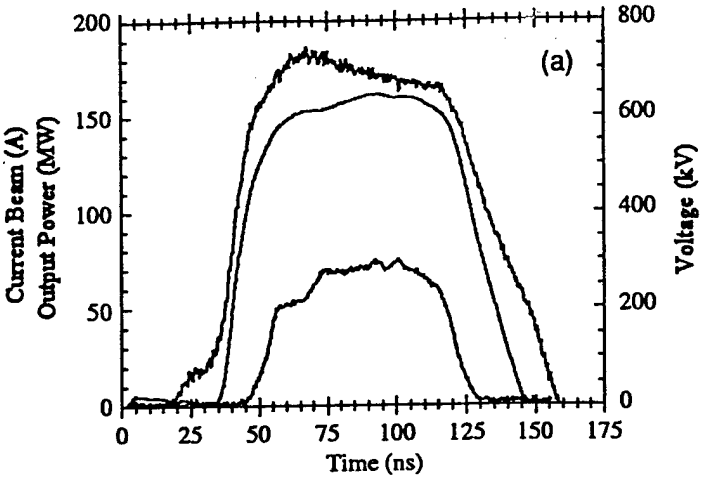


Figure 7: Typical beam noltage (730 kV), current (180 A) and rf power envelope (77MW) shown on the same time scale.

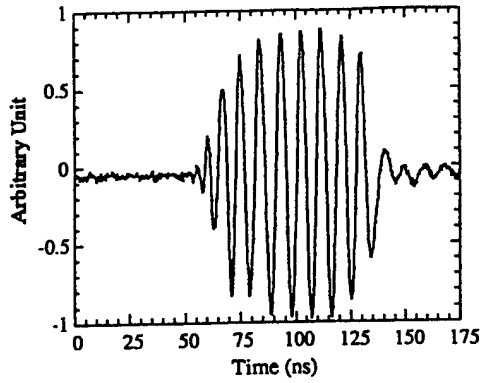


Figure 8: Downshifted signal from double balanced mixer.

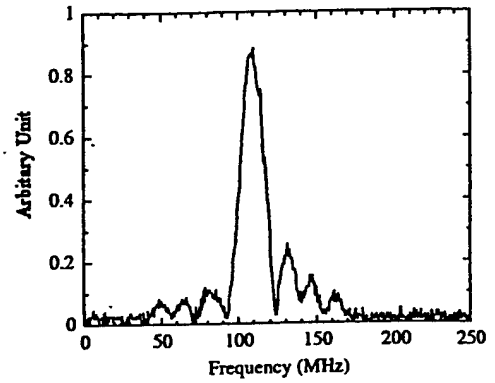


Figure 9: FFT of downshifted signal.

## 3.5 Bunch Compression

The axial extraction scheme takes advantage of the fact that a slow-wave is basically an evanescent wave that decays from the periodic structure inwards. This allows one to gradually decouple the wave from beam in the output section. The opposite situation may be utilized in the bunching section namely, we need maximum longitudinal electric field on axis. Consequently it may be advantageous to operate in a region where the phase velocity is larger than $c$ - provided this is done for a relatively short region. Recently, it was shown [29] that such a buncher may have substantial advantages. Such a buncher was implemented successfully in [27].

## 3.6 Ka-Band Studies

All the studies described above have focused on operation in X-band (9 GHz), however, future devices may need to be operated at higher frequencies (e.g. 35GHz). For this reason the 1D macro-particle approach was extended [28] to 2D i.e. longitudinal and radial motion. This analysis enables one to examine the basic requirements of a traveling wave structure driven by a beam similar to that which drives the present X-band system. Such a beam implies that the disk aperture (at 35GHz) relative to the cutoff wavelength is larger compared to the ratio for an X-band amplifier. The price for using at 35GHz a relatively large disk aperture,

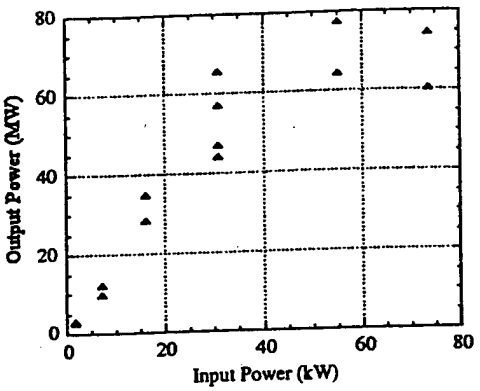


Figure 10: Output microwave power as a function of the input power.

is operation at high group velocity and low interaction impedance. This has two effects, namely:- a) for a given current and for maximum efficiency the required interaction length is longer and this in turn, leads to a higher sensitivity to beam-quality. On the other hand, b) it makes the transverse motion of the particles less "violent" reducing the probability of electrons hitting the wall for a given guiding magnetic field. Experiments are underway and first results from a single-stage system indicate that a few MWatts of rf power have been achieved from a 900 kV, 200 A. beam [30].

## 3.7 Hybrid Modes

Slow wave structures and their driving beam are in most cases azimuthally symmetric. However asymmetry in the system may occur either due to the input or output arm or the azimuthal electron distribution. A longitudinally modulated beam may couple energy from the main interacting symmetric transverse magnetic (TM) mode to asymmetric modes due to either one of these asymmetries. From the perspective of the interaction with the electrons, the main problem with an asymmetric mode is that it has a non zero azimuthal (and radial) magnetic field on axis. As a result, electrons that move at relativistic velocities in the longitudinal direction may be deflected by this field. In fact, these modes are used in the accelerator community in beam deflectors.

The first step in understanding the role of asymmetric modes is to investigate their "cold" characteristics. In the internal region ($r < R_{\text{int}}$) all the components of the electromagnetic field may be derived from the longitudinal components that read

$$\begin{aligned} E_z &= \sum_{n,\nu=-\infty}^{\infty} \mathcal{E}_{n,\nu} e^{j\omega t - jk_n z - j\nu\phi} I_\nu(\Gamma_n r)\,, \\ H_z &= \sum_{n,\nu=-\infty}^{\infty} \mathcal{H}_{n,\nu} e^{j\omega t - jk_n z - j\nu\phi} I_\nu(\Gamma_n r)\,; \end{aligned} \tag{5}$$

$k_n \equiv k + 2\pi n/L$, $|kL| < \pi$, $\Gamma_n \equiv \sqrt{k_n^2 - (\omega/c)^2}$ and $I_\nu(\xi)$ is the modified Bessel function of the first type and order $\nu$. The dispersion relation of a periodic structure may be written in

a matrix form as follows:

$$\begin{pmatrix} D^{\mathrm{TM}}(\nu) & C_{12}(\nu) \\ C_{21}(\nu) & D^{\mathrm{TE}}(\nu) \end{pmatrix} \begin{pmatrix} \mathcal{E} \\ \mathcal{H} \end{pmatrix} = 0\,, \tag{6}$$

where, in principle, the matrices $D^{\mathrm{TM}}$, $D^{\mathrm{TE}}$, $C_{12}$ and $C_{21}$, are infinite. This notation is instructive since in case of symmetric modes ($\nu = 0$) the coupling matrices $(C_{12}, C_{21})$ are identically zero and this equation has two uncoupled solutions $\mathrm{Det}\left(D^{\mathrm{TM}}\right) = 0$ and $\mathrm{Det}\left(D^{\mathrm{TE}}\right) = 0$ that represent all the symmetric transverse magnetic (TM) and transverse electric (TE) modes, respectively. For any other value of $\nu$ the coupling matrices are not zero and as a result, the nontrivial solution of (6) implies that each eigen-mode is a superposition of the two modes (TE & TM) - consequently the asymmetric modes are also called hybrid electro-magnetic modes (HEM).

Similar to the symmetric modes, for each radial number $\nu$ there are two modes that are referred to as "lower" and "higher" modes. When the ripple amplitude of the periodic structure is small they degenerates to the uniform waveguide result. The lower mode coincides with the TE mode and the higher with the TM mode. As a result, the lower cutoff of $\mathrm{HEM}_{11}$ ($kL = 0.0$) may be below that of the $\mathrm{TM}_{01}$.

Figure 11 illustrates the dispersion relation of all the modes up to 20GHz of two structures: in the left frame the internal radius of the disk is relatively small (8mm) such that $\mathrm{TM}_{01}$ and $\mathrm{HEM}_{11}$ are well separated and do not intersect. The right frame illustrates the case when the modes intersect since the internal radius is large and as a result, the modes are close to each other. Note that these two conditions correspond to the two experimental amplifier configurations described in the last section.

The relative weight of each basic mode (TM and TE) composing the hybrid mode changes at different frequencies. In order to illustrate the "character" of the HEM mode it is convenient to define the quantity $h_0 \equiv \eta_0 |\mathcal{H}_{n=0}|/|\mathcal{E}_{n=0}|$ that may be shown to control the equations of motion of the electrons. When $h_0$ is smaller than unity, "$E_z$" is dominant and the system behaves as a "TM" mode whereas for values larger than unity its behavior resembles the "TE" mode. In either case the mode has a nonzero magnetic field on axis.

Figure 12 illustrates the value $h_0$ for the two structures whose dispersion curves were presented above. In both cases the "TE" behavior is primarily in the lower part of the pass band of $\mathrm{HEM}_{11L}$ and "TM" behavior in its upper region. When referring here to "TE" or "TM" we refer to to asymmetric modes since, as long there is no structural (geometric) asymmetry or an asymmetric driving bunch, the $\mathrm{HEM}_{11L}$ and $\mathrm{TM}_{01}$ modes are decoupled.

Another aspect that is critical in the design of a slow-wave structure is the group velocity of the HEM mode. If the latter is negative an inherent positive feedback develops in the system and the system will oscillate. This problem is in particular vital in tapered structures where even if initially the system was designed for a positive group velocity, as the phase velocity of the $\mathrm{TM}_{01}$ mode is reduced, the group velocity of the HEM may become negative.

## 3.8 Interaction of Symmetric and Asymmetric Modes

After these comments on cold properties we may discuss the coupling between $\mathrm{TM}_{01}$ and $\mathrm{HEM}_{11}$. This is based on a quasi-analytic macro-particle approach that describes the interaction of a beam of electrons with both $\mathrm{TM}_{01}$ and the low branch of $\mathrm{HEM}_{11}$. It is again

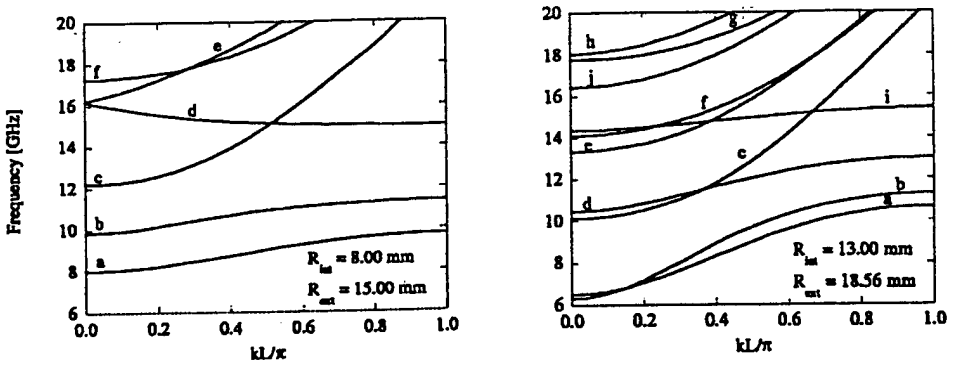


Figure 11: Dispersion relation of all the modes up to 20 GHz for two structures: in the left frame the internal radius of the disk is small (8mm) and the $TM_{01}$ and $HEM_{11}$ modes are well separated. The right frame illustrates the case ($R_{int}$ = 11.75 mm) and the modes overlap. In both cases the structure was designed to operate at 9 GHz with a phase advance per cell of $\pi/2$ and a phase velocity of $0.933c$. For evaluation of these dispersion curves 6 modes were used in the grooves and 50 Floquet harmonics in the inner space. Mode legend: a - $TM_{01}$, b - $HEM_{11L}$, c - $HEM_{11\overline{H}}$, d - $HEM_{21L}$, e - $HEM_{21H}$, f - $TM_{02}$, g - $HEM_{12L}$, h - $HEM_{12H}$, i - $HEM_{31L}$ and j - $HEM_{31H}$.

instructive to examine the 1D case where the coupling is due to asymmetric distribution of the electrons. Additional assumptions of the model include: positive group velocity of both modes, the basic form of both modes is preserved and no electrons are reflected. Subject to these assumptions the dynamics of the system is given by

$$
\begin{aligned}
&\frac{\mathrm{d}}{\mathrm{d}\xi}\left(\frac{a_1}{\sqrt{\alpha_1}}\right) = \sqrt{\alpha_1}\left\langle e^{-j\chi_{i,1}}\mathrm{I}_0(\bar{\Gamma}_1\bar{r}_i)\right\rangle\,,\\
&\frac{\mathrm{d}}{\mathrm{d}\xi}\left(\frac{a_2}{\sqrt{\alpha_2}}\right) = \sqrt{\alpha_2}\left\langle e^{-j\chi_{i,2}+j\phi_i}\mathrm{I}_1(\bar{\Gamma}_2\bar{r}_i)\right\rangle\,,\\
&\frac{\mathrm{d}}{\mathrm{d}\xi}\chi_{i,1} = \frac{\Omega_1}{\beta_i} - K_1\,, \qquad \frac{\mathrm{d}}{\mathrm{d}\xi}\chi_{i,2} = \frac{\Omega_2}{\beta_i} - K_2\,,\\
&\frac{\mathrm{d}}{\mathrm{d}\xi}\gamma_i = -\frac{1}{2}\left[a_1\, e^{j\chi_{i,1}}\mathrm{I}_0(\bar{\Gamma}_1\bar{r}_i) + a_2\, e^{j\chi_{i,2}-j\phi_i}\mathrm{I}_1(\bar{\Gamma}_2\bar{r}_i) + \mathrm{c.c.}\right];
\end{aligned}
\tag{7}
$$

The indices represent the modes: index 1 represents the $TM_{01}$ mode and index 2 the low $HEM_{11}$ mode; $\phi_i$ is the azimuthal location of the i'th particle; $\Gamma$ and $r$ are normalized with $R_{\mathrm{int}}$. All the other quantities were defined in the context of Eq.(4).

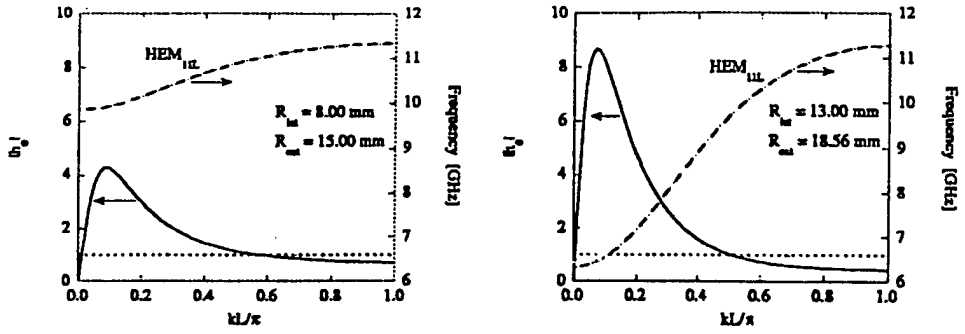


Figure 12: The value $h_0$ for the $\mathrm{HEM}_{11L}$ for the structures presented in Figure 01. In both cases the "TE" behavior ($h_0 > 1$) is primarily in the lower part of the pass band and the "TM" behavior ($h_0 < 1$) in its upper region.

Based on (7), the spatial growth of the system may be deduced from

$$\begin{aligned}
&\frac{\mathrm{d}^3}{\mathrm{d}\xi^3}a_1 + \left(\frac{j}{2}\alpha_1\Omega_1 p_1\right)a_1 + \left(\frac{j}{2}\alpha_1\Omega_1 U\right)a_2 \simeq -\alpha_1\left\langle\left(\frac{\Omega_1}{\beta_i} - K_1\right)^2 e^{-j\chi_{i,1}}\mathrm{I}_0(\bar{\Gamma}_1\bar{r}_i)\right\rangle \\
&\frac{\mathrm{d}^3}{\mathrm{d}\xi^3}a_2 + \left(\frac{j}{2}\alpha_2\Omega_2 p_2\right)a_2 + \left(\frac{j}{2}\alpha_2\Omega_2 U^*\right)a_1 \simeq -\alpha_2\left\langle\left(\frac{\Omega_2}{\beta_i} - K_2\right)^2 e^{-j(\chi_{i,2}-\phi_i)}\mathrm{I}_1(\bar{\Gamma}_2\bar{r}_i)\right\rangle
\end{aligned} \tag{8}$$

where $p_1 \equiv \left\langle \mathrm{I}_0^2(\bar{\Gamma}_1\bar{r}_i)(\gamma_i\beta_i)^{-3}\right\rangle$, $p_2 \equiv \left\langle \mathrm{I}_1^2(\bar{\Gamma}_2\bar{r}_i)(\gamma_i\beta_i)^{-3}\right\rangle$ and

$$U \equiv \left\langle e^{-j(\chi_{i,1}-\chi_{i,2}+\phi_i)}(\gamma_i\beta_i)^{-3}\mathrm{I}_0(\bar{\Gamma}_1\bar{r}_i)\mathrm{I}_1(\bar{\Gamma}_2\bar{r}_i)\right\rangle . \tag{9}$$

Ignoring the two noise terms in the right hand side of both equations we may calculate the eigen-wavenumber of the coupled system by assuming solutions of the form $a_1 = \bar{a}_1 e^{-js\xi}$ and $a_2 = \bar{a}_2 e^{-js\xi}$. The result is

$$\begin{pmatrix} s^3 + \frac{1}{2}\alpha_1\Omega_1 p_1 & \frac{1}{2}\alpha_1\Omega_1 U \\ \frac{1}{2}\alpha_2\Omega_2 U^* & s^3 + \frac{1}{2}\alpha_2\Omega_2 p_2 \end{pmatrix}\begin{pmatrix} \bar{a}_1 \\ \bar{a}_2 \end{pmatrix} = 0 . \tag{10}$$

As clearly revealed by this matrix, the term $U$, defined in Eq.(9), represents the coupling between the basic eigen-modes ($\mathrm{TM}_{01}$ & $\mathrm{HEM}_{11L}$) and, from its definition, it is realized that this is directly related to the correlation between the two phases $(\chi_{i,1}, \chi_{i,2})$, the radial and momentum distribution, and in particular, the correlation of all four with the azimuthal distribution of the electrons forming the beam.

When the coupling between the modes is zero each one of the modes, $\mathrm{TM}_{01}$ and $\mathrm{HEM}_{11L}$, develops independently according to $s^3 + S_1^3 = 0$ and $s^3 + S_2^3 = 0$ correspondingly; $S_\mu^3 \equiv \frac{1}{2}p_\mu\alpha_\mu\Omega_\mu$, $\mu = 1, 2$. The coupling between the $\mathrm{TM}_{01}$ and $\mathrm{HEM}_{11L}$ is determined by the *real*

parameter

$$\bar{u} \equiv \sqrt{\frac{UU^*}{p_1 p_2}} = \frac{\left| \left\langle \frac{e^{-j(\chi_{i,1}-\chi_{i,2}+\phi_i)}}{(\gamma_i\beta_i)^3} \mathrm{I}_0(\bar{\Gamma}_1\bar{r}_i)\mathrm{I}_1(\bar{\Gamma}_2\bar{r}_i) \right\rangle \right|}{\sqrt{\left\langle \frac{\mathrm{I}_0^2(\bar{\Gamma}_1\bar{r}_i)}{(\gamma_i\beta_i)^3} \right\rangle \left\langle \frac{\mathrm{I}_1^2(\bar{\Gamma}_2\bar{r}_i)}{(\gamma_i\beta_i)^3} \right\rangle}} \tag{11}$$

thus the solution of the coupled system can be determined from $s^3 + S_\pm^3 = 0$ where

$$S_\pm^3 = -\frac{1}{2}\left(S_1^3 + S_2^3\right) \pm \frac{1}{2}\sqrt{(S_1^3 - S_2^3)^2 + 4S_1^3 S_2^3 \bar{u}^2}\,; \tag{12}$$

the solution $S_+$ corresponds to the "$\mathrm{HEM}_{11}$"-like solution since at the limit $\bar{u} = 0$, $S_+ = S_2$, whereas $S_-$ corresponds to the "$\mathrm{TM}_{01}$"-like solution. The solid line curves in Figure 13 illustrate the variation of the growth per cell, $g_\pm \equiv (L/d)20\log(e^{\sqrt{3}S_\pm/2})$, as a function of the parameter $\bar{u}$. In case of complete correlation ($\bar{u} = 1$) the spatial growth of the "$\mathrm{HEM}_{11}$"-like mode is zero whereas the "$\mathrm{TM}_{01}$"-like is slightly larger than the case when there is no coupling ($\bar{u} = 0$). Although, the "HEM"-like wave becomes unimportant, we have to remember that the "$\mathrm{TM}_{01}$"-like mode is not a pure $\mathrm{TM}_{01}$ mode but rather a hybrid of $\mathrm{TM}_{01}$ and $\mathrm{HEM}_{11}$ therefore, the impact of the HEM is still destructive.

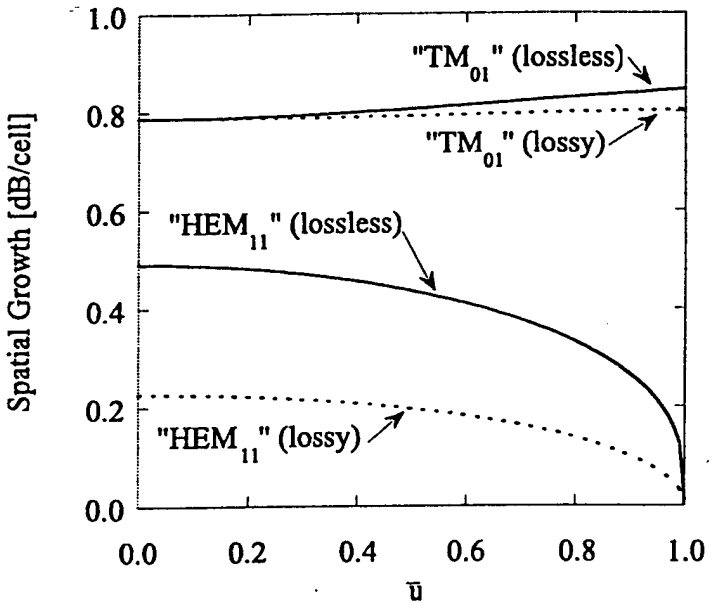


Figure 13: Wave growth per cell as a function of the correlation parameter $\bar{u}$.

In order to reduce the coupling effect, selective damping can be introduced in the structure. The dashed lines in Figure 13 illustrate the spatial growth per cell (in dB) in the case of damping the $\mathrm{HEM}_{11}$ mode for an attenuation of 1.7dB per cell in the absence of the beam. Two facts are evident: firstly, the "$\mathrm{HEM}_{11}$"-like mode is substantially suppressed though not as one would expect from the cold attenuation and secondly, the "$\mathrm{TM}_{01}$"-like mode is almost independent of $\bar{u}$ indicating that the "$\mathrm{TM}_{01}$"-like mode is close to the pure $\mathrm{TM}_{01}$ mode.

## 3.9 Discussion

Generation of high power microwave radiation using traveling wave tubes has many advantages primarily because the distributed interaction, bandwidth and the potential low sensitivity to manufacturing tolerances. Hundreds of mega watts were achieved in the past when the goal was high power and just to put that in perspective with, say the L-band relativistic klystron amplifier, 400 MW at 9 GHz is equivalent to 12 GW generated at 1.5 GHz assuming that the longitudinal electric field experienced by the electrons is the same i.e. $Power \times (frequency)^2$ =const. . However, the possibility to focus this energy to a small area is substantially enhanced at X band. Operation at high frequency has the potential advantage of reduced probability of rf breakdown.

Operation at high frequency has also its disadvantage since assuming single mode operation, the size of the structures is reduced and consequently, the amount of power in the beam is smaller. Furthermore the constraints on the guiding magnetic field are more stringent. The role of the latter is even more critical when high efficiency is required since small asymmetries of beam may generate hybrid modes that cause beam break-up. In such a case increasing the intensity of the guiding magnetic field is not sufficient and it is necessary to suppress the hybrid modes. Moreover, for high-power, high-efficiency, and high rf energy, the extraction of the energy from the beam in the output section becomes the most crucial issue. We believe that axial extraction is the sensible method for further investigation. Finally, the coaxial output structure seems to be the adequate approach when ultra-high power and high energies are required.

# 4 Ferroelectric Cathodes

## 4.1 Introduction

Research into the use of ferroelectrics as electron sources started with the work of Rosenman[31] who first observed low current emission from a ferroelectric ceramic. The work took on a practical interest when Gundel[32] and his co-workers later increased the emission by thirteen orders of magnitude. Shortly after, this work started in several other laboratories distributed throughout the world. The present state of the art has electron beams generated in ferroelectric guns operating at 500 kV and 300 A in 250 ns pulses. Current densities are typically less than or of order 100 $A/cm^2$, although higher current densities have been recorded from localized regions.

A ferroelectric material exhibits hysteresis in its polarization. If an applied cyclic electric field 10 kV/cm is applied to the material, the electric polarization curve P = P(E) follows a hysteresis loop. At zero applied electric field, there may exist a remnant polarization. Ferroelectrics have a non-linear permittivity $\epsilon = \epsilon(E)$. The peak value of the relative permittivity has a value of several thousand, so the internal polarization of the ceramic may result in an external field several thousand times larger than the field within the medium. Using values of $\epsilon = 5000$ and $E = 10^6$ V/m, we estimate electric field strengths external to the ferroelectric of order 5 x $10^9$ V/m. With field enhancements at triple points, the local external field may easily exceed 50 GV/m. These external fields pull in free charge from the surroundings to the surface of the ferroelectric. The charge screens the extremely large

electrostatic fields from the surroundings of the ferroelectric cathode due to the material polarization (and applied fields). The application of a rapidly changing electric field across the ferroelectric material may modify the amount of surface charge required to produce the electrostatic screening. The surplus charge is then emitted into the anode-cathode gap and may be used for the production of pulsed electron beams. Depending on the polarity of the trigger pulse used to initiate emission, it is also possible to generate the electron beam from the metallic grid on the front surface of the ferroelectric. In this configuration, the ceramic acts as a high dielectric constant, albeit non-linear, material which serves to enhance the field thereby causing the field emission from the triple points between a metal grid coating, the ceramic and the vacuum on the front surface of the ceramic.

Experiments have been carried out in various laboratories, [33, 34, 35, 36, 37, 38] on emission initiated by changing the material (e.g. PLZT) from an antiferroelectric to a ferroelectric state, and in other cases by cycling a ferroelectric material (e.g. PZT) around a minor hysteresis loop. In both cases, the role of the material polarization on the screening charge is crucial in determining the emission. The relative ease of generation of the electron beam current makes this source a potentially attractive option for high power microwave sources.

## 4.2 Recent Developments in Ferroelectric Emission

Since this area of investigation started in 1985 there have been a number of notable achievements. In 1990 Airapetov, [33] reported the highest ferroelectric current density obtained so far (400 A/cm2). Work in the United States was started at Cornell University in 1990 with first results reported in 1993 [50]-[51]. We observed emission from PZT with reverse triggering pulses, i.e. with a positive voltage applied to the rear surface of the ferroelectric. We also developed a comprehensive model of emission based on the formation of an electron cloud in the anode-cathode gap which acted as a medium for subsequent electron flow. A key conclusion of this work was that the electron cloud in the diode/gun would act to give a linear $I$-$\sqrt{V}$ characteristic. The effort has expanded to include groups at Integrated Applied Physics in collaboration with Jiang eta al. [36] (who measured beam emittance), Sampayan et al. [37] (who developed a phenomenological theory of the emission based on the energy of the emitted electrons), and the University of New Mexico (who extended the work started by Riege [20] on emission from PLZT). In parallel, the topic has been investigated in Japan [38], Germany [39], France, Israel [40]], and Russia[41].

We now summarize some of the key experimental results:

- The initial current flow is triggered and controlled by the pulsing of the ferroelectric. At later times, plasma closes the A-K gap and the current flow is then controlled by plasma processes [42].

- Current densities of more than 100 $A/cm^2$ were measured at CERN [32] and at Cornell with anode voltages ranging from 0-50 kV and with A-K gaps of up to 5 cm [42].

- At low voltages ($\leq$ 50 kV), the I-V characteristic of the diode is linear [58] within a reasonable approximation and the current exceeds that predicted by the Child-Langmuir

relationship. At higher diode voltages (V$\sim$ 250 kV), the current reverts to the usual $V^{3/2}$ scaling.

- The energy of the emitted electrons is measured by back-biasing of the anode and is found to depend on the polarity of the voltage applied on the back of the ferroelectric. In the case of a positive voltage the energy is of the order of 100 eV and in the case of a negative pulse the energy is approximately $\leq$ 1 keV [42]. Substantially higher energies ($\sim 25keV$) have been found by Riege and inferred by the group at LLNL.

- Several groups have measured the electron beam emittance and brightness. IAP [36] reported a brightness of $10^{10}A/m^2rad^2$ for a 36 A, 22.5 kV beam. At LLNL [37] the brightness was found to be $10^9A/m^2rad^2$ for currents of 6 A at 11 kV and 42 A at 21 kV. At Cornell the brightness was measured at 14 kV, 8 A and found to be 1.2 x $10^9A/m^2rad^2$.

- Several authors measured good repetitive pulses: Riege has reported reproducible 5 ns pulses at 1 MHz repetition rate over more than $10^6$ shots. At Cornell reproducible pulses at 15 kV, 20A and 600 ns were measured at 50 Hz. The LLNL group observed no degradation of the current pulse at 1 Hz for more than 20,000 shots with anode voltages between 15 to 60 kV. Some electron gun experiments have been carried out at beam energies of up to 500 keV with 200 A from a 1.9 cm diameter ferroelectric disk. These experiments will be described later in this section.

## 4.3 Theoretical Models

A comprehensive theory that can explain all the experimental results listed in the previous section does not exist; herein, we note only the basic concepts proposed.

Gundel [32] has summarized a qualitative explanation for the presence of the energetic electrons found in most experiments. If the polarization field in the material is altered by, for example, applying a short duration voltage pulse, then part of the free-charge screening charge attached to the surface by the original polarization field may be ejected from the cathode. If an applied field reverses the polarization field, then the surface neutralizing charge is repelled and acquires a kinetic energy associated with the energy stored in the reversed polarization field.

Schachter has developed a model based on the experimental data accumulated at Cornell [42]. It is the only detailed quantitative theory of ferroelectric emission that has been developed to date. When the ferroelectric is pulsed from its equilibrium state, a substantial fraction of the excess of surface charge redistributes within the A-K gap with the rest flowing to the surrounding grid. This charge forms a deep potential well which serves to control subsequent electron flow. The electrons oscillate in the potential well, however the net current associated with this motion is zero. When a (non-relativistic) anode voltage is applied, the motion of the oscillating electrons is perturbed and a net current flows. The current-voltage characteristic is linear and the diode impedance may be shown to be

$$R_{gap} \equiv \frac{\eta g^2}{36A}\gamma_0{}^2\sqrt{\frac{\gamma_0+1}{\gamma_0-1}}. \qquad (13)$$

where A is the diode surface area, $\eta = 377\Omega$, g the diode gap, and $g_0$ is the normalized kinetic energy of the oscillating electrons. The impedance is directly related to the amount of charge repelled into the gap. The amount of charge that traverses the A-K gap can be much larger than the initial charge on the surface of the ceramic. This is particularly important when a long duration anode voltage pulse is applied. The current flow is then due to electrons emitted from the surface of the ceramic by, for example, field emission. This may or may not be accompanied by significant plasma formation. The model predictions agree well with experiment over variations of more than three orders of magnitude in the anode voltage and two orders of magnitude in the diode gap spacing.

The LLNL group has developed a phenomenological model [37] based on the assumption that electrons are injected by the ferroelectric into the A-K gap with an initial kinetic energy W. It was assumed that the injected current was sufficiently large to cause a virtual cathode to be formed. When a voltage f is applied to the anode, the current density is calculated as

$$\frac{J}{J_{CL}} \equiv \frac{[1 + (1 + \phi_N{}^{3/4})]}{\phi_N{}^{3/2}}. \tag{14}$$

where $\phi_N = ef/W$ and $J_{CL}$ is the Child-Langmuir limiting current density. This model shows that at low voltages ($\phi_N << 1$) the current density may exceed the Child-Langmuir limit whereas at high voltages the C-L limit is asymptotically approached. Based on their experimental data, the authors infer that the initial kinetic energy of the electrons is approximately 5 keV.

In the previous models, no attention was paid to the processes which occur on the surface of the ceramic. In an attempt to explain the excess of the measured current beyond the Child-Langmuir limit, Mesyats and his co-workers [41], [43] suggest explosive electron emission due to field enhancements at triple-points (vacuum-metal-dielectric junctions). The emission can contribute directly to the anode current flow and also lead to plasma formation on the surface of the cathode. In addition to expanding across the surface of the cathode, the plasma propagates towards the anode with a typical velocity vp, and the limiting current may be approximated as a function of time by

$$J(t) \equiv J_{CL} \frac{g^2}{(g - \nu_p t)^2} \tag{15}$$

where g is the physical anode-cathode gap spacing. The triple-point emission almost certainly plays an important role in the emission process [43].

In many of the ferroelectric diode experiments carried out to date, the late time behavior of the diode is determined by the energy deposition in the anode. The effects include anode plasma formation and back-sputtering of the cathode surface. These effects are not observed in electron gun geometries where the beam dump is remote from the gun. We conclude this section with a brief outline of recent results on electron beam generation at current and voltage levels useful for high power microwave generation.

## 4.4 Electron Beam Generation Using a Ferroelectric Cathode

The electron gun used in this work [44] operates at 500 kV, 200A, 250 ns and uses a ferroelectric cathode as the electron source. The system operates at a repetition rate of about

0.1 Hz which is limited by the available power supplies. Vacuum levels are presently in the vicinity of 5 x $10^{-6}$ Torr. The experimental geometry is illustrated in Fig. 14.

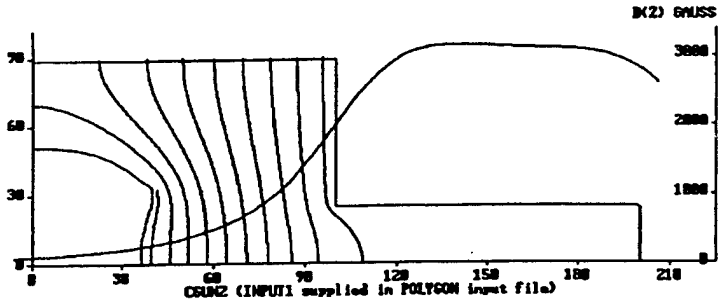


Figure 14: Diode/electron gun schematic. Equipotentials for the system and the amplitude of an applied magnetic field are indicated in the figure. Both axes are in mesh units equal to 1 mm.

The ferroelectric emitter is located on the cathode surface and has a diameter of 1.9 cm. The emitter is a 1 mm thick PZT sample, pre-poled, and mounted with the polarization vector pointing into the vacuum region. The emission is confined by an axial magnetic field. A thin ($\leq$ 1$\mu$m) grounded grid consisting of a number of 200 $\mu$m width silver strips spaced from each other by 200 $\mu$m is deposited on the front surface of the ferroelectric. In these experiments, we triggered emission via a positive trigger pulse applied to the rear surface of the ferroelectric. This method results in electron field emission from the metallic grids in the vicinity of the triple points. The duration of the field emission is determined by the applied pulse duration ( 100 ns) and by the hysteresis properties of the ferroelectric, so the total emission duration may exceed 1 $\mu$s [42]. The use of a positive polarity pulse was found to yield a consistent electron current. The electric field applied across the ferroelectric is about 10 kV/cm.

In Fig. 15., we show the voltage across the gun and the beam current for a 500 kV, 200 A beam with an effective gap spacing of 6.6 cm. The emission is triggered by a pulse applied to the ferroelectric about 50 ns prior to the start of current flow in the electron gun.

In Fig. 16. we show plots of the gun current versus the three halves power of the gun voltage for gap. The emission scales linearly with the three halves power of the gun voltage and was found to be within a factor of about two of that expected in space charge limited flow as predicted by the EGUN code. This result should be contrasted to the linear voltage scaling previously reported at lower ($\leq$ 50 kV) voltages.

The large spacing between the cathode and the collector surfaces makes it very unlikely that plasma closure, especially that due to plasma formed by collector bombardment, plays any significant role in determining the diode dynamics. Nevertheless, the possibility of explosive field emission, and hence, plasma formation on the cathode surface is not precluded. In these experiments the emission starts with the application of the trigger pulse to the rear

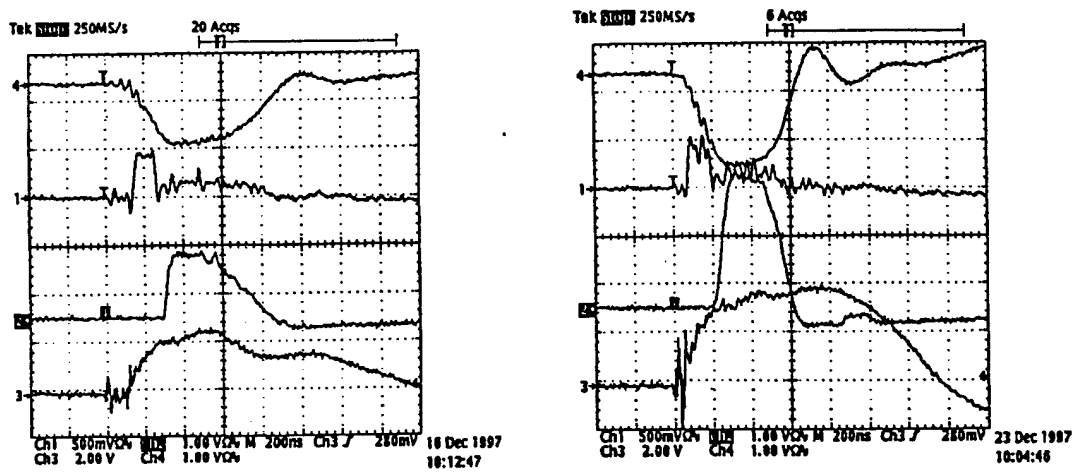

Figure 15: Data showing top, output voltage, ferroelectric trigger, beam current and bottom, of 500 kV, 200 A.

surface of the ferroelectric, and terminates with the end of the main gun acceleration pulse. It is consistent with field emission from the metallic grid at the vacuum/grid/dielectric boundary. Note, however, that field emission does not necessarily lead to explosive emission and plasma formation as described by Mesyats.

# 5 Recent Experimental Results

## 5.1 HPM Experiments

The work described above was extended during the last year. A full description of this work was recently submitted for publication and a copy of the paper is appended. There are two new important results:

- The beam voltage was increased to 800 kV and accompanied by an increase in the beam current to 300A. The microwave power pulse was observed to increase to 120 MW at an rf conversion efficiency of 44%. There was no evidence of pulse shortening.

- Substantial efforts were made to determine the role, if any, in these experiments of HEM modes on pulse shortening observed in many high power microwave experiments. The lower branch of the HEM mode is expected to be synchronous with the beam (i.e. have its maximum growth rate) at about 10.5 GHz. To measure HEM modes and their power levels we inserted a high pass filter in the envelope detector arm. The transmission of the $TM_{01}$ mode was, under these conditions, at least 55 dB down compared to the levels observed without the filter. We examined the HEM mode power levels for a variety of conditions as follows:

    (a) Under normal operational conditions the HEM mode level was about 100 W,

    (b) With the beam one radius off axis the HEM level increased to about 1 kW

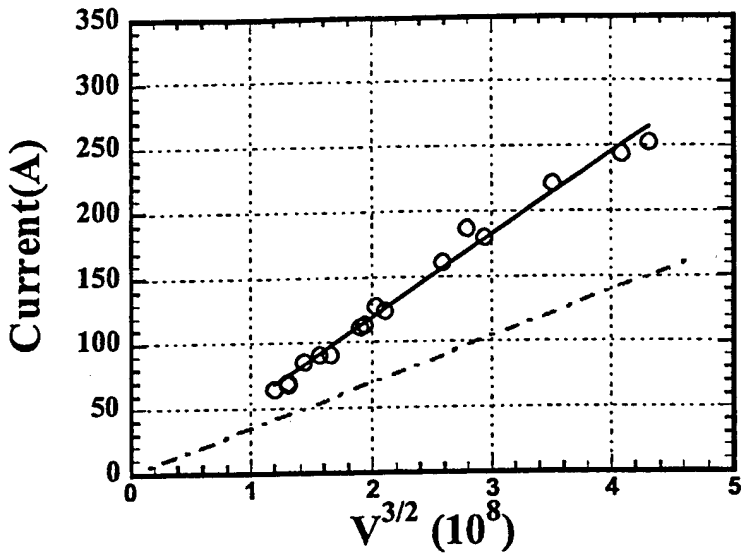


Figure 16: V-I characteristics of the electron gun for a cathode to drift tube (anode) spacing of 6.5 cm. The dashed line shows the current calculated using the EGUN code.

(c) For an elliptical cross section beam the power level remained about 1kW in both planes of polarization and,

(d) With the amplifier modified by the use of two fin severs and loads (The usual sever and load consisted of 4 SiC fins arranged perpendicular to each other) the HEM mode absorption in the severs/loads is dramatically reduced and we expect the HEM mode to oscillate and to compete with the TM01 mode. Under these conditions the HEM mode level approached 500 kW while the TM mode power declined from 70 MW to about 50 MW.

Under no circumstances did we detect any effects from the HEM modes which might be interpreted as causing beam pulse/microwave shortening. The problem was also examined theoretically as described in the appended report and the experimental results confirmed.

The hybrid modes are very important in disk loaded TWT accelerators and lead to beam loss. It is reassuring to find that the amplifiers do not seem to be plagued by the same beam loss. This is presumably due to the lower Q of the amplifiers.

In early experiments during the MURI program beam loss and rf pulse shortening were found to be important. The change in the results appears to be due to a re-alignment of the tube. At a flange about 25 cm downstream of the diode a 0.5 degree alignment error was detected so that the beam and magnetic field axes were not coaxial. Correction of this alignment error resulted in the elimination of the pulse shortening.

## 5.2 Ferroelectric Results

The work described above was extended in the last year to include a new gun design, one which allowed laminar beam flow at 500 kV and 200 A. The new configuration was tested using a single stage X-band TWT amplifier and found to produce about a 30 dB gain

with a power output of several megawatts. These results are currently being prepared for publication and will be submitted to the IEEE Trans on Plasma Science in the late summer.

During the Muri investigations the ferroelectric cathode program was taken from the generation of diodes with a few amperes of current at several hundred volts to the generation of 500 kV laminar flow beams suitable for use in HPM research. Tests were also carried out over short times ( a few seconds) which demonstrated that these cathodes can be satisfactorily operated at 60 Hz. The remaining un-tested feature is cathode lifetime.

# References


[1] J.A. Nation, "On the Coupling of a High-current Relativistic Beam to a Slow Wave Structure," Appl. Phys. Lett. v. 17, pp. 491-494, (1970).

[2] N. F. Kovalev, M. I. Petelin, M. D. Raiser, A. V. Smorgonsky, and L. E. Tsopp, "Generation of powerful electromagnetic radiation pulses by a beam of relativistic electrons," Pis'ma Zh. Eksp. Teor. Fiz., v. 18, pp 232-235 (1973) [ JETP Lett., v. 18, pp. 138-140 (1973)].

[3] Y. Carmel, J. Ivers, R. E. Kribel, and J. Nation, "Intense coherent Cerenkov radiation due to the interaction of a relativistic electron beam with a slow-wave structure," Phys. Rev. Lett., v. 33, pp. 1278-1282 (1974).

[4] S.A. Gilmour,"Principles of TWT's", Artech, 1994.

[5] A. Nordsieck, "Theory of the large signal behavior of traveling wave amplifiers," Proc. IRE, v. 41, pp. 630-637 (1953).

[6] "High Power Microwave Tubes: In the Laboratory and On-Line", IEEE Trans. on Plasma Science v.22, no.5, pp. 683-691, (1994)

[7] S. P. Bugaev, V. A. Cherepenin, V. I. Kanavets, A. I. Klimov, A. D. Kopenkin, V. I. Koshelev, V. A. Popov, and A. I. Slepkov, "Relativistic multiwave Cerenkov generators," IEEE Trans. Plasma Sci., v. 18, pp. 525-536 (1990).

[8] S. D. Korovin, G. A. Mesyats, V.V. Rostov, V.G. Shpak, and M.I. Yalandin, "Relativistic Millimeter Range microwave amplifier using a high-current electron miniaccelerator," Pis'a Zh. Tekh. Fiz. v.11, 1072, (1985). (Sov. Tech. Phys. Lett., v. 11, 445, (1985).

[9] D. Shiffler, J.D. Ivers, G.S. Kerslick J.A. Nation and L. Schächter; "A Two Stage High-Power Traveling-Wave Tube Amplifier," Appl. Phys. Lett. v. 58, p. 899, (1991).

[10] D. Shiffler, J.A. Nation, L. Schächter, J.D. Ivers and G.S. Kerslick; " A High Power Two Stage Traveling-Wave Tube Amplifier", J. Appl. Phys. v. 70, 106, (1991).

[11] P. Wang, Z. Xu, D. Flechtner, Cz. Golkowski, Y. Hayashi, Cz. Golkowski, J.D. Ivers, J.A. Nation, S. Banna and L. Schachter "A comparative Study of a High-Power, Multi-stage, X-band TWT Amplifiers," PAC'99, Particle Accelerator Conference, New York, (1999).

[12] J.R. Pierce, "Theory of the Beam-Type Traveling Wave Tube," Proc. IRE, p. 111 (1947). See also: "Traveling-Wave Tubes", by J.R. Pierce, D. van Nostrand Company Inc., Princeton, New Jersey (1950).

[13] L. Schächter, "Beam-Wave Interaction in Periodic and Quasi-Periodic Structures" Springer-Verlag, Heidelberg, (1997).

[14] L. Schächter, J. A. Nation and G.S. Kerslick, "On the Bandwidth of Short Traveling Wave Tubes", J. Appl. Phys., v. 68, p. 5874,(1990).

[15] L. Schächter, "Cerenkov Traveling Wave Tube with a Spatially Varying Dielectric Coefficient," Phys. Rev. A., v.43, p. 3785,(1991).

[16] L. Schächter, J.A. Nation and D. Shiffler, "Theoretical Studies of High-Power Cerenkov Amplifiers," J. Appl. Phys. v. 70, p. 114, (1991).

[17] L. Schächter and J.A. Nation, "Slow Wave Amplifiers and Oscillators: A Unified Study," Phys. Rev. A., v. 45, p 8820, (1992).

[18] L. Schächter and J.A. Nation, "Narrow Band High Power Traveling Wave Amplifier" Proceedings of the Third Workshop on Advanced Acceleration Concepts, Port Jefferson, Long Island NY 14-20, June 1992.

[19] E. Kuang, T. J. Davis, G. S. Kerslick, J.A. Nation and L. Schachter; "Transit Time Isolation of a High Power Microwave Amplifier" TWT", Phys. Rev. Lett. v. 71, p 2666 (1993).

[20] E. Kuang, T.J. Davis, G.S. Kerslick, J.A. Nation and L. Schachter; "Low Group Velocity Traveling Wave Tube Amplifier", IEEE - Trans. Plasma Science v. 22, p.511 (1994).

[21] L. Schächter and J.A. Nation; "An Analytical Method for Studying Quasiperiodic Disk Loaded Waveguide", Appl. Phys. Lett. **63**, 2441 (1993).

[22] L. Schächter and J.A. Nation; "Propagation of Electromagnetic and Space-Charge Waves in Quasi-Periodic Structures", Physics of Plasmas, **2**, 889 (1995).

[23] L. Schächter; "High Efficiency Beam-Wave Interaction in Quasi-Periodic Structures", Phys. Rev. E. **52**, 2037 (1995).

[24] L. Schächter, D. Flechtner, J.D. Ivers, G.S. Kerslick, E. Kuang, S. Naqvi, J.A. Nation and G. Zhang. "Studies of High Efficiency Interaction in Traveling Wave Structures". Proceedings of Pulsed RF Sources for Linear Colliders, Oct.2-7,1994, Montauck, Long Island, New York.

[25] S.A Naqvi, G. S. Kerslick, J. A. Nation and L. Schächter; "Axial Extraction of High-power Microwaves from Relativistic Traveling Wave Amplifiers", Appl. Phys. Lett. **69**, 1550 (1996).

[26] S.A. Naqvi, G.S. Kerslick, J. A. Nation and L. Schächter: " Resonance Shift in Relativistic Traveling Wave Amplifiers", Phys. Rev. E. **53** 4229 (1996).

[27] P. Wang, Z. Xu, D. Flechtner, Cz. Golkowski, Y. Hayashi, Cz. Golkowski, J.D. Ivers, J.A. Nation, S. Banna and L. Schachter "A comparative Study of a High-Power, Multistage, X-band TWT Amplifiers" PAC'99, Particle Accelerator Conference, New York 1999.

[28] L. Schächter and J.A. Nation; "Beam-quality and Guiding Magnetic Field Requirements for a High-Power Traveling Wave Amplifier Operating at 35GHz", Phys. Rev. E, **57** 7176 (1998).

[29] S.A. Naqvi, Nation J.A., Schächter L. and Wang Q. "High Efficiency TWT Design Using Traveling-Wave Bunch Compression", IEEE Trans. Plasma Science - Special Issue, Vol.26(3) p. 840-5(1998).

[30] Cz. Golkowski, J.D. Ivers, J.A. Nation P. Wang and L. Schächter " First Results from a High-Power KA-Band TWT", PAC'99, Particle Accelerator Conference, New York 1999.

[31] G. I. Rosenman, E. V. Okhapkin, Yu. L. Chepelev, and V. Ya. Shur, "Electron emission during the switching of ferroelectric lead-germanate," Sov. Phys.–JETP Lett., vol. 39, no. 9, pp. 477-480, 1984.

[32] H. Gundel, H. Riege, E. J. N. Wilson, J. Handerek, and K. Zioutas, "Fast Polarization Changes in Ferroelectrics and their Application in Accelerators", Nucl. Instrum. Meth. Phys. Res. A, vol. 280, pp. 1-6, Aug. 1989.

[33] [49] A. Sh. Airapetov, A. K. Krasnykh, I. V. Levshin, and A. Yu. Nikitskii, "Measurement of the Emission Current Accompanying the Reversal of Polarization of a Ferroelectric", Sov. Tech. Phys. Lett., vol. 35, no. 3, pp.182-184, 1990.

[34] J. D. Ivers, L. Schachter, J. A. Nation, G. S. Kerslick, and R. Advani, "Electron beam diodes using ferroelectric cathodes," J. Appl. Phys., vol. 73, no. 6, pp. 2667-2671, Mar. 1993.

[35] L. Schchter, J. D. Ivers, G. S. Kerslick, and J. A. Nation, "The analysis of a diode with a ferroelectric cathode," J. Appl. Phys., vol. 73, no. 12, pp. 8097-8110, 1993.

[36] B. Jiang, G. Kirkman, and N. Reinhardt, "High brightness electron beam produced by a ferroelectric cathode," Appl. Phys. Lett., vol. 66, no. 10, pp. 1196-1198, Mar. 1995.

[37] S. E. Sampayan, G. J. Caporaso, C. L. Holmes, E. J. Lauer, D. Prosnitz, D. O. Trimble, and G. A. Westenskow, "Emission from ferroelectric cathodes," Nucl. Instrum. Meth. Phys. Res. A, vol. 340, no. 1, pp. 90-95, Feb. 1994.

[38] M. Okuyama, J. Asano, and Y. Hamakawa, "Electron emission from lead-zirconate-titanate ferroelectric ceramic induced by pulse electric field," Japan J. Appl. Phys., vol. 33, pp. 5506-5509, Sep. 1994.

[39] H. Gundel, "Electron emission from ferroelectrics," Science and Technology of Electroceramic Thin Films, O. Auciello and R. Waser (eds.), Boston, MA: Kluwer Academic Publisher, 1995, pp. 335-51.

[40] V. D. Kugel, G. Rosenman, D. Shur, and Y. E. Krasik, "Copious electron emission from triglycine-sulfate ferroelectric crystal," J. Appl. Phys., vol. 78, no. 4, pp. 2248-2252, Aug. 1995.

[41] G. A. Mesyats, "Electron emission from ferroelectric ceramic," Tech. Phys. Lett., vol. 20, no. 1, pp. 8-9, Jan. 1994.

[42] D. Flechtner, C. Golkowski, G. S. Kerslick, J. A. Nation, and L. Schchter, "Electron emission from lead-zirconate-titanate ceramics," J. Appl. Phys., vol. 83, no. 2, pp. 955-961, Jan. 1998.

[43] V. L. Puchkarev and G. A. Mesyats, "On the mechanism of emission from the ferroelectric ceramic cathode," J. Appl. Phys., vol. 78, no. 9, pp. 5633-5637, Nov. 1995.

[44] J. D. Ivers, D. Flechtner, Cz. Golkowski, G. Liu, J. A. Nation, and L. Schchter, "Electron beam generation using a ferrroelectric cathode," IEEE Trans. Plasma Sci., PS-27(3) p.707 (1999).

# Refereed Journal Publications Arising from MURI Program at Cornell University

**Published papers**

"Resonance shift in relativistic traveling wave amplifiers," S. Naqvi, G.S. Kerslick, J.A. Nation and L. Schachter, Phys. Rev. E. 53, 4229 (1996)

"Axial extraction of high-power microwaves from relativistic traveling wave amplifiers," S. Naqvi, G.S. Kerslick, J.A. Nation and L. Schachter, Appl. Phys. Lett. 69, 1550 (1996)

"Electron emission from ferroelectric ceramics," D. Flechtner, Cz. Golkowski, G.S. Kerslick, J.A. Nation and L. Schachter, Journal of Applied Physics, 83, 955-961, (1998)

"Ferroelectric sources and their application to pulse power: A review," C.B. Fledderman and J.A. Nation, IEEE Transactions on Plasma Science, 25,2, 212-220, (1997)

"Beam-quality and Guiding Magnetic Field Requirements for a High-Power Traveling Wave Amplifier Operating at 35GHz", L. Schächter and J.A. Nation, Physical Review E, **57**, pp. 7176-7183, (1998).

"Annular Electron Beam Generation Using a Ferro-electric Cathode", Cz.,.Golkowski, D. Flechtner, J. Ivers, J .A. Nation, and L. Schächter. IEEE Trans. Plasma Science - Special Issue, Vol.26 (3) p. 835-9, (1998).

"Analytic Expression for Triple-Point Electron Emission from an Ideal Edge" L. Schächter , Applied Physics Letters, **72**(4) p. 421-3 (1998).

"High Efficiency TWT Design Using Traveling-Wave Bunch Compression", S . Naqvi., J.A Nation., L . Schächter, and Q. Wang. IEEE Trans. Plasma Science - Special Issue, Vol.26 (3) p. 840-5, (1998).

"Theoretical Study of a Diode with Dielectric-Gridded Cathode", L. Schächter, D. Fletchner, Cz, Golkowski., J.D. Ivers, and J. A. Nation, J. Appl. Phys., 84(12) p. 6528-6535 (1998).

"Advances in Non-Thermionic Cathode Physics and Technology" J.A.Nation, L. Schächter, F. Mako, L. Len, W. Peter, Cha-Mei Tang and Triveni Srinivasan-Rao, Proceedings of the IEEE, Vol. 87(5), p.865-889. Invited paper.

"Amplification of a Wake-Field Generated by a Charged Bunch in a Resonant Medium," L. Schächter , Phys. Rev. Lett., 83(1), p. 92 (1999).

"Electron Beam Generation Using a Ferrroelectric Cathode", J.D. Ivers, D. Fletchner, Cz. Golkowski, G. Liu, J.A. Nation, and L. Schächter, IEEE Trans. Plasma Sci., PS-27(3) p.707 (1999).

"High Power Microwave Amplification in Non-Uniform Slow Wave Structures", P. Wang, Zhou Xu, J.D. Ivers, J.A. Nation, S.A. Naqvi, and L. Schachter; Appl. Phys. Lett., 75(16), p.2506-7 (1999).

"Limiting Current from a Metallic Ideal Edge Attached to a Dielectric Edge", L. Schächter and J.A. Nation, Appl. Phys. Lett., 75(20), p.3084-6(1999).

**Papers Accepted For Publication**

S. Banna, J.A. Nation, L. Schächter and P. Wang. *The Coupling of $TM_{01}$ and $HEM_{11}$ in a High-Power, High-Efficiency Traveling Wave Amplifier,* Physical Review E , 2000

*S. Banna, J.A. Nation, L. Schächter and P. Wang, The Interaction of Symmetric and Asymmetric Modes in a High-Power Traveling Wave Amplifier, IEEE Plasma Science - Special Issue 2000*

P. Wang, Z. Xu, J.A. Nation, S. Banna and L. Schachter, *Symmetric and Asymmetric Mode Interaction in High-Power Traveling Wave Amplifiers,* IEEE Trans on Plasma Science. 2001

**Papers Submitted for Publication**

Y. Hayashi, X. Song, J. D. Ivers, D. Flechtner, J. A. Nation and L. Schachter, *High Power Microwave Generation Using A Ferroelectric Cathode Electron Gun,* IEEE Trans on Plasma Science. 2000